Delft University of Technology &
Scuola superiore Sant'Anna

BM51032

BME MSc Thesis

Design and Development of a Switchable Joint for Rehabilitation Purpose with the Focus on an Elbow Joint

---

Author:
Jessica Brand

Student Number:
4466160

September 12, 2017

Contents

Introduction **1**

Scientific Paper **4**

References **15**

Appendix **17**

1 Current Design by the Biorobotics Institute 17
2 Expanded Method 18
3 Creation Process of the Conceptual Designs 22
4 Non-backdrivable Mechanism 23
5 Conceptual Designs 23
6 Selecting Process of a Winning Concept 29
7 Finalizing the Winning Concept 32
8 FEM Analysis 37
9 Component Issues 54
10 MATLAB Codes 54
11 Technical Drawings 69
12 Abbreviation List 85

Introduction

The human body consists out of many joints to allow a high variety on movements and functions. One important joint of the upper limb is the elbow joint.

The elbow is a mechanical connection between the upper and lower arm (forearm) transferring the movement of the shoulder to the wrist/hand. Because of that, it is co-responsible for certain functions such as powerful grasping, positioning the hand, stabilization as well as being the center of rotation for the forearm. [1]

The stabilization elements of the elbow joint include active and passive features. The passive stabilization is achieved by ligaments as well as the compliant articulation between the forearm (ulna) and the upper arm (humerus). The active stabilization is caused by pressure forces acting on the joint. This forces are induced by the muscles crossing the joint. [1]

When being precise, the elbow joint consists out of three joints [2] (see Fig. 1). Hence, it not only allows flexion and extension, but also supination and pronation representing the rotation of the forearm. Consequently, the elbow joint is responsible for two Degrees of Freedom (DOF) [3].

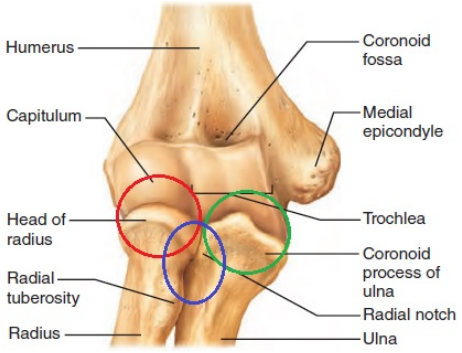

Figure 1: Elbow joint in anterior view. The colored circles indicate the three different joints: Red - humeroulnar joint, green - humeroradiales joint, blue - radioulnar joint. Modified Figure [4].

The first of the three joints is called the humeroulnar joint, which connects the ulnar and the humerus, allowing movements in the sagittal plane (extension - flexion) in a range of $-5\,^\circ$ [5] or $0\,^\circ$ [1] to $145\,^\circ$ [5] or $150\,^\circ$ [1]. However, most daily activities are performable between a range of 30°-130° [6]. The second joint in the elbow is named radioulnar [2] joint connecting ulna and radius. It performs its movement based on the rotation of the radius around the ulnar. It allows about $85\,^\circ$ ($80-90\,^\circ$[5]) supination and $75\,^\circ$ ($50-80\,^\circ$[5]) pronation for an healthy person. The last joint is the humeroradiales [2]. It keeps the connection between the humerus and the radius, while the radius is moved around the ulnar and allows for flexion/extension of the forearm. [1]

Due to its DOF and the previously named functions, the elbow is used in everyday life activities, for almost any tasks related to the upper limb. For instance, the elbow is used in easy tasks such as lifting a bottle, brushing teeth or when going grocery shopping. Yet,

it is also needed in more complex tasks such as when playing tennis, throwing a ball or when the elbow is used to balance the body with the help of the arm.

Occurs now a dysfunction or the loss of the elbow joint due to an disease, an traumatic incident [2] or based on congenital defects or even on an amputations due to malignant, vascular or traumatic conditions [7], then these daily activities become very difficult or even impossible to be performed. Consequently, the life quality of the affected population decreases.

However, several rehabilitation devices exist with the purpose to regain or to improve lost or decreased joint functions. For instance, prostheses are used to replace a missing body part [8] such as an entire arm or just a part of it. Yet, prostheses are either used to compensate for lost limb/joint functions or only for cosmetic reasons and in that case the prostheses would be without any functions. However, another example of rehabilitation devices are orthoses, which are externally applied to movable body parts [8] such as the elbow joint. Thus, orthoses are used when problems regarding the skeletal or neuromuscular system are present. For instance, when an abnormal posture and/or movement occurs. Therefore, orthoses are supposed to correct, align and support the body with its impairments [8]. Furthermore, orthoses can be static or dynamic, whereby a static orthesis fixes the joint and its limb in a certain position and a dynamic orthesis decreases or increases the movement of a joint [9].

Yet, many different elbow orthoses and prostheses have been developed to regain or to increase the elbow functions as much as possible. However, since human joints consist out of a complex structure with their bones, muscles and nerves, the devices focus often only on specific problems that they desire to solve. Hence, some prostheses are focused on increasing the DOF such as the developed CINESTAV IPN by Escudero et al. [10] or to balance the complexity and performance of the device, to encourage more amputees to wear a prostheses on a daily basis, which was, for instance, the goal of the RIC Arm by Lenzi et al. [11]. Instead, some ortheses may focus on specific diseases or functions of the joint. For instance, a Flexible Fluidic Actuation orthosis was developed by Pylatiuk et al. [12] to reduce the symptoms (reduced speed and power when performing movements) of patients with limited voluntary control of their biceps and triceps.
However, some developed prostheses and ortheses focus on the improvement of previous designs, just as the developed joint module by the Biorobotics Institute of the Scuola Superiore Sant'Anna (SSSA) in Pisa (Italy). The joint module was created to adjust the transmission mechanism of previous designs to allow multiple transmission stages such as a direct transmission between the input and output and a transmission including a compliant mode. In previous designs, for instance of the Dynamic Arm (Ottobock GmbH, Duderstadt, Germany) or the U3 Arm (Motion Control Inc., Salt Lake City, USA), rigid transmission stages are used. Only few prostheses [13] and orthoses allow the disengagement of the transmission to engage and copy the natural free-swing of the arm when walking. For instance, the patent US 8,591,443 B2 of an elbow orthesis by Bonutti et al. [14] can disengage its transmission when it unaligned its gear teeth.
Yet, other devices include an additional actuator to obtain a compliant mode, so that the design is able to absorb shocks and to reduce or even avoid compensatory movements when reaching to an object. However, when these additional actuators are used a second motor is required for their activation as it is the case in the elbow orthosis by Sulzer

et al. [15] where two motors are required to achieve the pretensions within the device. Consequently, the size and weight of the device increases. As a result, the purpose of the developed joint module by the Biorobitics Institute was to create a device that allows to disengage the transmission and to include a compliant mode within one mechanism resulting in a reduced power consumption. Based on that, an artificial joint was created which is a bidirectional, non-backdrivable roller clutch that can switch between three different modes, a locking, free movement and compliant mode. However, the design still needs to be optimized regarding its weight, dimensions and the selecting mechanism of the different modes. Especially, the latter one needs to be improved, since the mechanism tends to get stuck when switching between the three modes or it is very difficult to do so. Anyhow, these issues are based on internal generated lever arms due to the used force transmission of the selector mechanism. Consequently, leading to involuntary wedging problems. [13]

The Purpose of the Paper

Based on the previous introduced issues, the intention of this paper is to create either a new mechanism or an improved design of the current joint mechanism to reduce, or in the best case, to avoid the involuntary wedging problems between the selector elements. Therefore, the aim is to develop a switchable joint mechanism, where the selecting mechanism and the created forces act (preferably) within the same plane, reducing or even eliminating undesired force lever arms. In addition, ambitions will be put on lowering the weight and the dimensions.

As a result, this paper introduces a new mechanism and concept with the potential to outperform the current developed joint module, which is based on the obtained results of the first stage. Yet, the second stage still needs to be analyzed, manufactured and tested to prove that the entire design with its two stages surpasses the current mechanism.

The paper will introduce and explain the new mechanism. Furthermore, a prototype will be developed of the first stage and mechanically tested regarding its unlocking torque and its operability. In addition, a first subjective acceptance evaluation regarding the size of the device will be performed and two conceptual designs for the second (compliant) stage will be developed and discussed.

Design and Development of a Switchable Joint for Rehabilitation Purpose with the Focus on an Elbow Joint

Jessica Brand, Department of Mechanical, Maritime and Materials Engineering
Delft University of Technology, 2628 CD, Delft, Netherlands
The BioRobotics Institute, Scuola Superiore Sant'Anna, 56025, Pisa, Italy

***Abstract*—Artificial elbow modules are used in orthoses and prostheses, whereby orthoses correct, align and support the body with skeletal or neuromuscular impairments [1]. Instead, prostheses replace missing body parts and compensate for lost functions [1]. However, most designs do not allow the natural arm swing based on their transmission design or the devices use multiple actuators to achieve a compliant mode [2]. Consequently, the Scuola Superiore Sant'Anna (Pisa, Italy) developed an elbow module, which can switch between two transmission stages resulting in three selectable elbow modes (locked, free, compliant). Furthermore, it uses only one controlled input leading to a reduced power consumption. Yet, the design contains major problems regarding its selecting mechanism (based on involuntary created moments), weight and dimensions. Here we introduce a new design with the potential to outperform the previous design regarding its unlocking torque, weight and dimensions based on the retrieved results. Hence, the unlocking torque decreased by a factor of 9.2±4.1 to 124.1±35 Nmm and 606.2±97.6 Nmm when 450 g - 600 g were applied. The weight is reduced by ∼280 g reaching ∼410 g. The diameter and depth are reduced by 7 mm and 5 mm leading to a final size of 78 mm and 32 mm, considering the first stage in combination with a second stage concept. Yet, to prove that the entire introduced design surpasses the previous mechanism, the second stage needs to be finalized, manufactured and tested. However, we provide a successful design of the first stage that can be used for further investigations.**

Keywords - bidirectional, non-backdrivable, clutch, joint, orthoses, prostheses, rehabilitation, elbow

Abbreviations - SSSA - Scuola Superiore Sant'Anna, VSA - Variable Stiffness Actuators, FEM - Finite Element Method, ROM - Range of Motion, CAD - Computer Aided Design, d - diameter, Tui-x - unlocking torque (i = t-optimal theoretical, ts - theoretical including selecting mechanism, m - measured; x = ND - new design, OD - old design), Tro - resulting output torque, Fu - unlocking force, Lu - unlocking force lever arm

I. Introduction

The elbow is an important joint of the human arm providing two degrees of freedom, which helps us to perform daily easy tasks (e.g. getting dressed, preparing food), but also complicated movements such as during sports (e.g. when playing tennis or when throwing a ball). However, when a dysfunction or even loss of the elbow occurs, then these activities become very difficult to be performed and with that, the quality of life decreases.

Every year about 150-200,000 people worldwide become amputees, whereby 30% are affected by upper arm amputations [3]. Consequently, the affected people are missing their elbow and suffer from reduced life quality due to the missing elbow functions. Although, not only amputees but also people dealing with muscular/neurological diseases (e.g. muscular dystrophy) and traumatic incidents can suffer from reduced elbow functions [4].

To increase the life quality of these patients certain rehabilitation devices such as prostheses and orthoses are being developed to either regain or to improve their reduced elbow functions.

Several designs for elbow mechanism exists. Present elbow modules as in the powered prostheses called Dynamic Arm (Ottobock GmbH, Duderstadt, Germany) and U3 Arm (Motion Control Inc., Salt Lake City, USA) are based on a rigid transmission between the output and actuator. Only few prostheses [2] and orthoses allow the disengagement of the transmission to engage and copy the natural free-swing of the arm when walking. For instance, the patent US 8,591,443 B2 of an elbow orthesis by Bonutti et al. [5] can disengage its transmission when it unaligned its gear teeth.

Furthermore, variable stiffness actuators (VSA) are used in prostheses and orthoses to ease the reaching movement towards an object and with that to reduce or even avoid unnatural compensatory movements of other proximal joints [2]. Besides, due to these VSA shocks can be better absorbed lowering the risk of related injuries at the residual articulation [2]. Nonetheless, when VSAs are used an additional motor is necessary for the adjustment of either the transmission ratio between the elastic elements influencing the size and weight of the prostheses or to adjust the elastic elements regarding their preload [2]. As an example, the elbow orthosis by Sulzer et al. [6] uses a type of VSA requiring two motors to achieve the pretensions within the device.

The BioRobotics Institute of the Scuola Superiore Sant'Anna (SSSA) in Pisa (Italy) has been working on an elbow module to find a compromise of desirable but less important requirements (such as the ability to store energy, low power consumption, safety, small size, variable compliant behavior and to be a lightweight design) for an elbow mechanism. To satisfy all of these criteria the Biorobotics Institute has developed an actuator being able to switch between passive and active compliant actuators. Hence, their elbow module is able to switch between three different modalities (locked, free movement, compliant) by the use of two transmission stages between the input and output shaft. Despite, the selected mode depends on the position of the transmission selector. As a result, it is possible to obtain a certain mechanical transmission behavior with a low power consumption. [2]

Issues of the Current Design

The developed elbow module by the Biorobotics Institute still contains major problems.

1) When switching between the different selection modes the mechanism gets often stuck or it is difficult to do, which is based on the design of the selecting mechanism of the current elbow module (see App. 1).
   As it can be seen in Figure 1, the selector pin consists out of a flat basement which has a perpendicular cylindrical extrusion. The basements of the selector pins get in contact with the rollers on its left and right side (see 'Top view' in Fig. 1) and the cylindrical extrusion is responsible for transferring the movement of the selector disk in the movement of the selector pins. This resulting movement of the selector pins is due to the selector disk pushing/pulling the selector pins based on the rotation of the selector disk. However, the contact between the selector disk and the cylindrical extrusion is at the end of the extrusion as indicated in Figure 1. Therefore, forces on the pin act in two parallel planes (with a distance of 11 mm in the first stage and 5.5 mm in the second stage). Consequently, one plane is on the same level as the pin's basement, where the roller forces act on the selector pin and the other plane is at the level of the contact point between the cylindrical extrusion and the selector disk. As a result, the obtained lever arm between these two planes apply a moment to the selector pin leading to wedging issues between the pin and its supporting surface. Another similar cause for the wedging problem is that the selector disk does not only apply pure, one directional forces in the direction of the pins sliding cavity, but due to the rotational movement of the selector disk, the generated forces are also applied in the direction of the rotation, pushing the pins against it surrounding elements.
2) Furthermore, the elbow module has a weight of 685 g, which can be considered as quiet high for a bare mechanism that will be applied to the body.
3) The size of the device is still large with a diameter of 85 mm and a depth of 37 mm, which makes the device bulky and not compact.

Based on these previous mentioned problems, the main intention of this paper is to create either a new or improved design of the current joint mechanism to reduce, or in the best case, to avoid the mentioned issues. Therefore, the aim is to develop a switchable joint mechanism, where the selecting mechanism and the created forces act (preferably) within the same plane. In addition, ambitions will be put on lowering the weight and the dimensions of the design.

II. Method

Before the development of a new switchable joint mechanism was started, design criteria and therefore requirements for the new design had to be found. Afterwards, based on brainstorming and discussions with lab members eight potential conceptual designs were created (see App. 3, 5). Critical comparisons between the concepts were performed to select a final design (see App. 6), which was subsequently finalized (see App. 7). Thereafter, a 3D-printed prototype was produced, Finite Element Method (FEM) analyzes were performed using ANSYS Workbench (ANSYS, Inc., Canonsburg, USA) (see App. 8), a real prototype was manufactured and subjectively and objectively tested regarding the acceptance of its dimensions, handling and

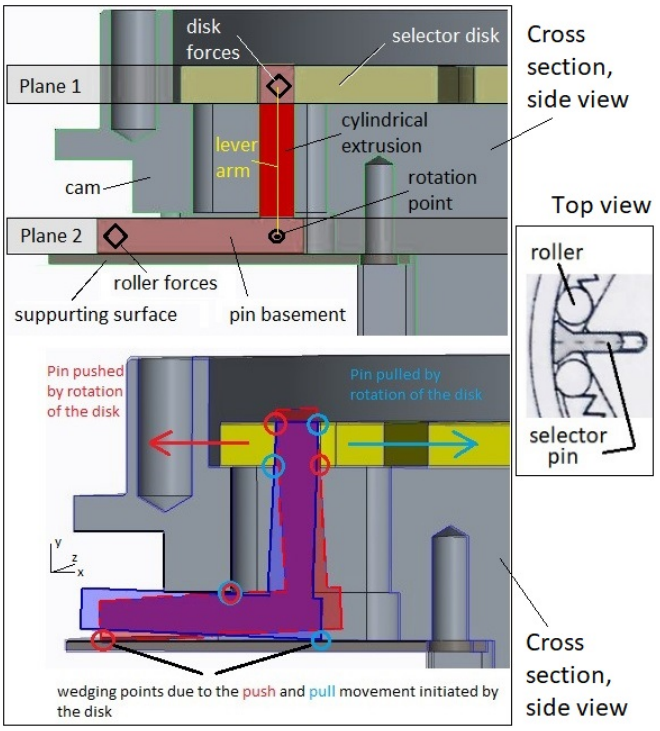

Figure 1: Left: Cross section of the input cam, selector pin and the selector disk. The upper figure indicates the two planes where forces are present. The areas with the applied forces are symbolized by squares. The lower figure is an exaggerated version of the wedging problem, showing the selector pin in the problematic positions when the selector disk applies pull (blue)/push (red) forces in a different plane than the basement part of the pin. The circles indicate possible problem areas of the design due to the disk forces. Right: Top view of the roller-selector pin formation.

unlocking torque (T_u).

(Calculations of these processes were performed with Excel (Microsoft, Redmond, USA) and MATLAB R2017 (The MathWorks Inc., Natick, USA); the MATLAB codes can be seen in App. 10. Technical drawings of included Computer Aided Design (CAD) models were created with Creo Paramatic 3.0 (PTC, Needham, USA) and are shown in App. 11.)

Design Criteria

The following design criteria apply to the development of the new design.

1) **Number of modes** - The new design should have at least two modes: A locking mode and a free mode. However, three modes are preferred, using a compliant mode as the third mode.
2) **Control of modes** - The new mechanism should be easily controllable, meaning that the switching from one mode to another should be able to be performed by one (bare) hand and that the unlocking torque (T_u)/force (F_u) should be lower than the T_u of the current device (which will be experimental measured in this paper). In addition, it should be difficult or (in the best case) impossible to switch between the modes by accident.
3) **Size** - The diameter (d) and depth of the device should be smaller than or at least equal to the dimensions of the current design. Hence, $d \leq 85$ mm and $depth \leq 37$ mm. Yet, the aim is to obtain a $d \leq 81$ mm (see App. 2).

4) **Design simplicity and number of components** - The design should be kept simple to allow an easy production, assembly, maintenance and therefore a low cost. Furthermore, a design with less components is preferred to warrant a light design and also a simple mechanism and assembly. The aim is to have the same or less amount of components as in the previous design (using 35 elements excluding screws).
5) **Weight** - The weight of the new device should be less or at least equal to the weight of the current design: 685 g. Yet, the aim is to reduce the weight by at least 200 g.
6) **Possibility to be automated** - The new mechanism should be able to be easily adjusted to an automated version by preferably one motor, in case patients are not able to control the device manually, or when the device is used for prosthetics.
7) **Range of Motion** - The new device should cover a Range of Motion (ROM) of at least 30°-130°, since most daily activities can be performed in this range [7]. Yet, the aim is to obtain the normal ROM of a healthy person which is between $-5\,^\circ$ [8] / $0\,^\circ$ [9] to $145\,^\circ$ [8] / $150\,^\circ$ [9]. However, it is preferred to achieve a ROM of 360° as in the current device, because than the range can be limited afterwards to every needed ROM as necessary for the patient.
8) **Natural appearance** - The new device should be related to the appearance of a natural arm, or at least the new design should be easily implemented in a natural appearance. This is needed to obtain a higher acceptance rate by the patients, since generally a natural look is preferred, which does not draw as much attention to the device as wearing an orthosis/prosthesis with an unnatural appearance.

In addition, a (bi-directional,) non-backdrivable system is preferred to hinder the accidental engagement of the mechanism by the output, and to reduce the power consumption [10]. Yet, brake systems will be considered as well.

The New Concept

The selected concept is based on the current design developed by the Biorobotics Institute of SSSA in Pisa (Italy). Consequently, it is again a bi-directional, non-backdrivable roller clutch. Although, only the engaging of the modes is different, even though the new concept still uses selector pins, which will be pushed out or pulled in, to either unlock or lock the stages. However, the mechanism that is responsible to move the pins is based on a crank-slider system (see Fig. 2) instead of using a selector disk that moves the pins due to the geometry of the cavities in the selector disk (see App. 1).

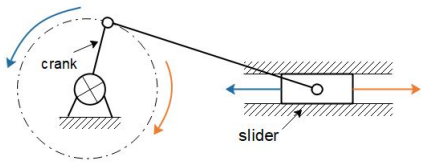

Figure 2: Overview of a crank-slider mechanism. By rotating the crank the slider gets either pushed or pulled in its sliding cavity.

In this new concept the crank will be called 'twister', the sliders will be represented by the 'selector pins' and the element connecting the twister with the selector pins will be called 'connector'.
The new mechanism uses two selector pins in each sliding cavity instead of one, which are pushed slightly to the side to transfer the translational, axial forces (obtained by the twister and the connector) to radial forces to unwedge the rollers. The selector pins are moved to the side due to the geometry of an additional pin (cam pin), which is part of the input cam. When unlocking the system, the selector pins are pushed against the cam pin, moving the selector pins aside and pushing the rollers away from the output ring. Furthermore, the previous force plane of the selector disk (plane 1, Fig. 1) is now substituted by the new crank/twister plane and the plane of the roller - selector pin force interaction and their movement (plane 2, Fig. 1) is substituted by two planes, whereby one plane is directly on top and the other one under the crank/twister plane. This is the consequence of using two selector pins for each roller pair instead of one, which are placed on top and bottom of the connector. Based on this placement, the force planes are closer to each other reducing the risk of involuntary wedging problems. A conceptual overview of the new mechanism can be seen in Figure 3.

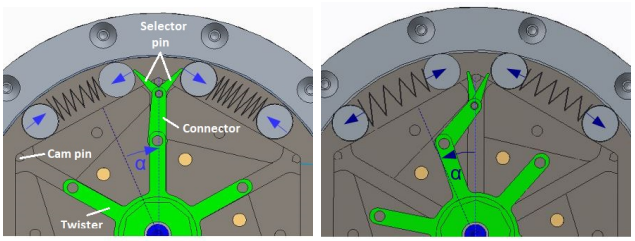

Figure 3: Overview of the basic principal of the new mechanism. (α represents in this case the angle of the rotation needed to push/pull the selector pins to unwedge/wedge the rollers.)

However, the previously shown mechanism represents only one stage, thus, when doubling this stage and adding a spring, the second stage can be obtained for the compliant mode. These two stages can either be designed to be in one component (see Concept 6, App. 3) or otherwise the stages can be separated as it is shown in Figure 4 and 5. When using the separated stage concept, the stages will be equally distributed around the elbow joint. Followed by that, one stage will be placed on the lateral side of the elbow and the other stage will be located on its medial side as demonstrated in Figure 5.

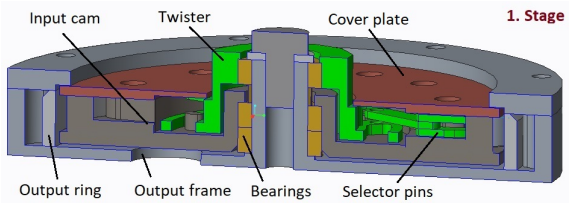

Figure 4: Overview of the first stage when the separated design is used. The cover plate will be attached to a forearm element, the output frame will be connected to an upper arm element.

Finalizing the Design

In the finalization process the geometry was tested against buckling, adjusted to the contact angle and the optimal roller radius (see App. 7). Besides, the radial roller-ring force was determined (see App. 7) and a FEM analysis was performed

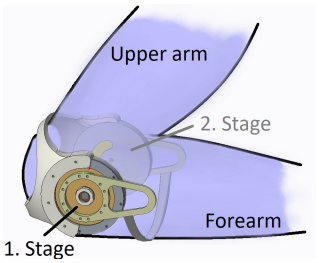

Figure 5: Example orthosis design of the entire separated stage mechanism, where the output frames of both stages are rigidly connected with each other, as well as the forearm elements. Furthermore, the forearm elements will be attached to the forearm and the output elements to the upper arm (not shown in this Figure).

of a normal and critical load case (5 kg, 50 kg) to check for possible stresses, deformations and pressures (see App. 8).

Furthermore, a 3D-printed prototype was manufactured of the important parts of the mechanism (output frame, output ring, input cam, twister, connectors, selector pins and the rollers). This was done to check whether the lock/unlocking mechanism works or whether the design has to be further changed before starting the real manufacturing process.

Mechanical Testing

First, a subjective test was performed to observe whether the mechanism locks/unlocks when rotating the twister as it was done for the 3D-printed prototype. Afterwards, an objective laboratory test was executed to compute the T_us of the old and new mechanism when 450 g, 1000 g, 2000 g and 3000 g were applied to the output with a load lever arm of 71 mm. The (input) unlocking forces (F_u) of each load condition were measured with the Instron 4464 (Illinois Tool Works Inc., Norwood, USA) using its associated ± 1 kN Static Load Cell. The input force was applied to an additional element mounted on top of the twister for the new design and on the middle of the selector disk for the old mechanism. With the applied force, the T_u was determined using an unlocking force lever arm (L_u) of 24 mm for the new design (see Fig. 6) and 61 mm for the old design. Each load condition was repeated five times. The F_u was introduced to the mechanism with a velocity of 10 mm/min. The raw data was analyzed with MATLAB R2017a (The MathWorks Inc., Natick, USA) to determine the measured T_u (T_{um}) (see App. 2, 10).

In addition, to obtain a first impression of the relation between the T_{um} and the operation of the mechanism by one (bare) hand, a second subjective experiment was performed by one person (female, 26 years). The purpose of this test was to evaluate until which applied load the mechanism is able to be operated by one (bare) hand. Therefore, the unlocking of the mechanism was first tested with no additional weight, and then it was loaded with 150 g at a load lever arm of 71 mm. After each successful performance (being able to unlock the mechanism with one hand) the weight was increased by about 148 g - 154 g until it was not possible anymore to unlock the mechanism with one (bare) hand. The test set up of the second subjective test is similar to the previous one in Figure 6. Only the unlocking force/torque is not applied by the test machine but directly by the use of one (bare) hand at the twister without an additional handle element.

Furthermore, two theoretical unlocking torques (T_{uts}, T_{ut}) of the new and one (T_{ut}) of the current mechanism were

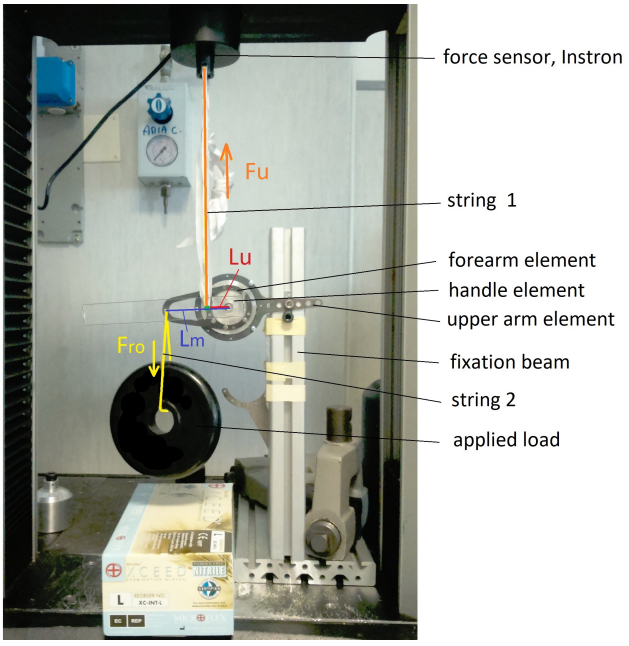

Figure 6: Test set up of the laboratory test. The weight(s) are connected by 'string 2' to the forearm element. The unlocking force (F_u) is applied to the twister by 'string 1' which is attached to an additional handle element, that is mounted on top of the twister. The upper arm element is mounted to a fixation beam. The lever arm of F_u is L_u and the lever arm of the responding output force F_{ro} is L_m.

calculated (see App. 2, 10). The T_{uts} represents the T_u with consideration of the entire selecting mechanism, whereas the T_{ut} only considers the optimal T_u with respect to the ring-roller-input cam formation while neglecting the selecting mechanism.

Besides, the device was weighted with the scale Kern EMS 6K1 (Kern & Sohn GmbH, Balingen, Germany).

Dimension Acceptance

To obtain a first impression of the acceptance of the design, regarding its size (diameter) a questionnaire was completed by eight subjects (five males, three females), whereby the mean circumference ($\pm SD$) of the flexed biceps was 28.14$\pm$2.06 cm (25.7$\pm$0.42 cm for females and 29.6$\pm$0.99 cm for males) and for the forearm 24.99$\pm$2.38 cm (22.47$\pm$1.03 cm for females and 26.5$\pm$2.3 cm for males). Hence, the diameter (circumference/π) of the arm varies from 7.95$\pm$0.76 (forearm) to 8.96$\pm$0.66 cm (biceps). The mean age ($\pm SD$) of all participants was 28.5$\pm$2.55 years. (The subjective evaluation of the weight and appearance were not included in the questionnaire, since only one of the two stages have been manufactured and because the prototype was assembled using few other temporary elements influencing the appearance of the device).

The circumference of the flexed bicep and forearm were measured of the subjects non dominant arm. The non dominant arm was chosen because it represents the more critical condition for the developed elbow prototype, since the non dominant arm has the tendency to be smaller in its circumference. Hence, it is assumed that the size of the device is more critically for a smaller circumference than for a larger one. However, for the bicep and forearm measurements the same positions were used as it was done by Greiner [11] (see App. 2).

After the measurements were performed, the device was put/held on the elbow of the subjects non dominant arm, whereby it was tried that the rotation axis of the device was near the rotation axis of the natural elbow. Afterwards, the subjects had to rate the size on a scale of one to three, with the following interpretations:

- 1 - not acceptable, changes of the design have to be made (decrease diameter by > 10 mm);
- 2 - acceptable, but slight changes are preferred (decrease diameter by 1-10 mm);
- 3 - acceptable, no changes required.

Furthermore, in case the subjects picked (1) or (2) they were asked to specify what and/or how much should be changed of the design.

III. Results

The manufactured design and performed analyses are presented of the new developed mechanism, whereby three versions of the new mechanism are visualized. First, the 3D-printed prototype, which is manufactured to see whether the principle of the mechanism works, but does not represent the final version. Second, the real manufactured prototype is shown. However, since possible problems of the mechanism were analyzed during the manufacturing, further optimizations were made that are not included in the produced prototype. Therefore, the last version contains one additional adjustment and the optimization of the FEM analysis (see App. 8).

Yet, all versions are based on the same principle mechanism, a bi-directional, non-back drivable roller clutch, which uses a crank-slider system to engage the different modes. Furthermore, the design was concentrated on using separated stages. Therefore, the basic structure of the mechanism was kept as it was shown in Figure 3 and 4. In addition, two possible conceptual designs for the second stages were developed.

3D-printed Prototype

The 3D-printed prototype (a) is shown in Figure 7, where the locked (b) and unlocked (c) conditions are shown in detail. Since the twister was able to rotate and to push/pull the selector pins and therefore the rollers in the unlocked/locked condition, the mechanism was considered as functional. Although, the 3D-printed prototype did not include the springs, which are responsible to bring the mechanism back into its locked (default) condition, when rotating the twister in the opposite direction.

The Manufactured Prototype and Its Functioning

The manufactured prototype does not include any adjustments regarding the FEM analysis, since the FEM analysis was performed during the manufacturing process. However, the manufactured first stage consists out of 32 components, without screws and pins, but including a separated input cam (see Fig. 8). Consequently, the input cam can be manufactured out of two materials using steel for the element in contact with the sides of the rollers and the selector pins and aluminum for the rest of the cam to reduce its weight.

In addition, only three springs (taken from pens) are included in the current prototype (as shown in Fig. 8) due to mechanical problems that occurred when using the originally planned six springs. These issues result from the different planes of the selector pins and their interaction with the rollers.

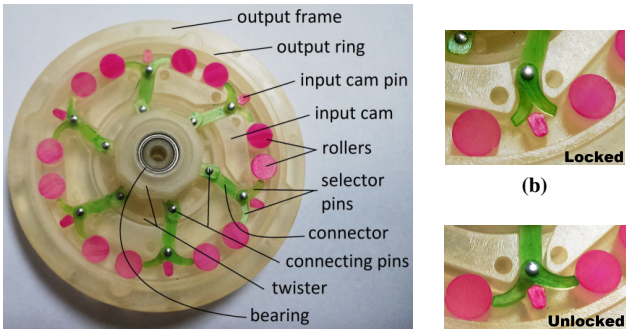

Figure 7: Left (a): 3D printed prototype of the new mechanism in its unlocked condition. Right top (b): Close up of the locked condition, wedged rollers between the input cam and the output ring. Right bottom (c): Close up of the unlocked condition, rollers are unwedged.

Hence, in the new developed design the two selector pins are separated by the connector element. Based on that, the selector pins act on different plane levels and therefore on different heights on the rollers. The bottom selector pins interact at the mid level of the rollers (see Fig. 9) preventing the rollers from being tilted, since no lever arm exists between the unlocking force and the mid point of the rollers. Yet, the upper selector pins act on the top of the rollers, resulting in a lever arm between the mid point of the roller and the selector pin force, that leads to the tilting of the rollers around their mid points (see black point in Fig. 9). When the rollers are tilted, their top and bottom edges get in contact with their bottom and top surrounding surface (bottom of the input cam, bottom of the cover plate, which is mounted on top of the input cam; see red circles in Fig. 9). Consequently, friction is developed hindering the rollers to be pushed away from the output ring. Furthermore, it was visible that few selector pins are moved upwards by the tilted rollers. This would also lead to a friction problem between the upper selector pins and the cover plate. Based on these observations, only three springs are used in the manufactured prototype, where the selector pins are located on the bottom.

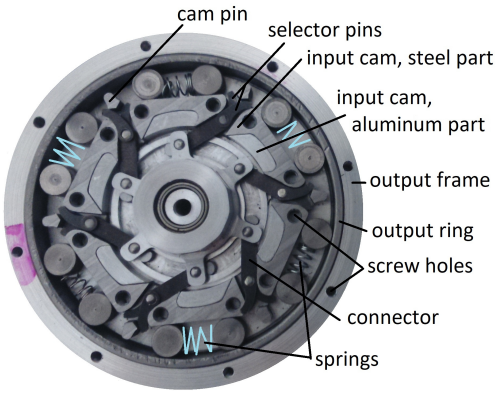

Figure 8: The manufactured prototype of the elbow joint mechanism. The light blue drawn springs indicate the springs that led to mechanical problems and were therefore excluded.

Moreover, due to the manufacturing process of important elements (e.g. selector pins) additional, unwanted material was obtained at some of their edges (see App. 9) influencing the performance. Consequently, temporary elements were included

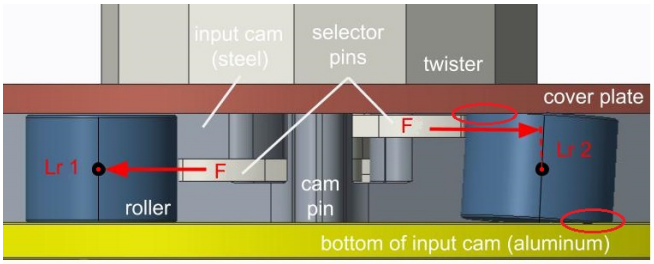

Figure 9: Demonstration of the upper and lower selector pin acting on the rollers. F represents the unlocking force that pushes the rollers away from the output ring. The bottom selector pin acts on the same plane as the rollers mid point, therefore the lever arm (Lr_1) between the mid point and the position of the force application is zero. Yet, this is not the case when the upper selector pin is used resulting in a larger lever arm (Lr_2 = 2.5 mm) leading to a tilted position of the roller. Resulting critical areas are circled.

to compensate for related assembly issues.

The prototype has normally a ROM of 360°, whereby in the current assembly the ROM is limited to about 180° by the use of additional screws, which block the movement of the forearm element. However, before the ROM was limited, it was noticed, that the rotation between the input and output element is not always fluent.

Even though the prototype has minor errors regarding its assembly, due to the previous mentioned issues, it can still be reported that the principle mechanism of the prototype works. Hence, when the twister is rotated to push out the selector pins, the rollers are being unwedged and the input can be rotated separately from the output. Yet, when the twister is rotated in the opposite direction pulling the selector pins back, then the springs push the rollers back into their wedged condition stopping the separate movement of the input and output. However, with the design of the manufactured prototype the twister has to be constantly hold to obtain the free movement. The included springs are responsible for this behavior pushing the selector pins back, without the need of actively rotating the twister in its default position (selector pins are pulled inside, rollers are wedged).

The weight of the new developed mechanism is 178 g for the first stage. Yet, the mechanism should normally consist out of two stages, thus the total weight can be assumed to be at least twice as much compared to the weight of the first stage. However, since the second stage might be slightly larger or contains more elements due to its compliant function, additional ∼50 g are added leading to an assumed final weight of ∼410 g. Hence, the new mechanism is approximately ∼280 g lighter than the old design.

The measured and theoretical T_u for the different loaded cases (1: 450 g, 2: 1000 g, 3: 2000 g, 4: 5000 g) of the new (ND) and old design (OD) are shown and compared in Table I and Figure 10.

As it can be seen from Table I, the ND has a positive input-output ratio, since its measured T_u (T_{um-ND}) is smaller than the resulting output torque (T_{ro}). Instead, the old design (OD) has a negative input-output ratio (T_{um-OD} > T_{ro}). Yet, only when considering the theoretical optimal unlocking torques of the old design (T_{ut-OD}), the previous

Table I: The measured and theoretical unlocking torques T_u of the new (ND) and old (OD) design in relation to the applied loads are shown. T_{ro} = resulting output torque; T_{um} = measured T_u; T_{uts} = theoretical T_u, including the selecting mechanism; T_{ut} = theoretical optimal T_u based on Controzzi et al. [12], neglecting the selecting mechanism; E = Error between T_{uts} and T_{um}. The absolute torque values are shown.

Load Cases	T_{ro} [Nmm]	$T_{um} \pm SD$ [Nmm]	T_{uts} [Nmm]	E [%]	T_{ut} [Nmm]
1-ND	313.4	124.1 ± 35	216.4	42.7	115.5
2-ND	696.5	208.2 ± 53	480.9	56.7	256.6
3-ND	1393.0	471.9 ± 82.1	961.9	50.9	513.2
4-ND	2089.5	606.2 ± 97.6	1442.8	58	769.9
1-OD	313.4	1777.5 ± 51.4	\	\	93.5
2-OD	696.5	2236.9 ± 90.4	\	\	207.7
3-OD	1393.0	2853.4 ± 100.7	\	\	586.9
4-OD	2089.5	3488.9 ± 565.2	\	\	623.1

design obtains a positive input-output ratio as well, which is not true when its T_{um-OD} is taken into account. The T_{um-OD} is larger than T_{ut-OD} by a factor of 10.6±6. Looking at the error between T_{uts-ND} and T_{um-ND}, it can be stated as relatively stable, but as high (with 52±7%). Besides, T_{um-ND} is 2.1±0.3 times smaller than its T_{uts-ND} and the T_{um-ND} is 1.1±0.2 times lower as its T_{ut-ND}.

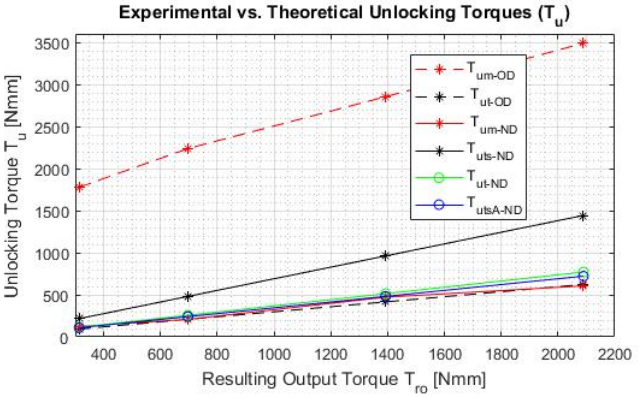

Figure 10: Theoretical (T_{ut}, T_{uts}) and measured unlocking torques (T_{um}) of the new (ND) and old (OD) design. (Note, that the theoretical T_{uts} of the ND takes the selector elements into consideration, instead the T_{ut} takes only the roller, the input cam and the output ring into account. T_{utsA} is the T_{uts} of the adjusted theoretical model.)

In addition, looking at Figure 10, it can be observed that the T_{uts-ND} is higher than the T_{ut-ND} and T_{ut-OD}. However, the T_{um-ND} is lower than its T_{uts-ND} and its T_{ut-ND}. Yet, it is similar to the T_{ut-OD}. Instead, the T_{um-OD} is higher than all T_{ut}s. However, the T_{um}s of both designs have a similar linear behavior as their T_{ut}s. Yet, an adjusted T_{uts-ND} ($T_{utsA-ND}$) is lower than the T_{uts-ND} and T_{ut-ND} and therefore closer to the T_{um-ND}.

Furthermore, after the new mechanism was tested in the fifth repetition of the last condition (3000 g), the mechanism got stuck. Yet, it can be stated that the problem is based on the temporary elements that are included in the assembly. Due to the sudden weight application on the system when the mechanism is being unlocked and the weight falls, the connector elements and the selector pins were partly or completely pushed into a gap or even further into the rotational space of

the twister, where these elements were pinched. Normally a cover plate is directly placed on the input cam hindering the selector pins and the connector elements to move out of their sliding cavity. However, since the fixating pins (connecting the selector pins with the connector elements), the selector pins and the connectors were slightly too high due to additional material on these elements, washers were placed between the input cam and its cover plate to prevent a pressure contact between all these parts. Consequently, a small space between the input cam and the cover plate was created. Hence, when the input cam rotated based on the attached weight, internal forces pushed the connector elements and the selector pins in these gaps or even further as stated above.

Furthermore, the subjective handling test of the device showed that the mechanism can be operated with one bare hand until an applied load of 1150 g. This means that the first and second load cases can be operated by one (bare) hand when the hand is able to provide a torque of about 208.2±53 Nmm. Afterwards, slipping of the hand on the small twister element occurred.

Subjective Evaluation of the Size

The evaluation of the size showed that 50% of the subjects (one female, three male) accepted the size of the new device without suggesting any changes. Thus, two subjects (25%, both female) rated the size as acceptable, but would prefer a diameter reduction by about 10 mm. However, two male subjects (25%) stated that they would prefer a diameter reduction of about 20 mm, yet, only if mechanically possible, otherwise they stated to accept the current design.

The acceptance of the new developed prototype regarding its size (outer diameter) in relation to the flexed forearm and biceps diameter can be seen in Figure 11.

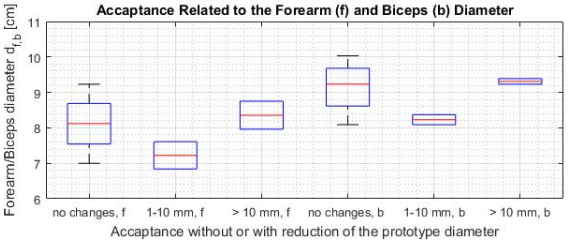

Figure 11: Relation between the acceptance of the prototype diameter and the flexed forearm/biceps diameter of all subjects.

As seen in Figure 11, when neglecting the category 'reduce by > 10 mm', a decreased diameter of the forearm and biceps leads to an increased wish to reduce the diameter of the prototype. However, when including the last category, this is not true, since a greater change of the prototype was preferred by subjects with larger forearm and biceps diameters.

However, in general a positive tendency regarding the acceptance of the new developed prototype was stated by the subjects.

Final Optimized Design

The finalized design of the first stage is visualized in Figure 12. Its main structure is still the same as it is shown in Figure 4, now only the input cam is divided into two parts as it is shown in Figure 8. However, due to the FEM analysis the design of the input cam and the selector pins changed since these parts are affected by the highest stresses. The changes (see Fig. 12) were made in order to allow that the mechanism can be loaded with nearly 50 kg. Besides, the twister and the inner input cam were modified to prevent the constant hold of the twister when the free movement is desired. Consequently, the twister obtains holes for spring plungers and the input cam includes corresponding pits for the rotational end positions of the twister. This prevents that the springs push the selector pins back into their default position inside the input cam.

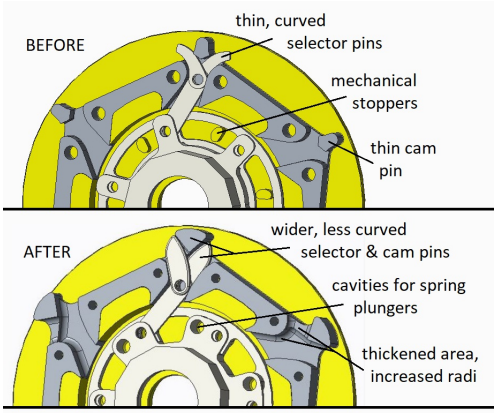

Figure 12: Visualization of the performed adjustments resulting in the final design. Top: CAD that has been manufactured and tested. Bottom: Adjusted model after the FEM analysis including an additional modifications with spring plungers.

The outer dimensions of the first stage are the following: The diameter is 78 mm and the depth from the bottom of the output frame to its cover plate is 12.6 mm and 16 mm when measured from the bottom to the top of the twister. (The cover plate is mounted on top of the input cam.)

Compliant Module: Two different conceptual designs for the corresponding second stage (compliant mode) were developed. The first version is based on the compliant mode of the previous prototype and can be seen in Figure 13. The second version is based on a new concept to include the compliant mode and can be seen in Figure 14.

The first version of the compliant mode uses the spring of the old design, which results in a larger depth of this second stage by 11.4 mm, while the diameter remains the same as the first stage. Besides, the compliant movement range stays the same compared to the old design with about 30°. The first conceptual version of the second stage consists basically out of the first stage of the new design. Yet, the output ring and the output frame had to be adjusted to allow the inclusion of the elements of the old design, which are needed for the compliant stage (see Fig. 13). Furthermore, the bottom of the frame includes now two radial aligned cavities (as in the previous design), which are responsible for the maximal limit of the compliant movement range. The output ring was extended in its depth, yet, not entirely, but using a specific pattern as indicated in Figure 13. This pattern allows a ridged connection to a counter element while blocking its rotational movement. Besides, the counter element provides two connection points for screws/pins, which will be in contact with the inner side of the spring. The translational movement of the counter element on the rotation axis is blocked due to a pressure connection of the surrounding elements. Moreover, the output ring and the output frame are not in contact anymore. Therefore, when the rollers are wedged between the input cam and the output ring,

the output ring with the connected counter elements and its screws rotate against the spring, which is fixated to the output frame by additional screws. However, the screws/pins of the counter element extend to the radial cavities at the bottom of the output frame. As a result, the movement range is firstly based on the springs stiffness and secondly it is limited by the cavities of the output frame.

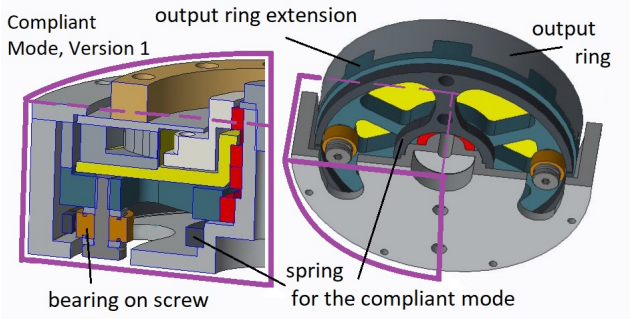

Figure 13: Compliant mode, first version, using the spring of the previous prototype.

The second conceptual version of the compliant stage uses the same outer dimensions as the first stage. Yet, only the geometry of the output frame and the output ring are slightly changed. Now, the output frame includes equally distributed spring cavities, which are mostly open to the side of the output ring as shown in Figure 14. Only towards the ends of the cavities a small wall exists towards the output ring. This wall is supposed to keep the springs centered in the output frame. Instead, the output ring includes equally distributed extrusions, which reach into the spring cavities. These extrusions obtain a hole for a pin, which should be used to center the springs on the sides of the output ring extrusions. Thus, when the rollers are wedged, the output ring is in direct contact with the springs for the compliant mode, which are placed on both sides of the output extrusions.

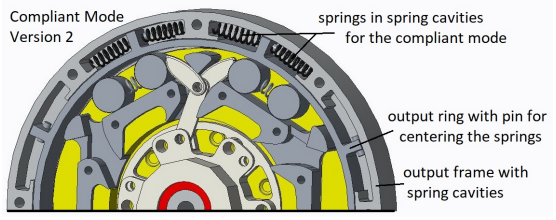

Figure 14: Compliant mode, second version, using a new concept, that includes the compliant springs within the output frame.

IV. Discussion

The Prototype

A separated stage mechanism was chosen for the final design, since it allows a better balanced weight distribution over the elbow joint. Besides, it allows patients to only use one stage if the design with its two stages will be to heavy for them. Yet, based on time constrictions only a prototype of the first stage was developed. However, two conceptual designs were developed, which have to be finalized, manufactured and tested. Yet, the design can still be considered as approved regarding the design criteria with respect to the required number of stages.

Furthermore, it can be assumed that a single stage can be easily automated, since the switching between the modes of one stage is done by one rotation. However, to automate the design with two stages, the automating process can be more complex, especially when used for an orthosis with the separated stage design. In that case, it can be considered that two motors will be needed to activate each stage, since the stages are separated by the patients arm. In that case the design would be outperformed by the old mechanism. Besides, the weight as well as the dimensions of the entire mechanism would increase compared to the design version, where both stages are placed on one side. Yet, when using the separated design for an prosthesis, the motor could be placed in between the stages making it possible to only use one motor as it is desired.

Moreover, the ROM of the new mechanism fulfills its design criteria as well. As long as the ROM of the design is not further limited it has a range of 360°, since the mechanism of the new developed design is still based on the previous clutch design. However, the rotational movement between the input and output is not always fluent. Yet this is mainly a problem of the unwanted, additional material, which is present on the upper arm and selector elements, interacting with the input elements. As a consequence, friction is developed, leading at specific spots to a higher resistance against the rotational movement.

The manufactured prototype uses in its assembly springs from pens. Therefore, the spring stiffness can be considered as not optimal for the design influencing the performance of the mechanism. Yet, not only the stiffness influences the performance, also the number of springs used. In the assembled prototype only three springs are used due to mechanical problems of the mechanism when six springs were included. As a consequence, only six of the twelve rollers are in the wedged position when the mechanism is put in its locked condition. Yet, without the missing springs, the other rollers cannot be moved back into their wedged position. (Although, some rollers may get into the locked position by coincidence due to the gravity effect depending on the position and orientation of the mechanism in 3D-space). The mechanical problem that occurs when six springs are used is based on the selector pins that are on the top of the connector element instead of on its bottom. Consequently, the upper selector pins act on the top of the rollers, leading to a tilt of the rollers. To solve this problem the order of the selector pins with respect to the connector elements can be changed. For instance, the connector elements could be moved to the top. As a result, the previous upper selector pins interact with the rollers on a lower level, but still not on the mid points of the rollers eliminating the lever arm not completely. Yet, the lever arms between the connector elements and the bottom selector pins increase again by ∼2.5 mm. In that case, similar side effects can be created, which were obtained in the previous design when referring to the lever arms between the selector disk and its selector pins (their basements, see Fig. 1). Another option would be to decrease the basement of the input cam. Yet, it can be assumed that this solution would increase the stresses at the rounding/curve between the cam pin and its basement, because less material would be present to compensate for the forces

pushing against the cam pin. Therefore, this option is not preferred as well. However, another option is the removal of the two selector pins and the cam pin and to use again only one selector pin. With the removal of the cam pin, the determined critical stress areas will disappear and the more complex (FEM adjusted) design will not be necessary anymore. Yet, the design of the input cam would need to be adjusted to the usage of only one selector pin. However, it can be assumed, that a new resulting design of the input cam and the selector pin will be less complex.

Mechanical Tests

As it was stated previously, the principal of engaging/disengaging the first stage of the new developed mechanism is functioning. Therefore, the first stage design can be considered as successful. Yet, the second stage has still to be manufactured to be able to judge the entire mechanism with its two stages. However, back to the manufactured first stage, minor errors still exist that need to be solved for the next prototype. As stated previously, the twister has to be constantly hold to be able to move the forearm into the desired position. Therefore, the final design was adjusted to use spring plungers allowing to keep each selecting position without the need of holding the twister constantly. This modification allows an improved handling of the device by one hand. Furthermore, the spring stiffness can be lowered (see App. 2). Besides, if spring plungers are used, they will get locked in small pits that are located at the rotating position for the locked and unlocked condition of the mechanism. As a result, the springs acting on the rollers will not be able to move the selector pins back into their default positions. This is due to the twister, which will be locked and only moves when it is actively rotated to force the included spring plungers out of their pits.

Moreover, the weight of the new mechanism (two stages) is assumed to be ∼410 g (doubling the weight of the first stage (178 g) and adding ∼50 g for additional elements that may be needed for the compliant stage). As a result, the ND fulfills the design criteria that the device has to be lighter by 200 g compared to the weight of the OD. Indeed, the new developed prototype is lighter by ∼280 g (and by ∼510 g when only the first stage is considered) even though it contains more elements.

In addition, the size of the mechanism, when using the first stage, can be rated as acceptable regarding the selected design criteria. The diameter (78 mm) is 7 mm smaller than the previous design and the depth is reduced by 21 mm (measuring the first stage from the bottom of the output frame to the top if the twister). However, these dimensions only include the first stage and therefore not the entire joint module. Yet, when taking the dimensions of the conceptual ideas into account, the dimensions are not necessarily acceptable anymore. When using the first conceptual version for the compliant stage, then the diameter is still the same, but the total depth increases by 6.4 mm to 43.4 mm (measuring each stage from the bottom of the output frame to the top of the twister). Yet, when only measuring the depth from the bottom to the top of the cover plate, then a total depth of 36.6 mm is reached, which is acceptable regarding the design criteria. However, when the second conceptual version of the compliant stage is considered, the total depth decreases by 5 mm to 32 mm, since the second stage is assumed to have the same dimensions as the first stage. In any case, the total depth is split into two elements. Based on that, the stages will be on opposite sides around the elbow instead of being placed on the same side. Although, even when the total depth is slightly larger than 37 mm, the depth of the current design, can still seem to be smaller due to an optical illusion based on the separated design, making the appearance less bulky compared to the previous design.

Looking at the mechanical and objective test it can be seen, that the T_{um-ND}s are lower than the T_{ro}s. However, the T_{um-ND}s were measured with a larger L_u (by 10 mm) then it is used by the twister itself. As a consequence, the computed F_u only represents the ND when an additional handle is added to the twister, otherwise the T_{um-ND}s are expected to be higher. Yet, the additional subjective test indicates that the operation of the system with one (bare) hand can be performed for at least the first and second load case. Afterwards, the grip of the twister was lost (due to its shape and surface condition) and the mechanism could not be operated anymore. However, since it was a subjective evaluation by one person the maximal weight to be able to operate the system by one hand might be slightly lower or higher than 1150 g, depending on the grip strength of the individual. Yet, to operate the mechanism when higher loads are applied, a design change of the twister is suggested. This can be done by increasing the grip area (changing the shape) as well as the lever arm (increasing dimensions) of the introduced torque, which will improve the grip and therefore the performance. Another option is to design an additional handle with the suggested adjustments and to place it on the current twister.

Now, since it is suggested to change the design of the twister, increasing its L_u, the previous findings can be considered as accurate and indicate a successful design regarding its input (unlocking)-output torque relation. Furthermore, as it was stated, the errors between T_{uts-ND} and T_{um-ND} are relatively constant (52±7%). The constant values indicate that the model is functioning. Nevertheless, since the values are quiet high it implies that the used theoretical model is not accurate yet. Although, it was noticed that the difference between T_{uts-ND} and T_{um-ND} is by a factor of 2,1±0.3. This can be explained with the fact that the mechanism uses two selector pins instead of one, which was not included in the theoretical model. Adjusting the T_{uts-ND} leads to improved result with reduced errors with respect to the T_{um-ND} for each load case 1-5: -14.7%, 13.4%, 1.9%, 16%. Yet, the remaining errors can be based on the force angles and lever arms within the selecting mechanism, since an exact determination was not possible. Besides, the theoretical model was created for the left selector pin assuming an symmetric behavior between the left and right selector pin.

In addition, the model by Controzzi et al. [12] is used to compute the radial roller force, which is again used to calculate the T_{uts-ND}. Yet the model assumes a symmetrical load spread of F_u across the rollers. However, it can be assumed that this is not completely true and leads therefore to an error. Hence, in the new mechanism the selector pins approach the rollers from the bottom, pushing them more to an open area based on the radius of the output ring. Since this behavior is

not considered in the model, it can be a reason for the higher obtained $T_{uts-ND}s$ compared to the $T_{um-ND}s$.

Instead, in the previous design, the selector pins approached the rollers from the top, pushing them not just aside, but also against the surface of the input cam creating additional friction. This can be one factor that contributes to the higher obtained $T_{um-OD}s$ compared to the $T_{ut-OD}s$. Additionally, the selecting mechanism with its generated friction and force transmissions are not taken into account in the T_{ut-OD}, leading to the large difference (by a factor of 10.6$\pm$6) between T_{um-OD} and T_{ut-OD}. Furthermore, the handle where F_u was applied used a L_u that was 33.5 mm longer than the original used handle for the OD. However, this would indicate an even higher T_{um-OD} as measured. Yet, the handle that was used for the test setup introduced a new lever arm to the design, due to the space of 35.5 mm between the selector disc and the handle. As a consequence, the element connecting the handle with the disc was slightly tilted. This could also be an influence on the determined T_{um-OD}. Another assumption for the higher achieved torques can be based on the fact, that the mechanism always engages/disengages two stages at the same time, whereby the new developed design engages/disengages the stages individually. However, the differences between $T_{um-OD}s$ and the $T_{ut-OD}s$ are not only high but also not consistent, but exponentially decreasing with increasing weight. This, indicates that with an increased weight the model becomes more accurate. Yet, since the selecting mechanism of the OD is not included in its T_{ut-OD}, the model needs to be adjusted and cannot be considered as accurate for the entire model. Although, it is assumed that the inclusion of the selecting process in the model (as it is done for the new mechanism) would reduce and stabilize the differences.

Yet, comparing the measured input torques of both designs, it can be seen that the $T_{um-ND}s$ are 9.2$\pm$4.1 times smaller compared to the $T_{um-OD}s$. Based on this and the positive input-output ratio of the ND, where the T_{um-ND} is smaller by a factor of 3.1$\pm$0.4, it can be stated that the new mechanism has the potential to outperform the previous design, due to the results of the first stage. Yet, the second stage needs to be tested in combination with the first stage to prove that the ND surpasses the OD.

Subjective Evaluation of the Size

In general, all subjects would have accepted the size (diameter) of the devise if they would have to wear it. However, two subject selected the 'not acceptable' section, because they prefer a reduction of the diameter by 20 mm. Yet, they also stated they prefer the reduction only if it is mechanically possible to do so, otherwise they accept the design. Furthermore, these two participants belong to the subjects with larger arm circumferences. Therefore, their statement was surprising, since other subjects with smaller arm circumferences, accepted the design without any complains or suggestions. However, since all subjects are working in the Biomedical Engineering field, critical evaluations can be expected, which can be assumed happened in the case where the two subjects selected the 'not acceptable' category. Hence, for further questionnaires and subjective evaluations a random selection of subjects with different backgrounds should be made, to obtain a better representation of the entire population. Besides, a higher number of subjects should be chosen.

Compliant Concepts

The two developed concepts for the compliant stage have both advantages and disadvantages. When looking at the first version its major draw back is the increased depth and with that an increased weight. Yet, it can warrant the compliant ROM of the previous design, since the same mechanism is used.
The major advantage of the second version is, that it has the same dimensions as the first stage, making the total device (with two stages) more compact and light. However, the compliant ROM is limited to the design of the output frame (compliant springs are located between mandatory screw holes of the output frame) and does not necessarily allow the same compliant ROM as the previous design. Furthermore, depending on future stress analysis, the dimensions (diameter) of the output frame might have to be increased, depending on the spring dimensions and the necessary wall thickness of the output frame to compensate occurring stresses.

Design Simplicity and Number of Components

The new developed mechanism has more components than the previous design, since the selector disk is exchanged by the twister and the connector element and because two selector pins are now used for each roller pair instead of one. For instance, the first stage consists out of 32 components (neglecting pins and screws) and it can be assumed that the entire design with two stages will have at least 63 elements when doubling the first stage. Yet, at least 28 more components will be used in the entire ND compared to the OD and as desired from the design criteria. Furthermore, the design is in general based on a simple concept, but due to the FEM analysis the design, especially the outer (steel) input cam changed to be more complicated to allow the application of higher loads. However, the design simplicity and number of components has not the highest importance as long as the more important criteria (e.g. weight, dimensions) obtain better results (outperforming the OD). Since this is the case, the complexity of the design and number of components can be neglected or be considered as acceptable.

Future Design Suggestion

Many suggestions regarding design improvements were made previously. Therefore, an improved design concept was created to visualize these suggested adjustments and to give an idea on which aspects should be focused for the next manufactured prototype. The suggestions can be seen in Figure 15.

As demonstrated in Figure 15, only one selector pin is used for one roller pair. The selector pins interact now with the entire surface of the rollers, preventing that the rollers are being tilted. Yet, the shape of the selector pins can be modified to allow to unwedge the rollers by pulling or pushing the selector pins. Additionally, the connector element, connects with the selector pin in its middle, warranting that the force transmission takes place in the same plane between these two parts preventing lever arms for unwanted internal torques. Furthermore, the selector pin is now centered by using two fixation pins which slides in a given cavity, with that a simultaneous engaging/disengaging of the rollers is guaranteed. The outer part of the input cam (steel) has now thinner walls decreasing the weight of the design even further.

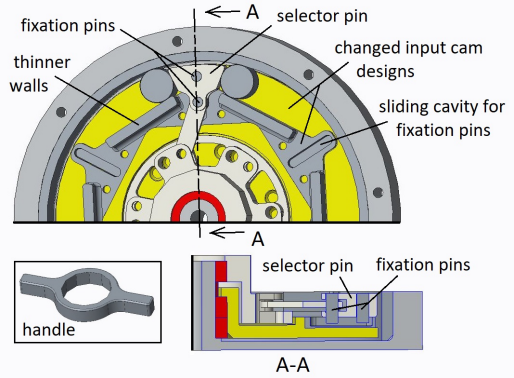

Figure 15: Adjustment suggestions of the new developed mechanism for the next prototype. In this example the selector pin unwedges the rollers when it is pulled into the input cam.

Besides, an additional element is introduced, the handle, which can be placed over the twister improving the operation of the mechanism by increasing the lever arm and the grip area.

V. Conclusion

A new design of the previous bidirectional, non-backdrivable roller clutch was developed, outperforming the current design in several categories when considering the second conceptual design as accurate. The new design has a decreased diameter and depth by 7 mm and 5 mm and a reduced weight by $\sim$280 g, while having the same amount of modalities and the same range of motion. Furthermore, its measured unlocking torque is lower than the resulting output torque by a factor of 3.1 ± 0.4. Besides, the measured unlocking torque of the new design is lower than the unlocking torque of the current design by a factor of 9.2 ± 4.1.

However, the new manufactured prototype does not include the entire design yet (two stages), but only one stage. Therefore, the concept of the second stage has sill to be finalized, manufactured and tested to be able to judge the functioning of the complete mechanism. Moreover, the next prototype should adjust its dimensions to warrant a smooth performance of the mechanism without being negatively influenced by a manufacturing process, otherwise the manufacturing process should be changed. It is also recommended to adjust the design to the suggested modification to guarantee the best performance for the next prototype.

When these changes will be made in a future prototype and the laboratory performance is judged as acceptable, especially when the entire design of two stages outperforms the previous design, then the developed artificial joint mechanism can be implemented in an orthosis or prosthesis design. Afterwards, clinical studies can be performed to judge the mechanism in daily life performances and to compare its results with other elbow orthoses and/or prostheses.

VI. Acknowledgments

This project was founded by the Biorobotics Institute of the Scuola Superiore Sant'Anna in Pisa (Italy). We thank Dr. Lorenzo Bassi Luciani and Dr. Marco Controzzi providing assistance of the methodology and the performance of the mechanical tests. Yet, they may not agree with all resulting interpretations of this paper.

References

[1] Kathleen Diane Pickrell. Miller-keane encyclopedia and dictionary of medicine, nursing, and allied health. *Hospitals & Health Networks*, 77(8):70, 2003.

[2] Modular upper limb. NEBIAS project founded by European Commission under FET Proactive: Evolving living technologies (EVLIT), project number: 611687, 2013-2016.

[3] A Ramírez-García, C Toledo, L Leija, and R Muñoz. Status of elbow myoelectric prosthesis: Cinvestav-ipn prosthesis. *Revista Mexicana de Ingeniería Biomédica*, 30(1):66–73, 2009.

[4] Innes Vanderniepen, Ronald Van Ham, Michael Van Damme, and Dirk Lefeber. Design of a powered elbow orthosis for orthopaedic rehabilitation using compliant actuation. In *2008 2nd IEEE RAS&EMBS International Conference on Biomedical Robotics and Biomechatronics*, 2008.

[5] Boris P Bonutti, Peter M Bonutti, Kevin R Ruholl, and Glen A Phillips. Elbow orthosis, November 26 2013. US Patent 8,591,443 B2.

[6] James S Sulzer, Michael A Peshkin, and James L Patton. Marionet: an exotendon-driven rotary series elastic actuator for exerting joint torque. In *9th International Conference on Rehabilitation Robotics, 2005. ICORR 2005.*, pages 103–108. IEEE, 2005.

[7] Daniel A Bennett, Jason Mitchell, and Michael Goldfarb. Design and characterization of a powered elbow prosthesis. In *Engineering in Medicine and Biology Society (EMBC), 2015 37th Annual International Conference of the IEEE*, pages 2458–2461. IEEE, 2015.

[8] Subrata Kumar Kundu and Kazuo Kiguchi. Development of a 5 dof prosthetic arm for above elbow amputees. In *Mechatronics and Automation, 2008. ICMA 2008. IEEE International Conference on*, pages 207–212. IEEE, 2008.

[9] Stefan Fornalski, Ranjan Gupta, and Thay Q Lee. Anatomy and biomechanics of the elbow joint. *Techniques in hand & upper extremity surgery*, 7(4):168–178, 2003.

[10] Jonathon W Sensinger and R Fff Weir. Design and analysis of a non-backdrivable series elastic actuator. In *Rehabilitation Robotics, 2005. ICORR 2005. 9th International Conference on*, pages 390–393. IEEE, 2005.

[11] Thomas M Greiner. Hand anthropometry of us army personnel. Technical report, Army Natick Research Development and Engineering Center MA, 1991.

[12] Marco Controzzi, Lorenzo Bassi Luciani, and Federico Montagnani. Unified approach to bi-directional non-back drivable roller clutch design. *Mechanism and Machine Theory*, 116:433–450, 2017.

References

[1] Stefan Fornalski, Ranjan Gupta, and Thay Q Lee. Anatomy and biomechanics of the elbow joint. *Techniques in hand & upper extremity surgery*, 7(4):168–178, 2003.

[2] Innes Vanderniepen, Ronald Van Ham, Michael Van Damme, and Dirk Lefeber. Design of a powered elbow orthosis for orthopaedic rehabilitation using compliant actuation. In *2008 2nd IEEE RAS & EMBS International Conference on Biomedical Robotics and Biomechatronics*, pages 801–806. IEEE, 2008.

[3] Vladimir M Zatsiorsky. Kinematics of human motion, human kinetics. *Urbana Champaign*, 1998.

[4] Elaine Nicpon Marieb and Katja Hoehn. *Human anatomy & physiology*. Pearson Education, 2007.

[5] Subrata Kumar Kundu and Kazuo Kiguchi. Development of a 5 dof prosthetic arm for above elbow amputees. In *Mechatronics and Automation, 2008. ICMA 2008. IEEE International Conference on*, pages 207–212. IEEE, 2008.

[6] Daniel A Bennett, Jason Mitchell, and Michael Goldfarb. Design and characterization of a powered elbow prosthesis. In *Engineering in Medicine and Biology Society (EMBC), 2015 37th Annual International Conference of the IEEE*, pages 2458–2461. IEEE, 2015.

[7] P. H. Robinson Douglas and A. S. Jain. *Synopsis of Causation: Upper Limb Amputation*. Veterans UK and Ministry of Defence, 2008.

[8] Kathleen Diane Pickrell. Miller-keane encyclopedia and dictionary of medicine, nursing, and allied health. *Hospitals & Health Networks*, 77(8):70, 2003.

[9] Grant Cooper. *Essential physical medicine and rehabilitation*. Springer Science & Business Media, 2007.

[10] AZ Escudero, Ja Alvarez, and L Leija. Development of a parallel myoelectric prosthesis for above elbow replacement. In *Engineering in Medicine and Biology, 2002. 24th Annual Conference and the Annual Fall Meeting of the Biomedical Engineering Society EMBS/BMES Conference, 2002. Proceedings of the Second Joint*, volume 3, pages 2404–2405. IEEE, 2002.

[11] Tommaso Lenzi, James Lipsey, and Jonathon W Sensinger. The ric arm—a small anthropomorphic transhumeral prosthesis. *IEEE/ASME Transactions on Mechatronics*, 21(6):2660–2671, 2016.

[12] C Pylatiuk, A Kargov, I Gaiser, T Werner, S Schulz, and G Bretthauer. Design of a flexible fluidic actuation system for a hybrid elbow orthosis. In *Rehabilitation Robotics, 2009. ICORR 2009. IEEE International Conference on*, pages 167–171. IEEE, 2009.

[13] Modular upper limb. NEBIAS project founded by European Commission under FET Proactive: Evolving living technologies (EVLIT), project number: 611687, 2013-2016.

[14] Boris P Bonutti, Peter M Bonutti, Kevin R Ruholl, and Glen A Phillips. Elbow orthosis, November 26 2013. US Patent 8,591,443 B2.

[15] James S Sulzer, Michael A Peshkin, and James L Patton. Marionet: an exotendon-driven rotary series elastic actuator for exerting joint torque. In *9th International Conference on Rehabilitation Robotics, 2005. ICORR 2005.*, pages 103–108. IEEE, 2005.

[16] Thomas M Greiner. Hand anthropometry of us army personnel. Technical report, Army Natick Research Development and Engineering Center MA, 1991.

[17] Marco Controzzi, Lorenzo Bassi Luciani, and Federico Montagnani. Unified approach to bi-directional non-back drivable roller clutch design. *Mechanism and Machine Theory*, 116:433–450, 2017.

[18] Sébastien Krut and Vincent Begoc. A simple design rule for 1st order form-closure of underactuated hands. In *UG: Underactuated Grasping*, pages 1–7, 2010.

[19] Richard F Weir and Jonathon W Sensinger. Design of artificial arms and hands for prosthetic applications, 2003.

[20] Michiel Plooij, Glenn Mathijssen, Pierre Cherelle, Dirk Lefeber, and Bram Vanderborght. Lock your robot: A review of locking devices in robotics. *IEEE Robotics & Automation Magazine*, 22(1):106–117, 2015.

[21] S.J. Kochan. Non-backdrivable gear system, August 18 2011. URL `https://www.google.it/patents/US20110201473`. US Patent App. 13/030,068.

[22] Robert C Juvinall and Kurt M Marshek. *Fundamentals of machine component design*, volume 83. John Wiley & Sons New York, 2006.

[23] Arthur Peter Boresi, Richard Joseph Schmidt, and Omar Marion Sidebottom. *Advanced mechanics of materials*, volume 6. Wiley New York, 1993.

[24] Metallurgica Veneta. Material information brochure: 39nicrmo3. URL `http://metallurgicaveneta.it/pdf_eng/acciai-al-carbonio-da-bonifica/39NiCrMo3.pdf`.

[25] Marco Controzzi. Ingegneria della riabilitazione - approccio alla verifica dei cuscinetti radenti - durabilità dei contatti (usura e fatica superficiale). University Lecture, 2016.

Appendix

1 Current Design by the Biorobotics Institute

The developed elbow module can either be used for prostheses or orthoses. It is a bi-directional, non-backdrivable clutch that offers three modes. These modes cover a locking mode, a free movement mode and a compliant mode, whereby the latter mode is used to allow a more natural behavior of the device. For instance, the compliant mode copies the natural free swing of the arm when walking or it allows to absorb shocks preventing/reducing the risk of injuries.
An overview of the elbow module and its mechanism can be seen in the following Figure 2.

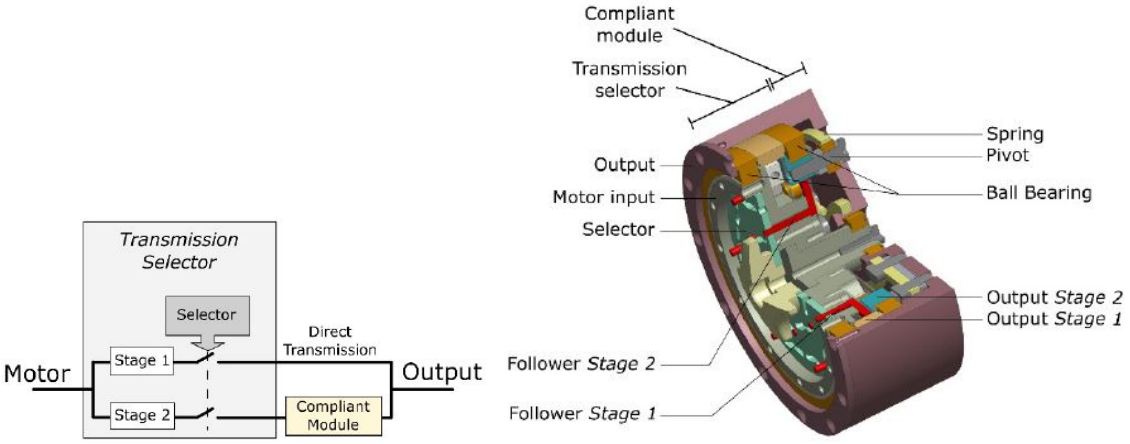

Figure 2: Overview of the current prototype. Left: Block scheme of the working principle. Right: Computer aided design of the current mechanism. The transmission consists out of two stages, which are either engaged or disengaged depending on the position of the selector element. [13]

The module consists out of two stages, which are responsible to obtain the three available modes. Engaging the first stage leads to a direct transmission between the input and output; the mechanism gets locked and the elbow gets fixated in the desired position. When the first and second stages are both disengaged, then the second mode (free movement) is obtained. As a result, the input and output are not fixated to each other and therefore the forearm can be moved in any desired position. Now, when engaging the second stage (while disengaging the first stage), the transmission between the input and output includes a compliant module (a spring) to obtain the previous mentioned third mode (compliant mode). The selecting mechanism, which is shown in Figure 3, is based on a roller-cam clutch. The (input) cam includes selector pins, which are either pushed out of the cam or pulled back into the input cam. To engage the first or second stage, the pins of that stage have to be pushed out, resulting in a fixation between the output and input element. The fixation occurs due to the springs, which are located between the rollers, to push the rollers aside. This leads to the contact between the rollers, the input cam and the output ring. Consequently, the input cam cannot be rotated anymore since the rollers are wedged between the input and output elements. To unlock the system and

with that to unwedge the rollers, the selector pins are pulled back into the cam. The rollers are moved away from the output ring by the selector pins since they push the rollers on the same side towards each other. Based on that condition, the rotation of the input cam is again possible. The second stage is based on the same mechanism of the first stage, the only difference is, that the input interacts with a different output element. This output element is connected to two pivots, which interact with the inner surface of a spring allowing the compliant behavior. Thus, when the input is fixated to this output element a rotation is still possible. However, this rotation is limited since in acts on the spring forcing a certain elastic resistance against the initiated rotation. As a result, the compliant model allows a movement of about 30°. [13]

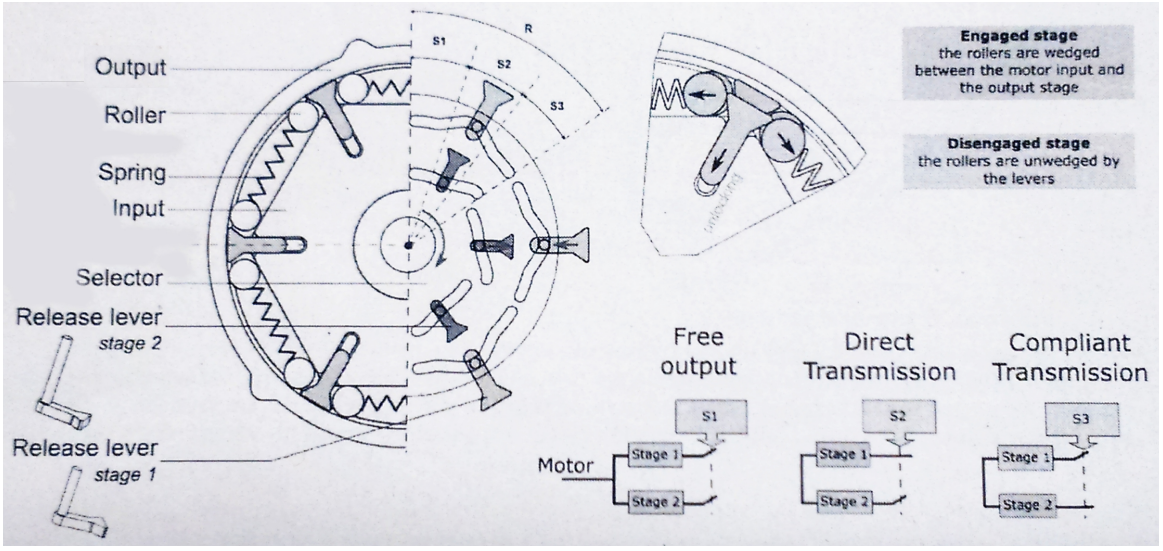

Figure 3: Overview of the mechanism of the roller based clutch with its release levers (selector pins) and the selector (disk). Depending on how far or to which position (s1, s2, s3) the selector disk is rotated, the different modes are selected due to the cavities in the selector disk. [13].

To select the different modes, an additional disk is mounted on top of the stages. This selector disk, as shown in Figure 3, has cavities with a specific pattern for each selector pin (see Fig. 3) of each stage. Now, when rotating the disk the cavities are responsible to move the selector pins in the correct position for the desired mode.

2 Expanded Method

In the following, one design criteria will be shown more detailed, the computation of the experimental and theoretical unlocking torque will be explained, characteristics for the included springs will be mentioned and details about the subjective evaluations will be given. Yet, the method of the FEM analysis will be explained in a different section together with its results and discussion (see App. 8).

Design Criteria - Size

The size of the device should be smaller than or at least equal to the dimensions of the current design. Hence, the diameter (d) should be smaller or equal to 85 mm and the depth should be below or equal to 37 mm. However, when using the 50^{th} percentiles, the circumference of a female forearm is around 25.3 cm ($d_1 = 81$ mm) and for a male around 30.3 cm ($d_2 = 97$ mm). The 50^{th} percentile of the circumference of a flexed biceps is for a female 28 cm ($d_3 = 90$ mm) and for a man around 33.7 cm ($d_4 = 108$ mm) [16]. Therefore, the elbow module can be in the range from 81 mm to 108 mm, whereby it is preferred to be closer to the lower value (d_1), or even to be below d_1, to keep the weight low and because the human elbow has not exactly a circular shape. Thus, it is always easier to add a cover to the mechanism to increase the arm circumference for adjusting its appearance to the patients anthropometry (especially when the new mechanism is used for prosthetics) than to decrease its size. Besides, using a lower value than 81 mm might allow that the design could be used for children as well.

The Experimental Unlocking Torques

To compute the experimental/measured unlocking torque T_{um}, the obtained raw data from the experiment was analyzed with MATLAB R2017a (The MathWorks Inc., Natick, USA), where the unlocking force of each repetition of one weight was determined by a sudden (positive or negative) jump in the recorded force data (maximal difference between two data points). Yet, the data point before the maximum difference occurred was used as the unlocking force F_u (as demonstrated in Fig. 4), However, in some cases the used data point was individually adjusted, when the graph pattern slightly varied.

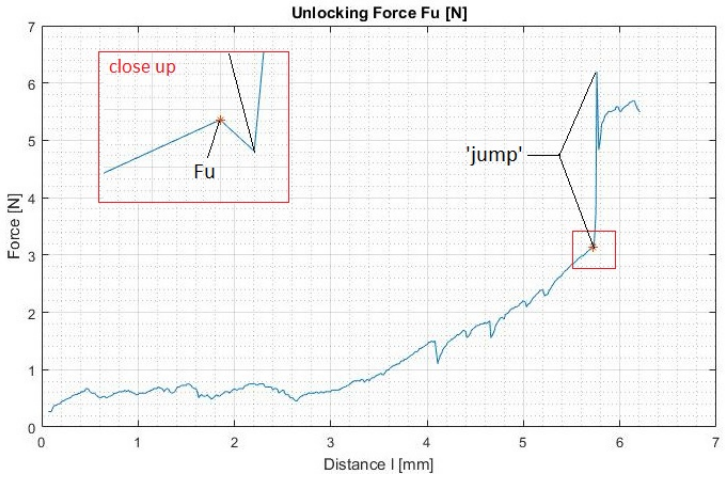

Figure 4: Example of the measurement output and the determination of the unlocking force F_u (indicated by the red point). The graph represents the output of a test trial when 150 g were used.

After all measurements were finished, the determined unlocking forces of the repetitions were averaged for each load case and transferred into the unlocking torque by multiplying the F_u with the corresponding lever arm (L_u) for the new and old mechanism. The applied

load (m) was transferred into the resulting output torque (T_{ro}) by using the equation $T_{ro} = m * g * L_m$, whereby $g = 9.81\ m/s^2$.

The Theoretical Unlocking Torques

The theoretical optimal unlocking torque T_{ut} was determined by using the equations of the paper by Controzzi et al. [17], that were implemented in an Excel table (Excel, Microsoft, Redmond, USA).

Yet, the optimal unlocking torque only includes the force and friction relation between the rollers, the input cam and the output ring and neglects the selecting mechanism with its force transmission and friction.
Consequently, a second theoretical unlocking torque (T_{uts}) was calculated for the new mechanism including the selector elements. The calculations can be seen in the MATLAB code (see App. 10). Yet, the related Free Body Diagram that was used for the calculations can be seen in the following Figure 5. Besides, the radial-roller force was used as the output force that had to be overcome by the unlocking torque. The radial roller force was determined by the equations of the paper by Controzzi et al. [17].

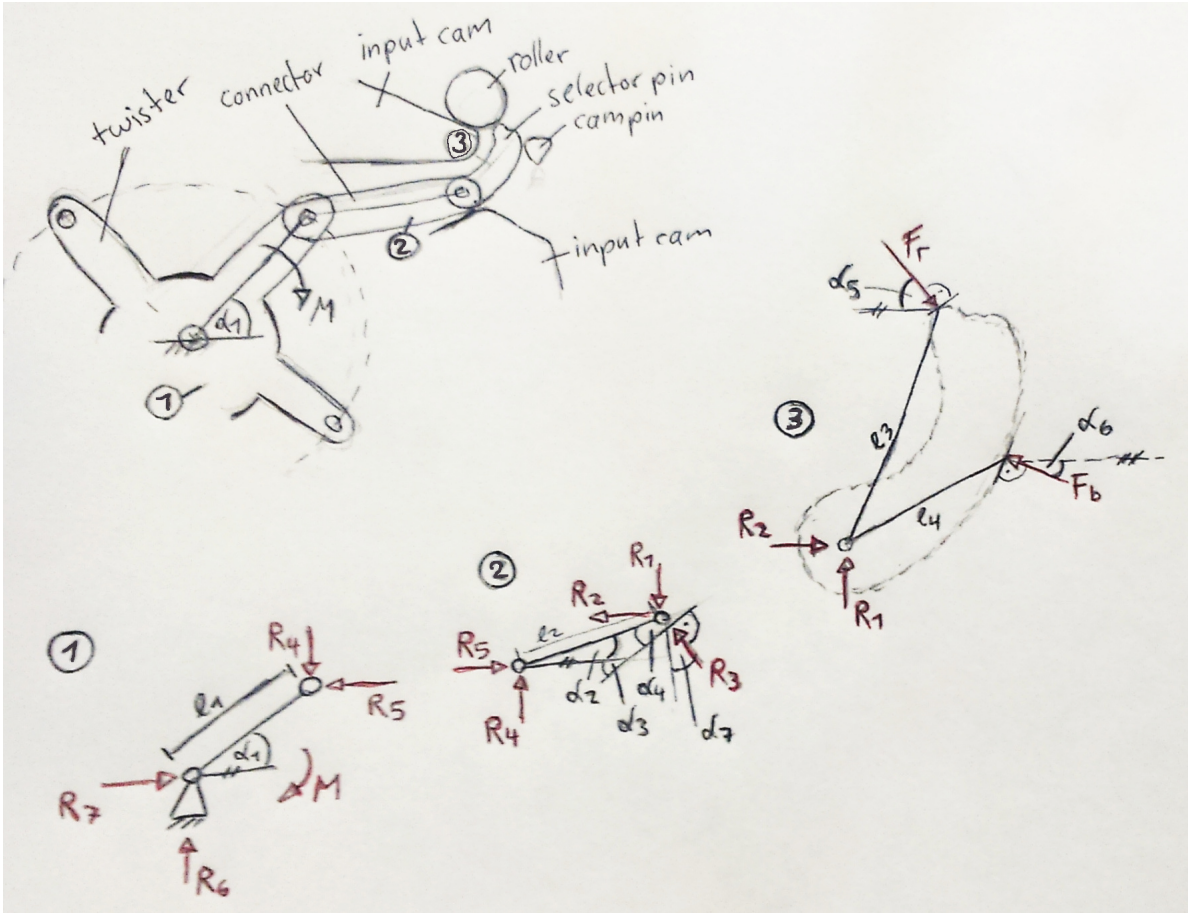

Figure 5: Free Body Diagram of the selecting mechanism of the new design.

Springs

The springs that should be used for the new mechanism of the first stage should have a very low stiffness, at least below 5 N/mm and preferably around 1 N/mm. The low stiffness is required because the springs only have to push the rollers apart from each other and should not add a high extra force on the rollers, which has to be overcome when unlocking the system. However, for the first manufactured prototype we will only use springs from pens or temporary 3D printed springs will be designed.

Subjective Evaluation

In the following, the position of the bicep and forearm measurements are shown. The positions are the same as used by Greiner [16] (see Figure 6).

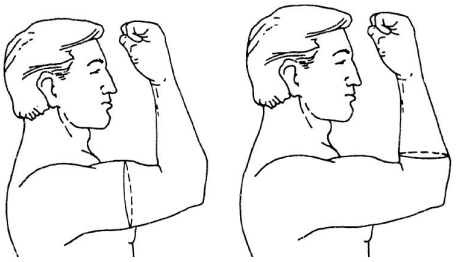

Figure 6: Indication of the measurement location on the biceps (left) and on the forearm (right). [16]

Besides, an example of the questionnaire is shown in the following:

Questionnaire

Subjective Evaluation of the Size of the New Developed Elbow Mechanism

The device will be placed on the elbow of the subject (as indicate below). The subjects have then to judge by themselve if they would accept the size of the device or not for an elbow orthosis.

Figure 1: Flexed bicep

Figure 2: Flexed forearm

Subject 1:
Gender: Female [ ] Male [ ]

Circumference flexed bicep : _____cm → diameter: _____mm
Circumference flexed forearm: _____cm → diameter: _____mm

Size
Rate the size of the prototype regarding its acceptance by a patient (you):
Would you accept the **size** of the mechanism for an orthosis that you have to wear? Please, circle one of the wollowing numbers:

[1]*	[2]*	[3]
not acceptable	acceptable	acceptable
changes of the design have to be made	but slight changes should be made	no changes needed

***In case [1] or [2] was chosen,** please specify what needs to be changed in your opinion:*

_____
_____
_____
_____

Figure 7: Example of the questionnaire for a subject.

3 Creation Process of the Conceptual Designs

The conceptual designs were created using creative methods (e.g. Brainstorming), by performing a brief literature research regarding non-backdrivable mechanisms (see App. 4) and by discussions with lab members. In total eleven concepts were created whereby only eight designs were further considered, since they were assumed to have a certain potential. The concepts were ranging from hydraulic/pneumatic, gear, crank-slider systems to drum/disk brakes or push mechanism (e.g. based an a pen).

4 Non-backdrivable Mechanism

A system is stated to be non-backdrivabale when it cannot transmit power and motion from the output to the input [18]. Examples for non-backdrivable mechanisms are 'wheel and worm drive,' 'rack and worm drive,' 'lead screw and nut' as well as 'triangular wedge' mechanisms [18]. In addition, roller clutches can be seen as non-backdrivable mechanism as well using a wedge mechanism [19], where the rollers wedge with the input cam and a corresponding output element. Moreover, non-backdrivable mechanism are passive locking devices, whereby the locking is based on friction that is created within the system [20].

5 Conceptual Designs

In the following, a brief explanation and a visualization of the developed conceptual designs will be given. Yet, only the concepts, which were considered to have a certain potential to become a final concept will be shown. Consequently, only eight out of eleven concepts are explained. Although, all concepts are focused on the selecting mechanism and will consider the same structure of the compliant mode of the current design. Besides, the first expected unlocking force/torque of the concepts are mentioned (for the calculations see the MATLAB code, App. 10). However, only brief calculations have been made for the first version of the concepts. Consequently, accuracy errors are expected.

Concept 1

The first concept is still based on the bidirectional, non-backdrivable roller clutch, yet, the mechanism of moving the selector pins and adding the compliant mode is different (see Figure 8).

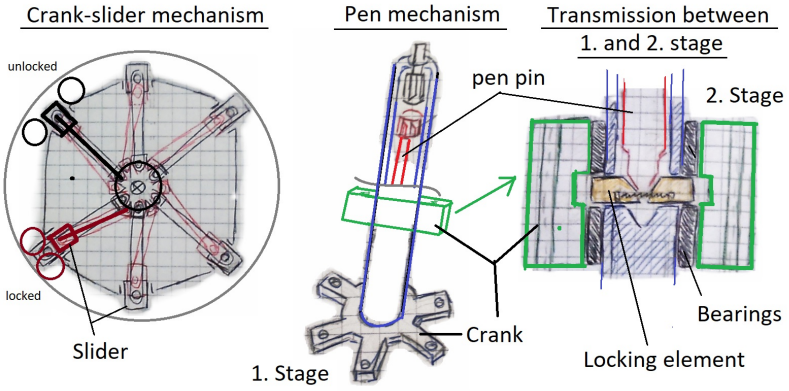

Figure 8: Concept 1: Using a crank slider mechanism to move the selector pins (sliders). Engaging the first stage to the crank of the second stage by the use of a pen mechanism. When the 'pen' is pushed a locking element connects with pits of the second crank, when the pen is pushed again, the locking element is pulled back by connecting springs.

As it can be seen in Figure 8, the concept is based on a crank slider mechanism. Depending in which direction the crank is rotated the input gets connected with the output (red slider)

or disconnected (black slider) and therefore it is responsible to engage or disengage each stage. Both stages use a crank slider mechanism, but in different levels. To connect the second stage (visualized in green) to the first stage, the 'click' mechanism of a pen is used.

The crank of the first stage has a hollow cylindrical extrusion, which would represent the frame of the pen. Around the frame, above the first crank, a second crank will be placed. Yet, the pen frame and the second crank will be connected by a bearing, so that the second stage does not rotate with the first stage, when it is disengaged. To engage the second stage, the pen mechanism needs to be used. When the pen pin in the hollow extrusion is pushed down, then the pen pin activates the locking element. This element is pushed to the sides into pits of the second crank. As a consequence, the crank is fixated with the hollow extrusion of the first crank. Hence, when rotating the first crank, the second one will be rotated as well. To disengage the second stage, the 'pen' needs to be clicked again. As a result, the pen pin moves up and the locking elements are pulled together by connecting springs. Therefore, the connection to the second stage is lost and an individual rotation of the first stage is possible again.
The expected unlocking torque is 1.8 Nm when an output force of 100 N is considered.

Concept 2

The second concept is based on a push and twist mechanism which is still based on the bidirectional, non-backdrivable roller clutch design. In this case, all selector pins (of each stage) are in one elastic component, which is slightly bended. When the bended element is pushed down, its diameter increases and therefore the single ends of this element, representing the selector pins, are pushed out. To keep the mechanism in this position, the element that is connected to the bended element can be rotated. Based on this rotation, extrusions on sides of that element are moved into a gab, hindering that the bended elements move back into their default position due to their elastic energy and additional springs that are placed below the bended element, as demonstrated in Figure 9.

The second stage will be engaged/disengaged in the same way. However, the push element, will be fixated by rotation, to the push element of the first stage.

The expected unlocking force is 17.6 N when an output force of 100 N is considered.

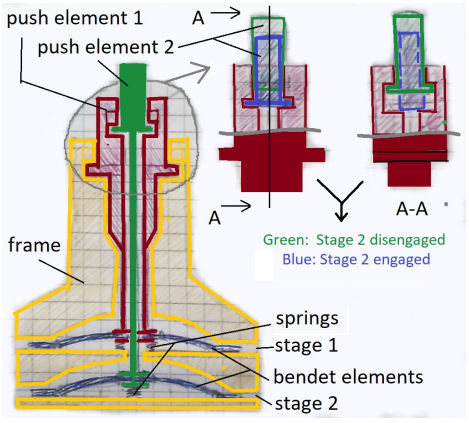

Figure 9: Concept 2: Using a push mechanism of elastic components to move the selector pins. The fixation of the pins in the desired position is achieved by twisting the push element that pushes the elastic element down. The two smaller figures in the top, right corner, visualize the different positions of the push element on the example of the second stage. A-A is the cross section of the left small figure. The same mechanism applies between the push element one and the frame.

Concept 3

This concept is just as the previous two, based on the bidirectional, non-backdrivable roller clutch. Yet, the mechanism is based on a pneumatic or hydraulic system. Therefore, a bellow will be located in the center of the clutch which will be pressurized to push the selector pins out and depressurized to allow them to move back into their default position. However, the selector pins will only move back in their default position due to springs, which were compressed during the pressurized condition. The second stage will be activated by the use of valve or a second independent bellow. This concept is shown in Figure 10.

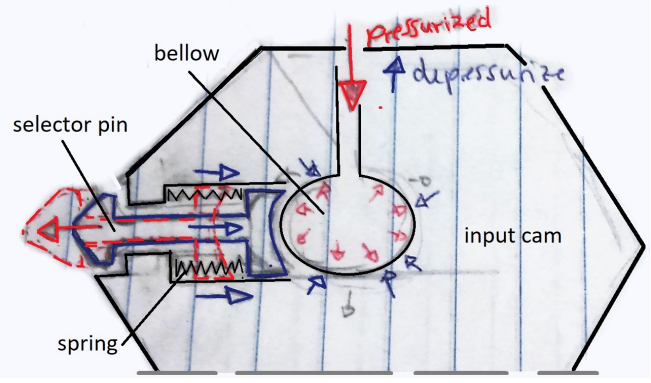

Figure 10: Concept 3: Using a pneumatic or hydraulic system where a bellow gets pressurized to push the selector pins out. When the bellow is depressurized, compression springs will push the selector pin back in its default position.

The expected unlocking force is 5.7 N and 11.1 N for the first and second stage, when an output force of 100 N is considered.

Concept 4

This concept is similar to the third concept. The selector pin will be moved back in its default position in the same way using compression springs. However, the pins will be pushed out by the geometry of an element that will be pushed down as indicated in Figure 11. To warrant that the selector pins will not be moved back, the push element has to be rotated and locks with the bottom of the input cam.

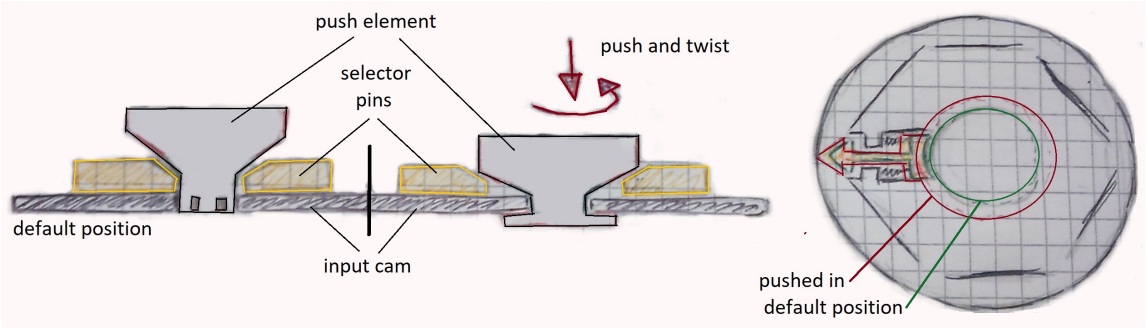

Figure 11: Concept 4: When the push element is pushed down, the selector pins are moved partly out of the input cam. When the push element is twisted, then the position of the elements will be fixated. When moving the push element back in its default position, springs push the pins back into the input cam.

The expected unlocking force is 17.6 N when an output force of 100 N is considered.

Concept 5

This concept is based on the patent US 20110201473 A1 [21]. Therefore, the roller clutch design is exchanged with a planetary gear system (see Fig. 12). The input gear is connected to two other gears which are all located on a cam. The other two gears are also in contact with the gear ring, the output. As a result, the cam rotates within the output ring. Considering the compliant stage of the current design, it can be added to this concept, when the element with the pivots for the spring will be connected to the cam and the spring to the output. Furthermore, a bearing will be needed between the output and the element carrying the pivots. Yet, the engagement of the second stage could be done with some type of pressure connection, where the second stage is pressed to the first one to obtain a fixation to the cam.
The expected unlocking torque is 0.8 Nm when an output force of 100 N is considered.

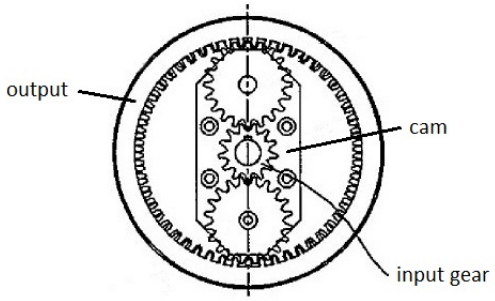

Figure 12: Concept 5: Selflockig, non-backdrivable mechanism based on a planetary gear system. Modified Figure [21].

Concept 6

This concept, which is the winning concept, is based on the first concept using a crank slider mechanism, but in this case the pen mechanism is neglected. Yet, the two stages can be individually engaged, just by twisting each crank (twister). Besides, for each roller pair are two selector pins used instead of one (see Fig. 13). When the selector pins are pushed outside, by the rotation of the crank, then they push against a pin, which is part of the input cam. Due to the geometry of the cam pin, the selector pins are pushed aside, pushing the rollers away, obtaining the free movement.

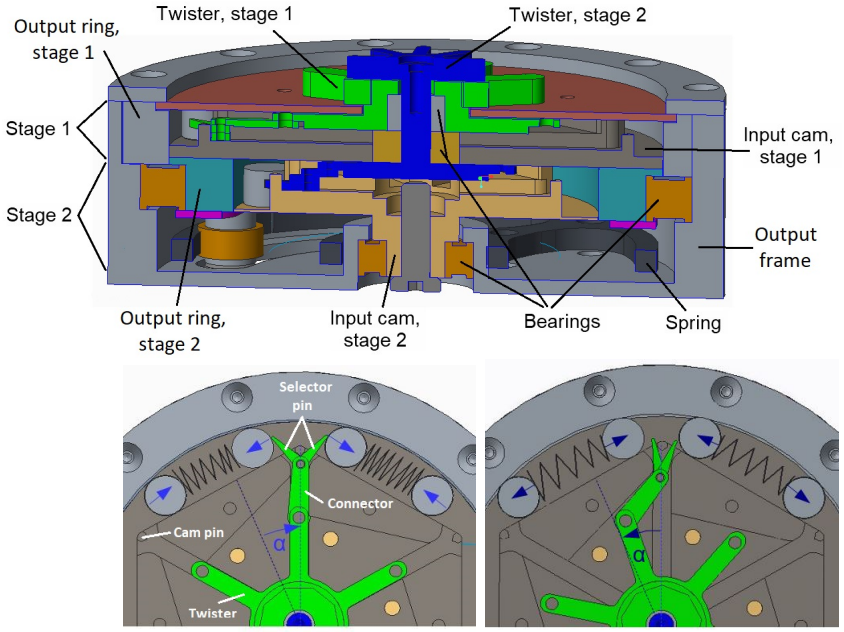

Figure 13: Concept 6: CAD model of the concept. Top: Overview of a possible assembly with both stages. Bottom: Position of the elements when rollers are unwedged (left) or wedged (right). (α represents the rotating angle of the twister).

The expected unlocking torque is the same as of concept one when an output force of 100 N is considered. Yet, with following calculations that were made since the concept were successful in the first selecting rounds, the expected unlocking torque changed to be 3.4

Nm when 100 N are considered for the output force. Furthermore the expected unlocking torque, which is needed when a load of 5 kg is applied, is 6.9 Nm.

Beside the shown design in Figure 13 represents the design version where the two desired stages are combined in one component, as it was done in the previous elbow module. The second stage in this new design version is achieved by doubling its first stage and adding a spring to it (similar to the previous design). Consequently, the compliant mode is integrated in the mechanism as demonstrated in Figure 13. As a result, the created elbow module will only be on one side of an elbow orthosis, otherwise the stages can be separated, as it is done in the new developed and manufactured design.

Concept 7

This concept focuses on disk based systems. Hence, either on a disk clutch as shown in Figure 14 or on disk brakes, as they are used in motorcycles. To engage the first stage, the corresponding nut has to be tighten. Consequently, the stage element gets pulled forward and pushes the disks and the spacers together, whereby the spacers are connected to the output frame. The same principle is applied to the second stage, whereby in that case the stage does not connect to the output but to the first stage.

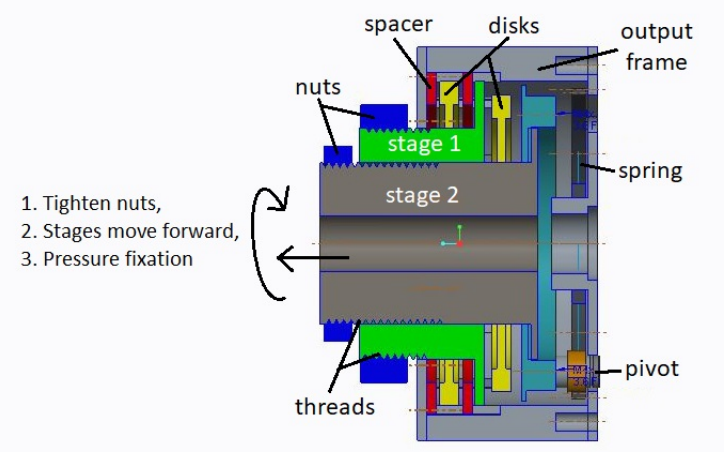

Figure 14: Concept 7: CAD model of a disk clutch example with one disk per stage. When tightening both nuts, then the stages are pressed against each other and against an element of the output frame.

The expected unlocking torque for the disk clutch concept is 4.9 Nm (using one disk) or 1.2 Nm (using four disks) when an output force of 100 N is considered. When an applied load of 5 kg is considered, then the expected unlocking torque is 0.8 Nm (using one disk) or 0.2 Nm (using four disks).

For an hydraulic disk brake, the expected unlocking force is 177.8 N, when an output force of 100 N is considered. The expected unlocking force for an applied load of 5 kg is 288 N.

Concept 8

This last concept is based on a drum brake systems, which can either be activated based on a hydraulic or mechanical mechanism (see Fig. 15).

When the hydraulic system is used, a piston pushes due to the receiving hydraulic pressure two lever arms against the output drum, initiating the locked condition. When the pressure is released, a spring connected to the levers, pulls them back in their default position. Yet, when a mechanical system is used, the two levers are pushed against or pulled away from the drum by rotating a handle, which is connected to these levers. To allow the activation of two stages with the mechanical system, the handle of stage one is hollow, so that a second handle can pass through it to the next level, where another pair of levers will be placed to activate the compliant mode. In the hydraulic system the second stage can be connected by a valve to the first stage.

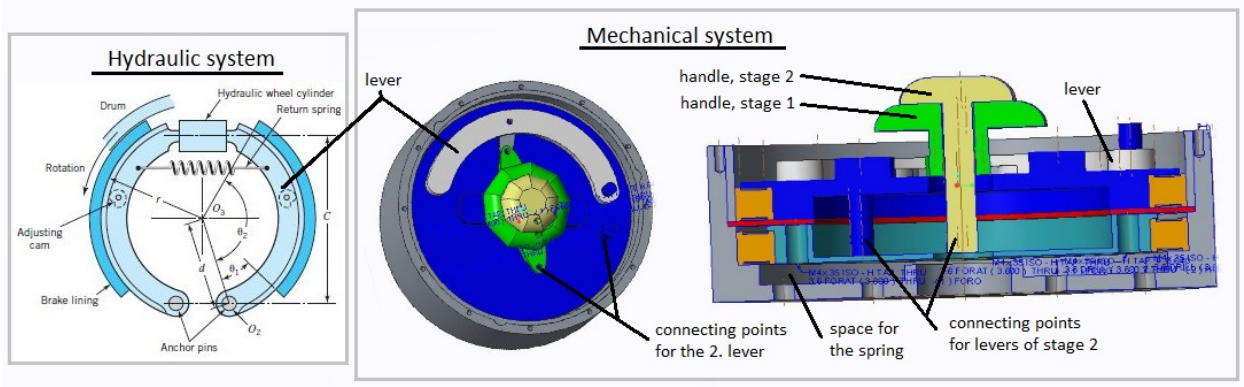

Figure 15: Concept 8: Showing an overview of the hydraulic mechanism on the left [22] and a partly assembled CAD model of the mechanical mechanism for two stages on the right.

6 Selecting Process of a Winning Concept

To select one of the conceptual designs as a final concept, selecting criteria have been used with specific weighting factors to make a comparison in different categories of the concepts possible. However, during the selection process the weighting factors of the selecting criteria have been adjusted according to a statement of a professor (of the hand surgery department at the hospital of Florence) regarding the importance of specific criteria. Therefore, criteria related to forces obtained at the end a lower weighting factor and criteria related to the weight and to the compliant mode obtained higher weighting factors (which was at the beginning of the selecting process vise versa). With that, it will be ensured that the new design is in line with the patients need according to the professor's evaluation.

However, multiple evaluation rounds have been performed of the conceptual designs changing/adjusting the evaluation criteria and eliminating, but also specifying concepts during each round.

The first selecting round included nine concepts and used only two selecting criteria, the 'natural appearance' and the 'potential of the design'. These criteria were only evaluated

by 'yes' and 'no'. Hence, only if a concept received a 'yes' for both criteria, then the concept was considered for the next round, otherwise the concept was eliminated. Due to this selection round, three out of nine concepts were excluded (see Table 1).

Table 1: Selection Round 1

Designs / Criteria	1	2	3	4	5	6	7	8	9
Potential of design	✓	✓	✓	✓	✓	✓	✘	✘	✘
Natural appearance	✓	✓	✓	✓	✓	✓	✘	✓	✓

The followed selecting rounds rated the criteria with either 1 (bad) to 3 (good) or 0, which was generally used when a criteria was not eligible for a concept or when the criteria did not meet the requirements. During these selecting rounds, the following criteria were used with the given points for specific conditions of the criteria :

1. **Number of modes** - Two modes = 1, three modes = 2, more than three modes = 3. (Concepts with only one mode were not included.)
2. **Control of modes** - Bad control = 1, moderate control = 2, good control = 3.
3. **Size** - Diameter (d) $\leq$ 81 mm = 3, 81 $\leq$ d $\leq$ 85 mm = 2, d $\leq$ 108 mm = 1, d $>$ 108 mm = 0.
4. **Design simplicity and number of components** - Rated in comparison between the conceptual designs. Simplest design/less parts = 3, most complex design/most parts = 1.
5. **Movement range** - Range of Motion (ROM) $< 130°$ = 0, minimal wanted ROM: 0 - 130°= 1, for the desired ROM: -5 – 150° = 2 and for ROM $> 150°$ = 3.
6. **Output force (F) or torque (T) higher then the input F or T** - Rated in comparison between the conceptual designs. Concept(s) with the best input-output relation = 3, with a medium input-output relation = 2 and the concept(s) with the worst input-output relation = 1.
7. **Negative friction** - Friction that influences the mechanism in a negative way (lowering output forces/torques and/or increasing input forces/torques). Rated in comparison between the conceptual design. Assuming a concept has no negative friction = 3, less negative friction = 2 or most negative friction = 1.
8. **Self-locking** - It means that no slipping in the mechanism (at the wedged elements) occurs when high forces/torques are applied, and that failure of the mechanism only occurs due to breakage of the material. Concept is self-locking = 1, not self-locking = 0. (Only used for the fourth selecting round.)
9. **Force (F) or Torque (T) to unlock the system when loaded with 5 kg** - Rated in comparison between the conceptual design. Lowest F or T = 3, medium F or T = 2, highest F or T = 1. (Only used for the fourth selecting round.)
10. **Manufacturing** - Rated in comparison between the conceptual designs. Assuming that the concept is easy to be manufactured = 3, moderate for manufacturing = 2

or difficult to be manufactured = 1. (Only used for the fourth selecting round.)

For the second and third round, the weighting factors were focused on the force/torque criteria and less on the weight, since the discussion with the professor of the hospital of Florence took place after Round 3 was performed. However, basic computer aided models were created of the concepts that seem to have the best potential for the final concept. The models were created using the software Creo Paramatic 3.0 (PTC, Needham, USA). However, looking at Round 2 (see Table 2) it can be seen that the winning concept of that round is Concept 6, whereby it only obtained a difference of 0.1 points to Concept 1 and 5 and a difference of 0.2 point to Concept 3. Therefore, the Concepts 3, 5 and 6 were evaluated in a third round. (Concept 1 was neglected since it is similar to Concept 6, but did not surpass the design in the selecting round).

Table 2: Selection Round 2

Designs **Criteria (weighting factor)**		1 'pen'	2 twist	3 pneu/hy	4 s. push	5 gears	6 combi
Fout > Fin	0.25	2	0	1	0	3	2
Number of modes	0.05	2	2	2	2	1	2
Size (excluding possible motors)	0.05	3	3	3	3	3	3
Assumed weight	0.05	1	1	1	1	1	1
Control of stages	0.15	3	3	3	3	1	3
Design/assembly	0.1	1	2	1	2	2	2
Possibility to be automated and to be passive	0.15	2	2	2	2	2	2
Negative Friction	0.15	2	2	3	0	2	2
Movement range	0.05	3	3	3	3	3	3
SUM	**1**	2.1	1.7	2	1.4	2.1	2.2

In Round 3, the selecting criteria, where all concepts performed equally in the previous round, were excluded. Consequently, the weighting factors increased in each category, as it can be seen in Table 3. Although, the winning concept in this round changed from Concept 6 to Concept 1 with a difference of 0.23 points. The difference to Concept 5 was by 0.25 points. However, all concepts are still very close to each other, therefore, based on a discussion with members of the Biorobotics Institute, Concept 6 was chosen as the winning concept of Round 3.

Yet, another final selecting round was performed with the previously 'winning concept' and three new developed promising concepts, whereby then, the weighting factors were adjusted to the previously mentioned professor's suggestions (more weight on the criteria related to the weight and the compliant mode, and less weight on the forces). The last selecting Round 4 can be seen in Table 4.

As it is shown, with this adjustment three of the four concepts obtained the same rank. One concept had a lower rank with 1.9 points, but only by 0.05 points (max. available points: 3). Hence, no large differences between the final points of the four concepts existed. At the end, the design was chosen which is the most related to the current design, because a specific knowledge regarding this design already exists and is therefore assumed to be easier realizable and assumed to have less complications.

Table 3: Selection Round 3

Designs Criteria (weighting factor)		1 'pen'	2 twist	3 pneu/hy	4 s. push	5 gears	6 combi
Fout > Fin	0.25	2	0	1	0	3	2
Number of modes	0.05	2	2	2	2	1	2
Size (excluding possible motors)	0.05	3	3	3	3	3	3
Assumed weight	0.05	1	1	1	1	1	1
Control of stages	0.15	3	3	3	3	1	3
Design/assembly	0.1	1	2	1	2	2	2
Possibility to be automated and to be passive	0.15	2	2	2	2	2	2
Negative Friction	0.15	2	2	3	0	2	2
Movement range	0.05	3	3	3	3	3	3
SUM	**1**	2.1	1.7	2	1.4	2.1	2.2

Table 4: Selection Round 4

		Drum based		Roller based	Disk based
Designs Criteria (weighting factor)		3a hydraulic (non self-locking)	3b mechanic (non self-locking)	6 combi.	7a clutch
Fout > Fin	0.05	2	2	2	3
F or T needed to unlock when 5 kg are applied	0.1	/	/	2	3
Self-locking/ can withstand high torques until breakage of device (no slipping occurs), yes = 1, no = 0	0.1	0	0	1	0
Negative friction	0.1	3	2	2	2
Number of components	0.25	3	3	1	2
Size (based on first CAD sketches)	0.35	2	2	3	2
Manufacturing	0.05	2	3	1	2
SUM	**1**	1.95	1.9	1.95	1.95

7 Finalizing the Winning Concept

For the finalization of the new design, the focus was on the first stage, since the main principle of the second stage will be the same, only a spring needs to be included in the design of the second stage to obtain the compliant mode. Therefore, only when the first stage will be finished in its design and can be considered as satisfying, the second stage will be finalized.

The geometry of the new design, especially the contact angle (between the rollers and the input cam) was specified and adjusted to the previously determined friction coefficient ($\mu_s = 0.14$) of the contact areas when using steel (39NiCrMo3) for the contact elements. Instead, for the other elements, where no high stresses were expected, an aluminum alloy (ERGAL7075) was used. The equations for determining the contact angle, optimal roller size, cam size, the inner output ring diameter and the radial forces were taken form the paper by Controzzi et al. [17], since the new design is based on the current roller-based clutch mechanism. However, the equations will be mentioned later on (see Equation 3 - 11).

All calculations of the following sections were performed by using Excel (Microsoft, Redmond, USA) and MATLAB R2017a (Inc. The MathWorks, Natick, USA).

Buckling

The new mechanism contains slim elements (selector pin, connector, twister), which will be loaded with pressure when unlocking the system. Therefore, a check regarding buckling of these elements was performed. The following equation was used:

$$\sigma_{cr} = \frac{\pi^2 * E * I}{A * L^2}, \tag{1}$$

where σ_{cr} is the buckling strength, E is the Young's Module, I is the moment of inertia, A is the area and L is the length of the slim element. To ensure that no failures occur due to buckling, the following had to be true:

$$\sigma_{cr} < S_y, \tag{2}$$

where S_y represents the yield strength of the material. The buckling failure mode was calculated using two materials, steel (39NiCrMo3, $S_y = 785$ MPa, E = 210000 MPa) and aluminum ($S_y = 414$ MPa, E = 27000 MPa).
Only when the Equation 2 is true, the design process will be continued of the selected conceptual design.

Contact Angle

The contact angle between the roller and the input cam influences the torque that needs to be applied to unlock the system. The contact angle is influenced by the friction coefficient, which can be seen in Figure 16. As it is shown, the optimal contact angle α is about 6.6° when using the determined friction coefficient $\mu_s = 0.14$.

To relate the contact angle to the other geometry elements of the mechanism, the following equation by Controzzi et al. [17] was used:

$$\alpha = 0.5 * \arccos(\frac{l + r}{R_{in} - r}), \tag{3}$$

where r is the roller radius, l is the distance between the centerline and the side surfaces of the input cam and where R_{in} is the inner radius of the output ring. By trial and error different values were used for the parameters l, r, and R_{in} to obtain the desired contact angle. In addition, every change of the geometry parameters were controlled in a CAD model regarding the feasibility of the design. Hence, to obtain a contact angle of 6.6, we used the following values: $l = 24.43$ mm, $r = 4$ mm and $R_{in} = 33.2$ mm.

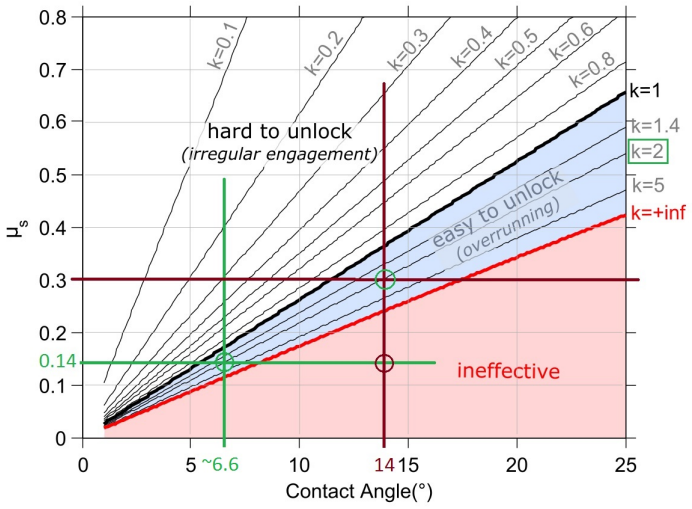

Figure 16: Graph of the relation between the friction coefficient and the contact angle with respect to the ease of unlocking the system. The crossing of the red lines indicate the optimal contact angle for the previously assumed friction coefficient of 0.3. The crossing of the green lines represent the optimal contact angle for the determined friction coefficient of 0.14. Modified figure [17].

Radial Force (Roller-Ring)

As it is shown in the paper by Controzzi et al. [17] the radial force (F_r) acting between the rollers and the output ring is determined by

$$F_r = F * \cos(\alpha) \ , \tag{4}$$

where F represents the related tangential force:

$$F = \frac{T_{max}}{R_{in} * \sin(\alpha) * N_a} \ , \tag{5}$$

whereby T_{max} is the maximal applied output torque, R_{in} is the inner radius of the output ring as mentioned previously and N_a represents the number of rollers that are in use when a load is applied to the mechanism at its locked condition. Hence $N_a = N/2$, where N represents the total number of rollers. For T_{max} two cases were used. The first case uses a torque of 1600 Nmm representing an applied load of 5 kg and the second case uses a torque of 16000 Nmm representing a load of 50 kg. The first load case was chosen to represent the applied forces of daily activities such as during grocery shopping (carrying the shopping bags), yet, the second load case was chosen to represent more rare conditions such as lifting heavy boxes and additionally to be a safety condition. However, in both cases a lever arm ('forearm length') of 32 cm is used. The forearm length of 32 cm was chosen, since the minimal length from the elbow to the 'center of grip' is for females 23.7 cm (50^{th} percentile of 32.9 cm) [16] and the maximal length for males is 43.60 cm (50^{th} percentile of 35.8 cm) [16], therefore, a random value between these two sizes was picked.

Consequently, the used radial roller force for the first case is 71.57 N and for the second case 715.67 N.

Optimal Roller Radius

At the end, the chosen geometry was analyzed regarding its optimal roller size. In general, the larger the rollers or the higher the number of the rollers, the better it is regarding the forces. More rollers are better for the force distribution and the larger the rollers (= increased contact angle) the better is the force transmission and therefore lower stresses on the material occur [17]. However, the complexity of the design might increase for fulfilling these requirements [17] and also the weight will increase with a larger amount of rollers. Furthermore, as already indicated the roller size is related to the contact angle and the friction coefficient. Therefore, the roller size cannot be maximized to the available space in the design, since the unlocking condition might become too difficult (see Fig. 16). Based on that, the optimal roller size has to be found, which keeps all the other related requirements fulfilled. For that, the maximal principle stress (σ) and the maximal number of rollers (N_{max}) were plotted over the roller radius, whereby the radius corresponding to the minimal value of the maximal principle stress is used in the plot of the maximal number of rollers (see Fig.17, 18). Yet, the following equations were used for the plots:

$$N_{max} = \frac{2 * \pi * (l - r)}{z + s} \text{ , where} \tag{6}$$

$$z = 4 * \arcsin(\frac{r}{2 * (l - r)}) * (l - r) \text{ and} \tag{7}$$

$$\sigma = \frac{b}{\Delta} * C_{f1} \text{ , where} \tag{8}$$

$$b = \sqrt{\frac{2 * F_{rx} * \Delta}{\pi * z}} \text{ and where} \tag{9}$$

$$F_{rx} = \frac{Fr}{\frac{N_{max}}{2}} \text{ and} \tag{10}$$

$$\Delta = \frac{1}{\frac{1}{2} * r + \frac{1}{2} * l} * (\frac{1 - {v_1}^2}{E_1} + \frac{1 - {v_2}^2}{E_2}) \text{ ,} \tag{11}$$

where v_n, is the Possion's ratio and E_n the Young's Module of the two used Materials for the rollers and for the output ring ($n = 1, 2$). Besides, C_{f1} is a parameter used in the context with determining the maximum compressive principle stress that occurs in the surface between $x = 0$ and $x = 0.3 * b$ in relation to the friction coefficient. According to Boresi et al. [23] $C_{f1} = -1.13$ for a $\mu_s = 0.11$ and when $C_{f1} = -1.19$ the $\mu_s = 0.17$. Since our friction coefficient, with $\mu_s = 0.14$, is in the middle of these values, we decided to use the mid value for the C_{f1} as well, resulting in a C_{f1} of -1.16.

In the following two Figures 17 and 18, the maximal number of rollers is indicated in relation to the roller radius. However, in these graphs the previous determined roller radius was used to compute the optimal roller radius. For that, a small range of ± 0.6 was placed around the previous determined radius ($r = 4$). The range is indicated by the vertical red lines. To find the optimal roller radius and number of rollers within the

range of 4 ± 0.6, the highest absolute number of the maximal number of rollers (N_{max}) was chosen. Consequently, the corresponding radius was the optimal roller radius, which was obtained from Figure 18 (close-up of Fig. 17).

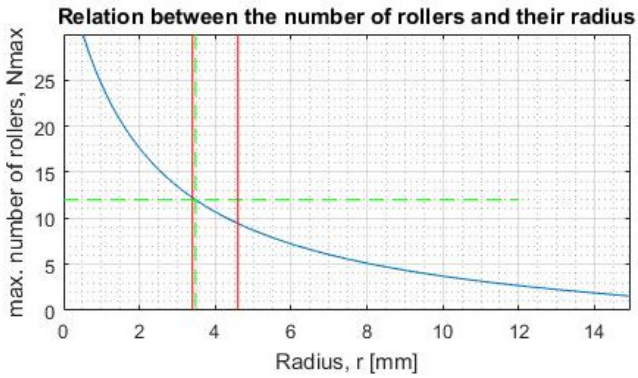

Figure 17: The relation between the maximal number of rollers regarding their radius is shown by the blue curve. The space between the red lines indicate the range for finding the optimal roller radius. The green dotted lines indicate the optimal roller radius and therefore the optimal number of rollers.

As it can be seen in Figure 18 the maximal number of rollers is 12 and the corresponding, optimal roller radius is therefore 3.48 mm.

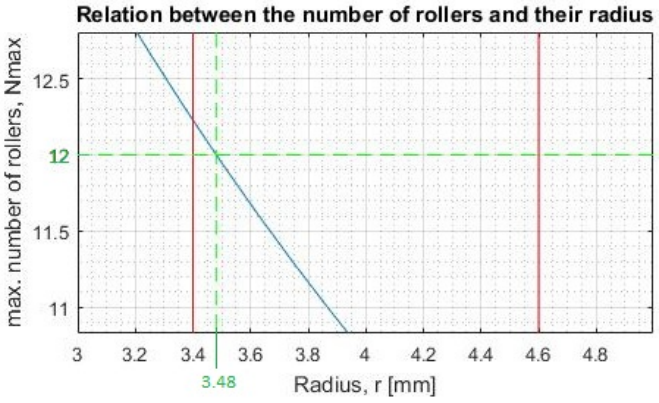

Figure 18: A close up visualization of the previous plot in Figure 17 showing the optimal roller radius and optimal number of rollers.

Since the optimal roller radius has been determined to be $r_{optimal} = 3.48$ mm instead of the previously used roller radius of $r_{previous} = 4$ mm the geometry of the design had to be adjusted to warrant the new determined roller radius as well as the determined contact angle. For the adjustment the same method as for finding the contact angle was used. Yet, it was tried to stay as close as possible to the previous determined geometry values, by changing for instance mostly the angle between the cam surfaces (the angles of the cam edges). Due to that we received the following parameter values which were used as the basic condition for the new conceptual design: $\alpha = 6.61°$, $l = 24.43$ mm, $r = 3.48$ mm and $R_{in} = 32.15$ mm.

8 FEM Analysis

In the following, the method of the FEM analysis will be explained, followed by summarized results. Afterwards, more figures of all results of the total deformation, (van-Mises) stresses and pressures are shown while only mentioning the maximal values of each category. At the end, the obtained results will be discussed.

Method

A static structural FEM analysis was performed of critical areas (areas with the risk of high stresses) using the ANSYS Workbench (ANSYS, Inc., Canonsburg, USA) software. The selector pins and the pins of the input cam were considered as critical areas when the mechanism switches its mode from its locked to its unlocked condition, especially when the mechanism is loaded. During that phase high forces are acting on the wedged rollers making it more difficult for the selector pin to push the rollers away from the output ring and the input cam. Hence, the selector pins and the pins of the cam have to withstand these high forces as well. Therefore, a FEM analysis of this condition was performed on the selector pins and the cam pin while the mechanism was virtually loaded with 5 kg (Case 1, representing a normal loaded condition) and 50 kg (Case 2, representing a critical loaded condition).

To obtain a model that is more related to the real condition regarding the contact force transmissions, the selector pin and the cam pin were analyzed together in a frictionless contact assembly instead of individually. Furthermore, two FEM models were created. The first model is used to obtain the interactions between the input cam and the left selector pin and the second model is used for the interactions between the input cam and the right selector pin.

In each model the two contacting surfaces (one on the selector pin and one on the cam pin) were selected for the frictionless contact area (see Fig.19).

The applied forces and constrictions for the FEM analysis are demonstrated on the first model in Figure 19 as well as the chosen refinement areas for the mesh generation. The previous determined radial roller force is applied at the red surface (B) and the direction of the force is indicated by the red arrow (depending on further adjustments of the design additional surface might have been created on the selector pins application (which was done only for the FEM analysis to obtain a better surface for the radial roller force ($F_r = 715.76$ N for the first case and $F_r = 71.6$ for the second case)). The displacement constriction is visualized by the yellow surface (D) and was added because a (cover) plate above the pins hinders the movement of the selector pins in the z-direction. Besides, a cylindrical support (blue, C) is added to the hole of the selector pin, since the real model obtains in that point support due to another fixating/connecting pin. Finally, a fixed support (A) was placed on the backside of the input cam (not directly visible in Figure 19).

For the mesh generation, first the default ANSYS mesh size was used, where a refinement was added in the contact areas and the surface of the force application. Later on, in some cases when the elements still appeared to be to large for specific critical areas, then the

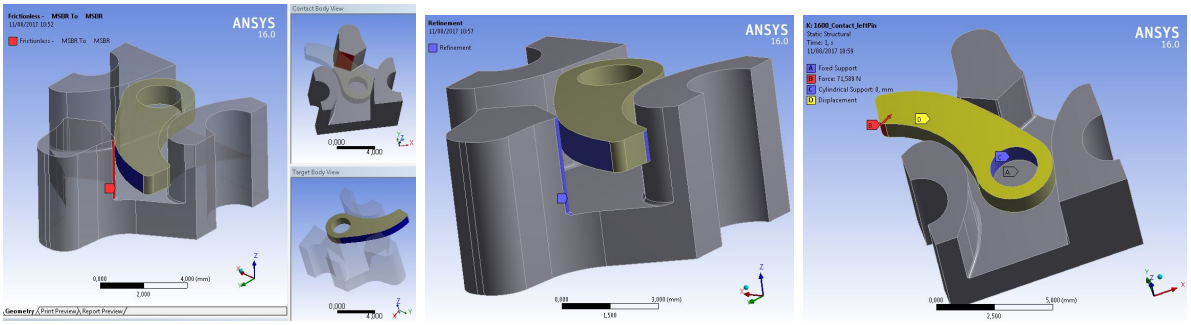

Figure 19: FEM set up demonstrated on the first default model. Left: Frictionless contact areas. Middle: Refinement areas of the mesh. Right: Static structural characteristics (constrictions, force application).

mesh was reduced to the following settings: Min size: 0.0005 mm, max size: 0.2 mm, minimum edge length: 0.015 mm.

The FEM analysis was solved for (von-Mises) stresses, total deformation and for the pressure in the contact area. Furthermore, the design of the mechanism has been adjusted multiple times until the resulting stresses of the analysis were within an acceptable range, which is based on the materials properties, such as its yield strength.

In addition, the resulting pressure values were used to relate the results of the virtual model to the real model. For that the following equation was used:

$$P_{Hz,10^7} = a * HB - b, \tag{12}$$

where $P_{Hz,10^7}$ is the pressure that the material can withstand when it has been loaded for 10^7 times; HB represents the Brinell hardness of the material ($HB_{39NiCrMo3}$ = 295-354 [24]), and a and b are material and its condition related parameters. Hence, for steel $a = 2.8$ and $b = -70$ MPa when considering sliding steel and a good lubrication. [25]

Results

The results of the FEM analysis of the two models (Model 1: Left selector pin; Model 2: Right selector pin) for two different cases (Case 1: 5 kg; Case 2: 50 kg) are presented in the following. First, the results are demonstrated on the left model. This is done, because the first model is considered as the more critical model, because it is assumed that its longer lever arm between the basement of the input cam and the applied force near the open end of the cylindrical extrusion (the cam pin) result in higher stresses. However, afterwards figures of all results will be shown for each condition.
An overview of the obtained results for both cases, both models and for the default and adjusted version can be seen in Table 5. Yet, the pressure values of the default models in the second case were not evaluated, because the obtained (van-Mises) stresses were already exceeding the allowable yield strength by far ($Rp_{0.2}$ of 39NiCrMo3 = 785 MPa [24]).

In general, it can be said that the maximal (van-Mises) stresses occur in the contact area of the selector and cam pin (such as in Fig. 20, 21). In the contact area, especially on the

Table 5: (Maximal) values of the FEM output. D_{tot} = total deformation; σ_{sp} = max. stresses of the selector pin; σ_{cp} = max. stresses of the cam pin; σ_r = stresses in the rounding/curve between the cam pin and its basement; σ_h = stresses at the area of the selector pin's hole; Diff. = difference between the default and adjusted design of the same case using the same model. Values in brackets '(x)' indicate maximal values given by ANSYS, yet, these values were in the analysis neglected since they only occur either on very small areas or on single nodes. The given stresses represent van-Mises stresses. (* Reduced mesh was used.)

Case 1: 5 [kg]						
max.	$M1_{de}$	$M1_{ad}$	Diff. [%]	$M2_{de}$	$M2_{ad}$	Diff. [%]
D_{tot} [mm]	0.012	0.0043	64.2	0.0036	0.0046	-27.8
σ_{sp} [MPa]	(633), 475	(372), 172	64.2	704	(248), 174	75.3
σ_{cp} [MPa]	(2058), 1425	(200), 172	87.9	(1584), 1408	174	87.6
σ_r [MPa]	316	57	82	880	148	83.2
σ_h [MPa]	158	114	27.8	176	99	43.8
p [MPa]	(1550), 1087	(726), 645	48.1	(4158), 3234	(566), 440	86.4
Case 2: 50 [kg]						
D_{tot} [mm]	0.13	0.034	73.8	0.11	0.036	67.3
σ_{sp} [MPa]	5374	(799), 686	87.2	(6817), 4870	703	85.6
σ_{cp} [MPa]	(17465), 10748	963*	91	(9739), 6817	(904), 703	89.7
σ_r [MPa]	2687	688*	74.4	6817	402	94.1
σ_h [MPa]	1344	571	57.5	974	602	38.2
p [MPa]	\	(2833), 2518	\	\	(2371), 1844	\

adjusted cam pin, the maximal stresses have the tendency to be located near the top and bottom edges of the tangential contact area (see Fig. 22). Same is true for the pressure distribution of the adjusted models (see Fig. 24). The maximal stresses on the adjusted selector pin are either equally distributed over the contact area (see Fig. 23) or behave with their distribution similar to the stresses of the cam pins contact area.

Looking at the default models, the maximal (van-Mises) stresses and the pressures are more equally distributed over a linear contact area of the cam pin compared to the adjusted designs (see Fig. 24), whereby a small increase of the stresses towards the bottom of the contact area are still present. Same occurs, at the selector pins, the stresses are generally equally distributed, yet with a slighter increase at one side of the contact area.

However, stresses occurred as well at the rounding/curve between the cam pin and its basement, at the hole of the selector pin and also within the selector pin, especially when the second case is applied. Nevertheless, these stresses, are always lower than the maximal obtained stresses.

The maximal deformation occurred in all but one condition at the tip of the selector pin, near the area of the applied force. Yet, in the second model, when analyzed with 5 kg, the maximal deformation still occurs on the selector pin, but in the contact area instead of at the tip.

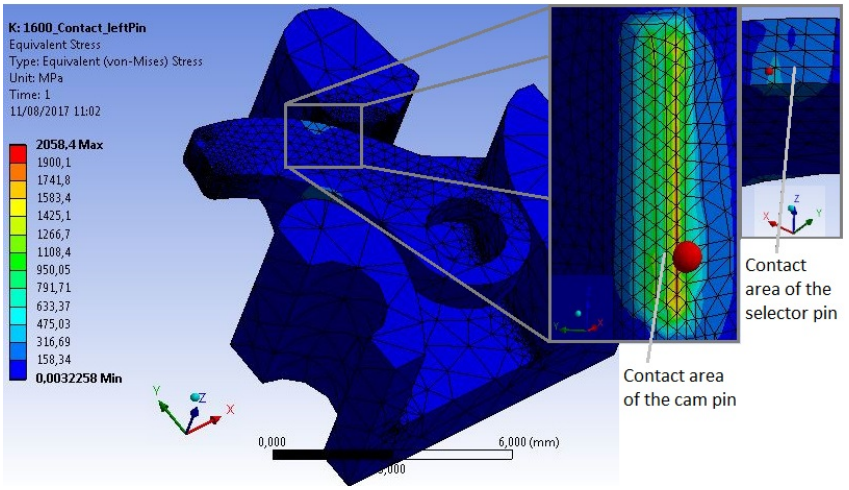

Figure 20: Case 1: Maximal (van-Mises) stresses of the default model, when the left selector pin is used. Close ups of the contact areas of the selector and cam pin are shown.

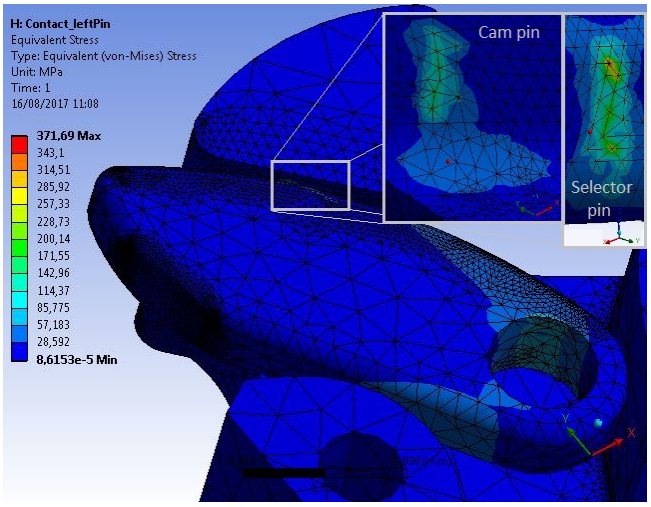

Figure 21: Case 1: Maximal (van-Mises) stresses of the cam pin, when the first adjusted model is used. A close up of the contact area of the cam pin as well as the selector pin are shown as well.

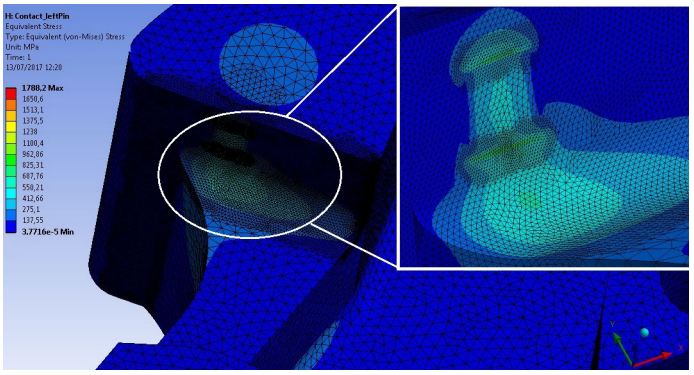

Figure 22: Case 2: Maximal (von-Mises) stresses of the adjusted cam pin, when the left adjusted selector pin is used. A close up of its contact area is shown in the upper right corner.

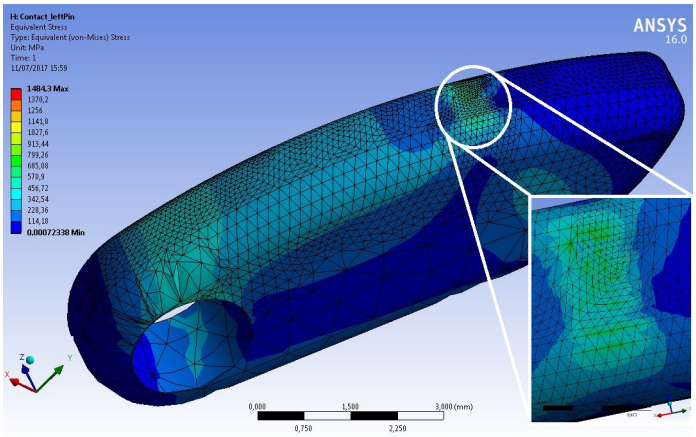

Figure 23: Case 2: Maximal (von-Mises) stresses of the left adjusted selector pin with a close up of its contact area is shown in the bottom right corner.

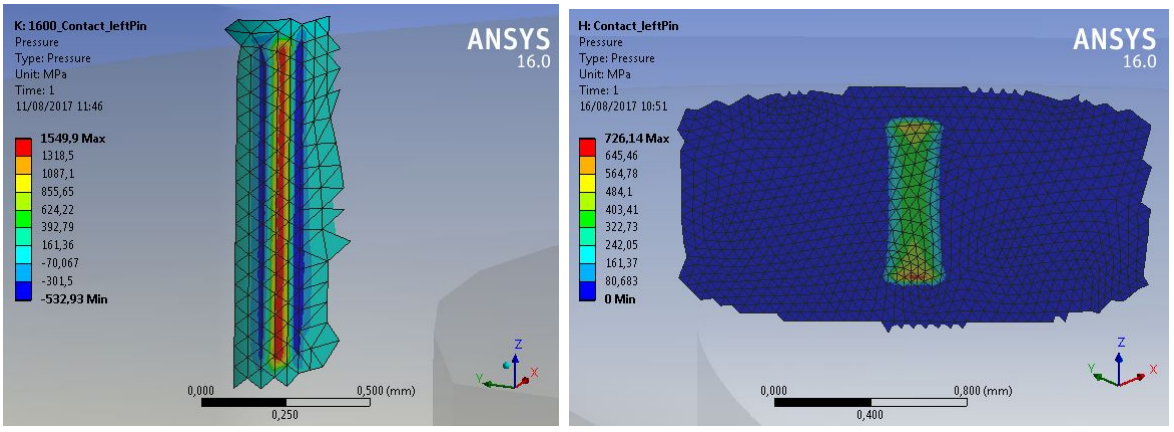

Figure 24: Case 1: Pressure of the contact area of the first default (left) and adjusted model (right), using the left selector pin.

Moreover, two irregularities of the results are noticed. First, the given pressure of the first default model shows in its first case not only compression, but also tension values next to the maximal pressure, reaching a negative maximum of -533 MPa.

Second, the performance of the models improved with the adjusted models in all categories, but one. As it can be seen in Table 5, the second adjusted model decreases its performance in the first case by 27% regarding the maximal deformation.

In addition, when using the Equation 12 for the stainless steel 39NICrMo3 we retrieve a maximal allowed pressure ($P_{Hz,10^7}$) of 954.8 MPa when loading the device 10^7 times. Since the obtained pressures are higher by 132 MPa and 2279.2 for the first and second default models of the first case, surface fatigue will occur when loading the device 10^7 times.

Additionally, the adjusted models for the first case have lower pressure values by 391 MPa and 515 MPa compared to the $P_{Hz,10^7}$. As a result, no surface fatigue will appear for the life cycle of 10^7. Yet, when the second case is applied to the adjusted models, the pressures increases again above $P_{Hz,10^7} = 954.8$ MPa with values between 1844 MPa and

2518 MPa.

Figures of All Results

In the following, the results of the FEM analyzes of both models (left and right selector pin) are shown for the first and second case (Case 1: 5 kg, Case 2: 50 kg) in the default and adjusted version. First, the results of the unadjusted (default) designs are shown for both cases and afterwards the results of the adjusted models. Here, only the maximal values of the total deformation, (van-Mises) stresses and the pressures will be mentioned beside the visual FEM output. (Notice that in almost all conditions the first mentioned value of the stresses and pressures are based on the chosen mesh size. Yet, the second mentioned values can therefore be considered as the actual (van-Mises) stresses and pressures that occur.

Model 1 and 2, Default Design, Case 1:

The maximal deformation of the first model is at 0.012 mm and of the second model at 0.0036 mm as shown in Figure 25.

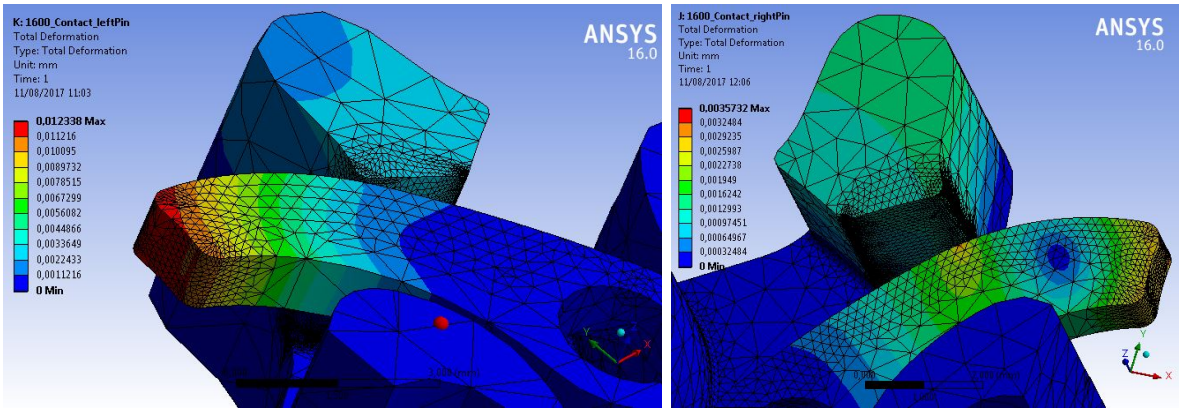

Figure 25: Default models, Case 1: Total deformation of the first (left) and second (right) model.

The maximal (van-Mises) stresses within the first model are between 1425-2058 MPa and within the second model between 1584-1408 MPa as shown in Figure 26-29.

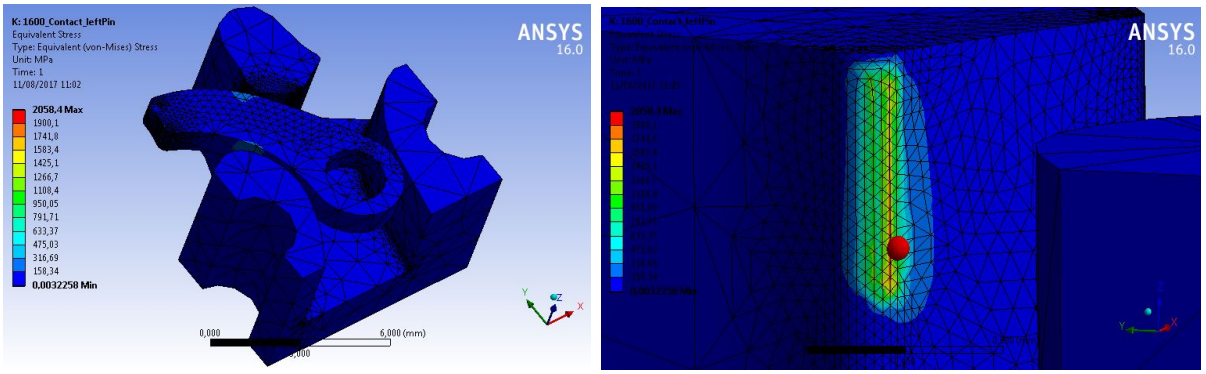

Figure 26: Default Model 1, Case 1: (Van-Mises) stresses. Left: Entire model. Right: Cam pin, contact area.

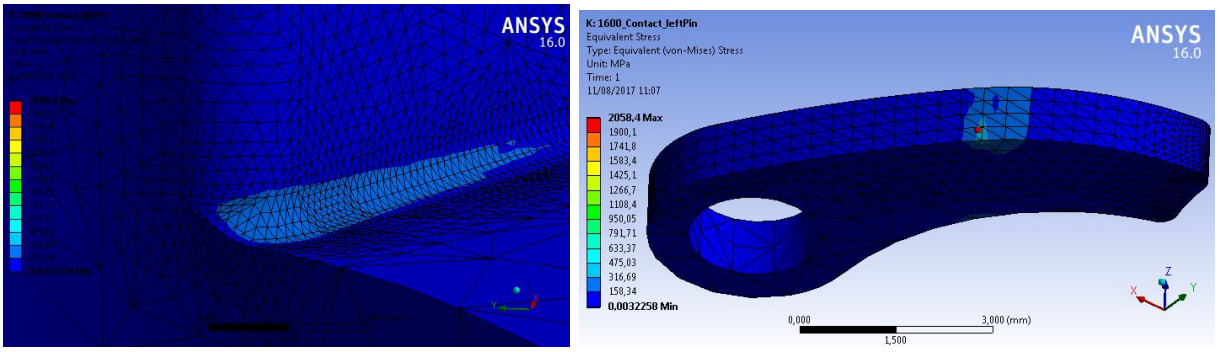

Figure 27: Default Model 1, Case 1: (Van-Mises) stresses. Left: Rounding between cam pin and its basement. Right: Contact surface of the selector pin.

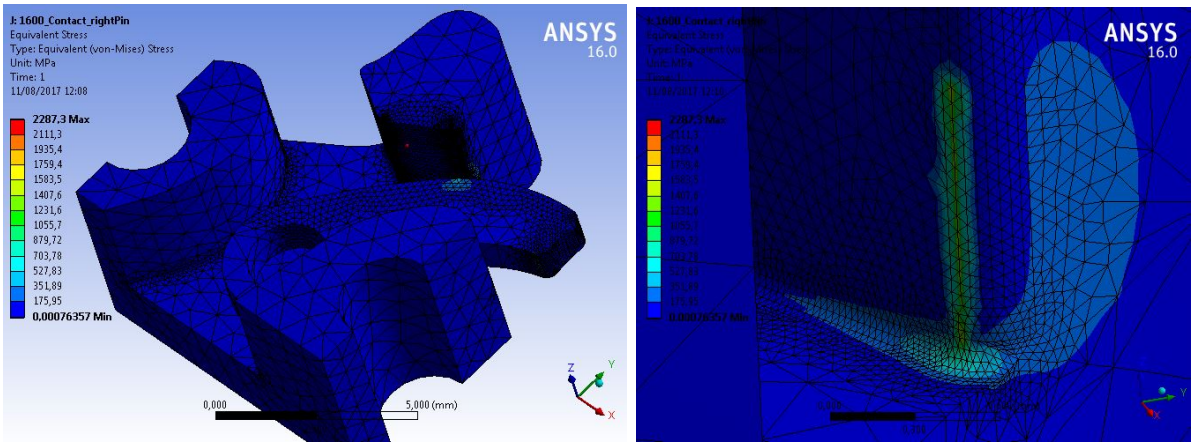

Figure 28: Default Model 2, Case 1: (Van-Mises) stresses. Left: Entire model. Right: Bottom of the cam pin, contact area.

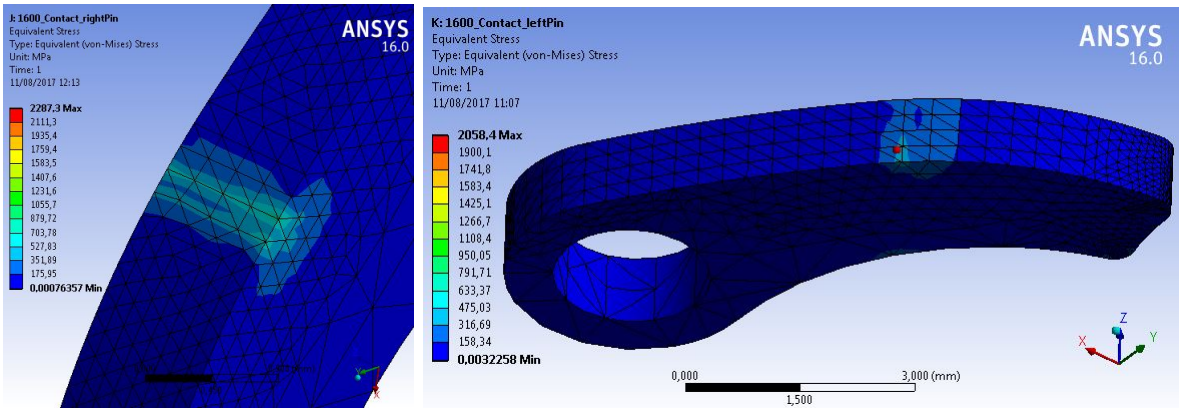

Figure 29: Default Model 2, Case 1: (Van-Mises) stresses. Contact surface of the right selector pin.

The maximal pressure at the contact area of the first model is between 1550 MPa and 1087 MPa and of the second model between 726 MPa and 645 MPa. as shown in Figure 30.

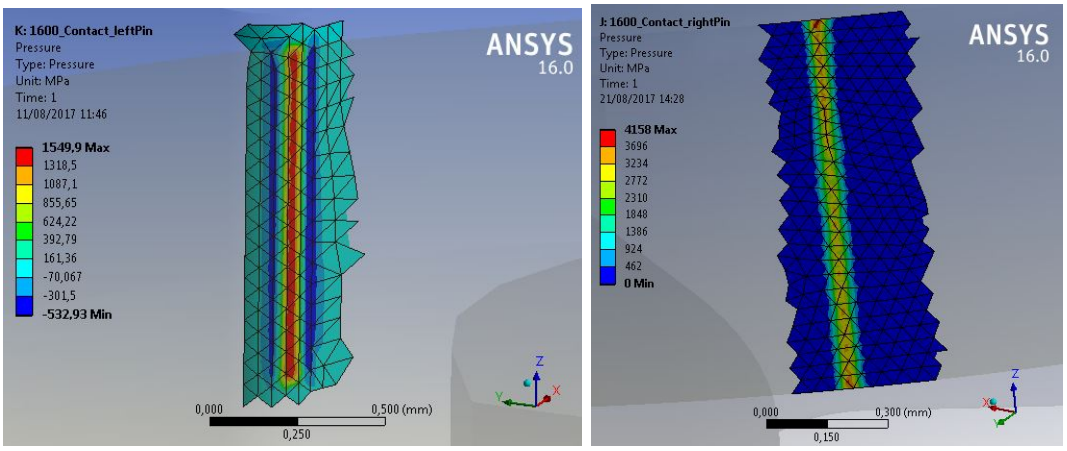

Figure 30: Default Model 1, 2; Case 1: Pressure at the contact area of the first (left) and second (right) model.

Model 1 and 2, Default Design, Case 2:

The maximal deformation of the first model is at 0.13 mm and of the second model at 0.11 mm as shown in Figure 31.

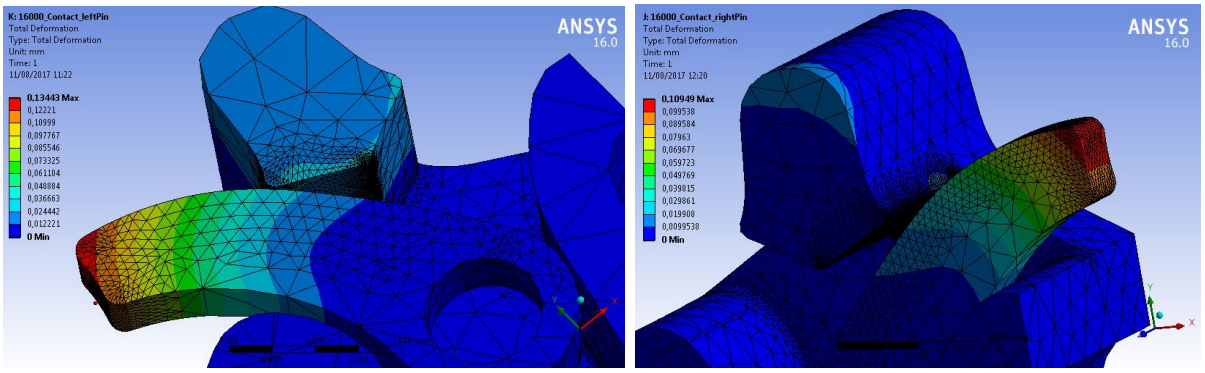

Figure 31: Default Model 1, 2; Case 2: Total deformation of the first (left) and second (right) model.

The maximal (van-Mises) stresses within the first model are between 17465 MPa and 10748 MPa and within the second model between 9739 MPa and 6817 MPa as shown in Figure 32 - 35.

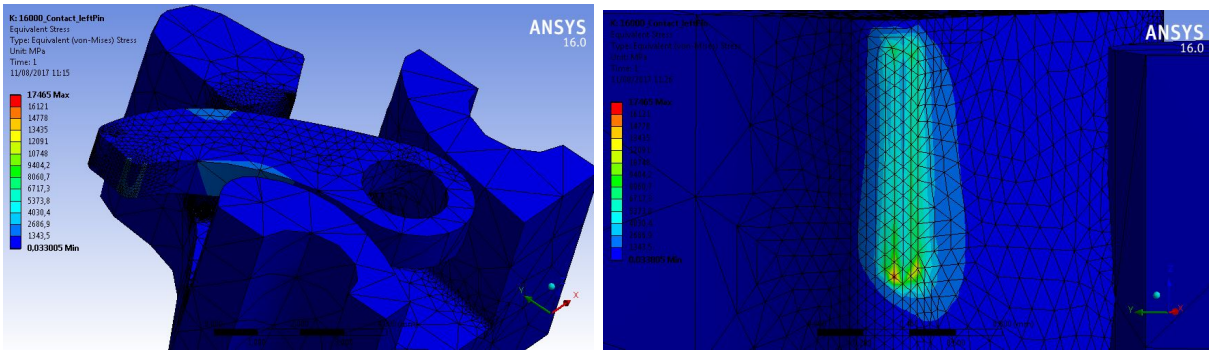

Figure 32: Default Model 1, Case 2: (Van-Mises) stresses. Left: Entire model. Right: Cam pin, contact area.

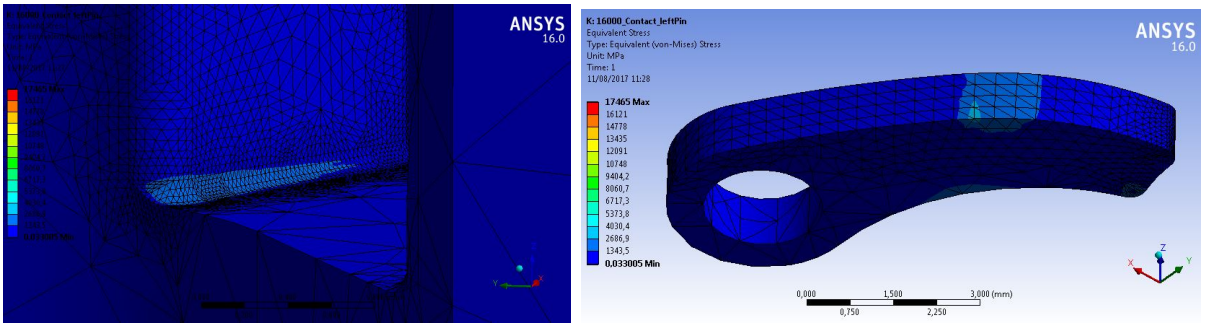

Figure 33: Default Model 1, Case 2: (Van-Mises) stresses. Left: Rounding between cam pin and its basement. Right: Contact surface of the left selector pin.

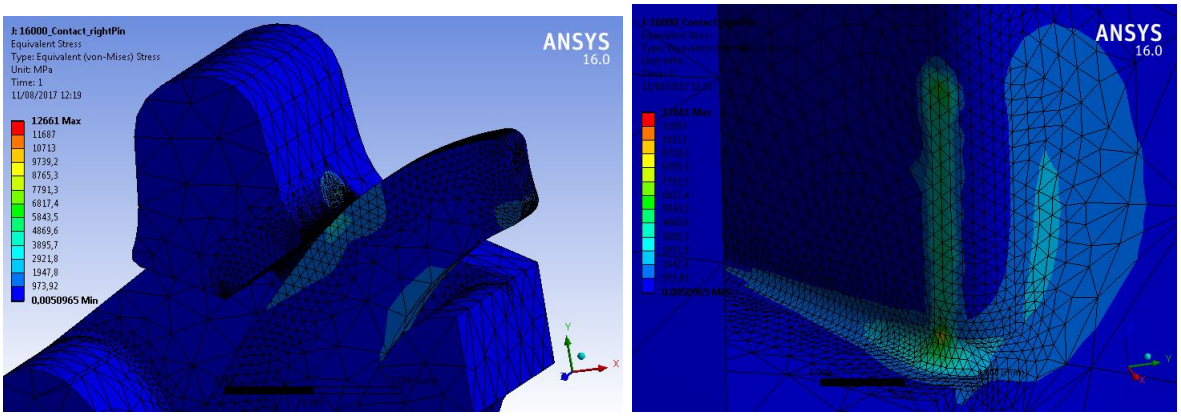

Figure 34: Default Model 2, Case 2: (Van-Mises) stresses. Left: Entire model. Right: Cam pin, contact area with rounding between the cam pin and its basement.

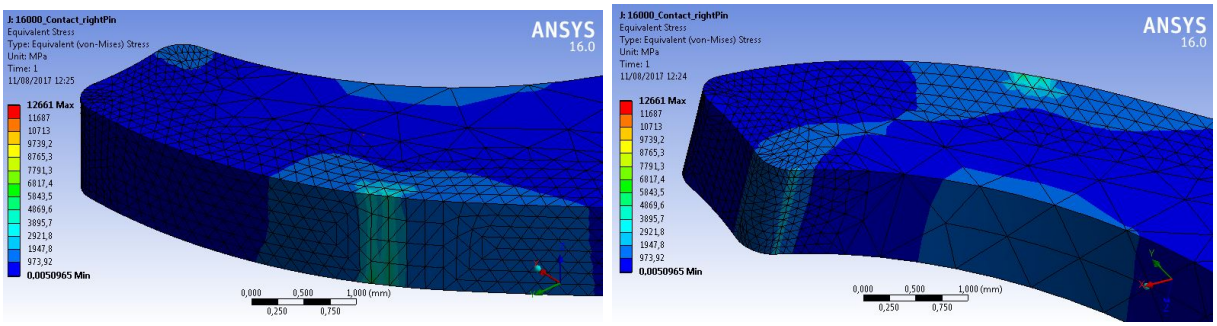

Figure 35: Default Model 2, Case 2: (Van-Mises) stresses. Selector pin seeing its contact surface (left) and its opposite surface (right).

Model 1 and 2, Adjusted Design, Case 1:

The maximal deformation of the first adjusted model is at 0.0043 and at 0.0046 for the second adjusted model as shown in Figure 36.

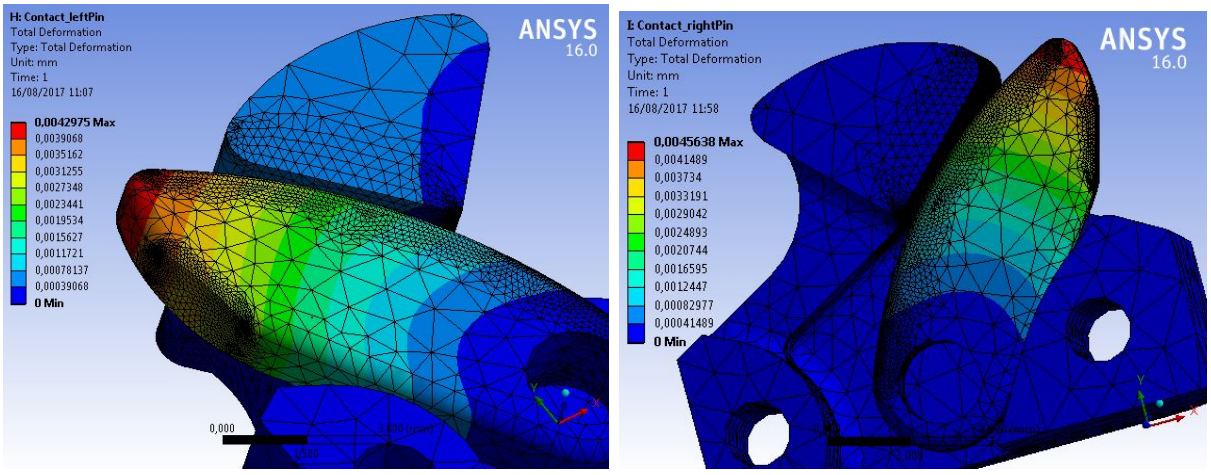

Figure 36: Adjusted Model 1, Case 1: Total deformation of the first (left) and second (right) model.

The maximal (van-Mises) stresses within the first adjusted model are between 372 MPa and 172 MPa and within the second adjusted model between 248 MPa and 174 MPa as shown in Figure 37-40.

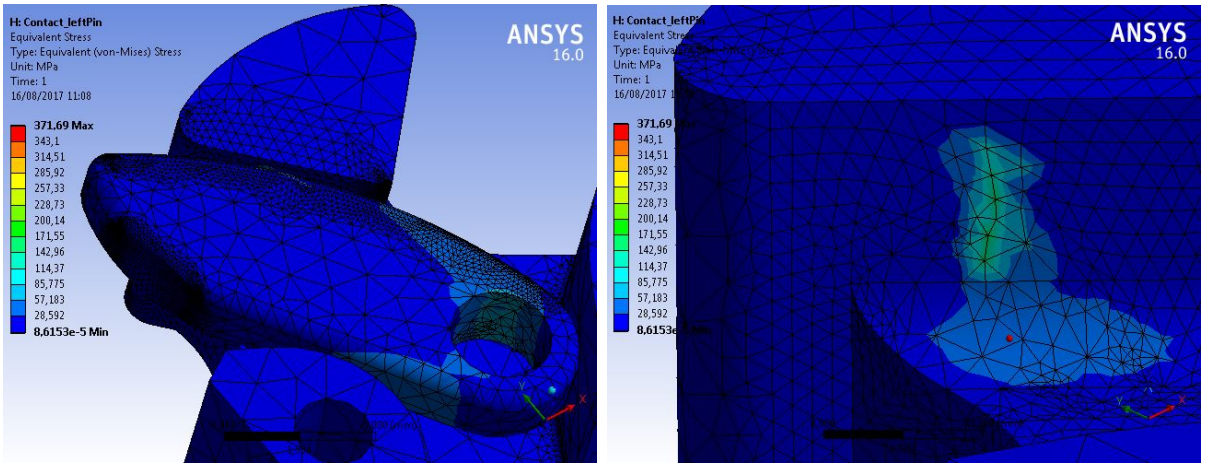

Figure 37: Adjusted Model 1, Case 1: (Van-Mises) stresses of the first model. Left: Entire model. Right: Cam pin, contact area with rounding between cam pin and its basement.

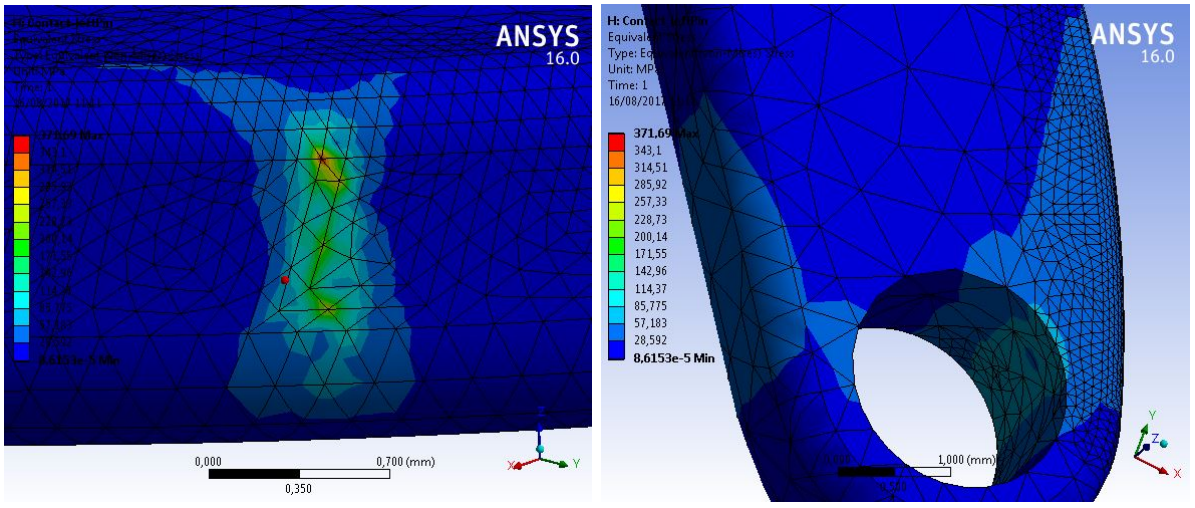

Figure 38: Adjusted Model 1, Case 1: (Van-Mises) stresses. Left: Contact area of the selector pin. Right: Hole area of the selector pin.

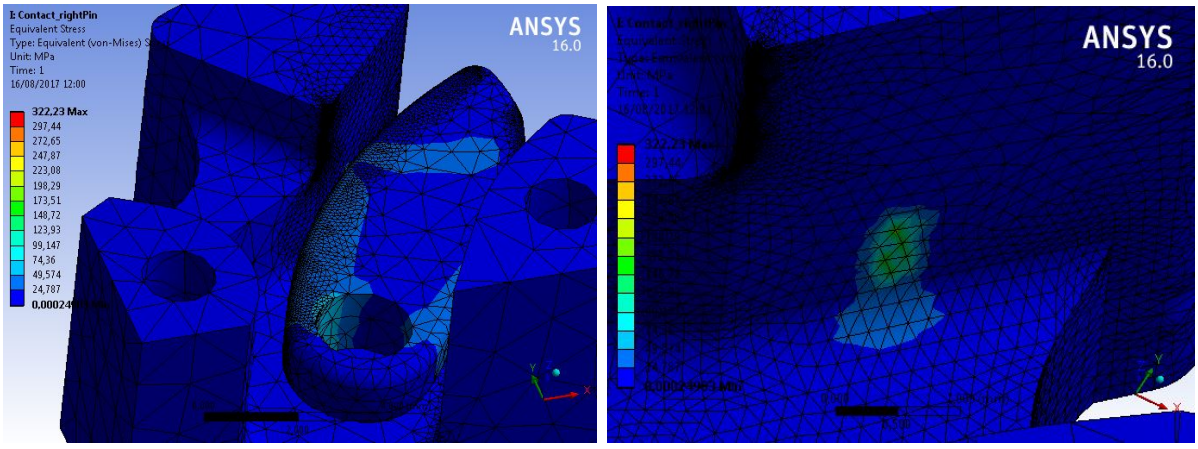

Figure 39: Adjusted Model 2, Case 1: (Van-Mises) stresses. Left: Entire model. Right: Cam pin, contact area with rounding between the cam pin and its basement.

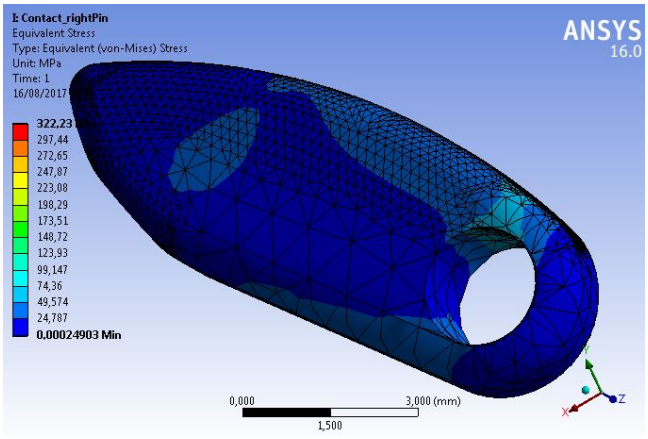

Figure 40: Adjusted Model 2, Case 1: (Van-Mises) stresses of the selector pin.

The maximal pressure at the contact area of the first adjusted model is between 726 MPa and 645 MPa and of the second adjusted model between 566 MPa and 440 MPa as shown in Figure 41.

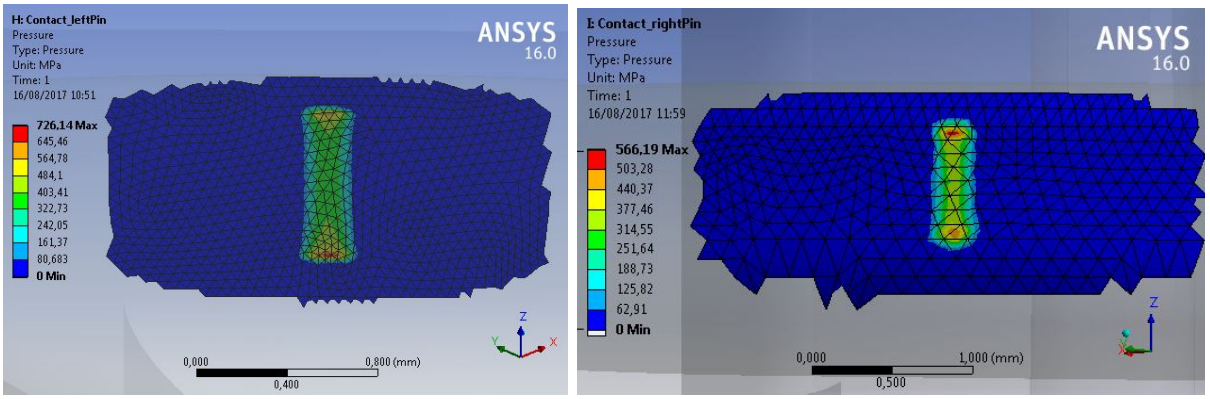

Figure 41: Adjusted Model 1, 2; Case 1: Obtained pressures at the contact areas of the first (left) and second model (right).

Model 1 and 2, Adjusted Design, Case 2:

The maximal deformation of the first adjusted model is at 0.034 mm and of the second adjusted model at 0.036 MPa as shown in Figure 42.

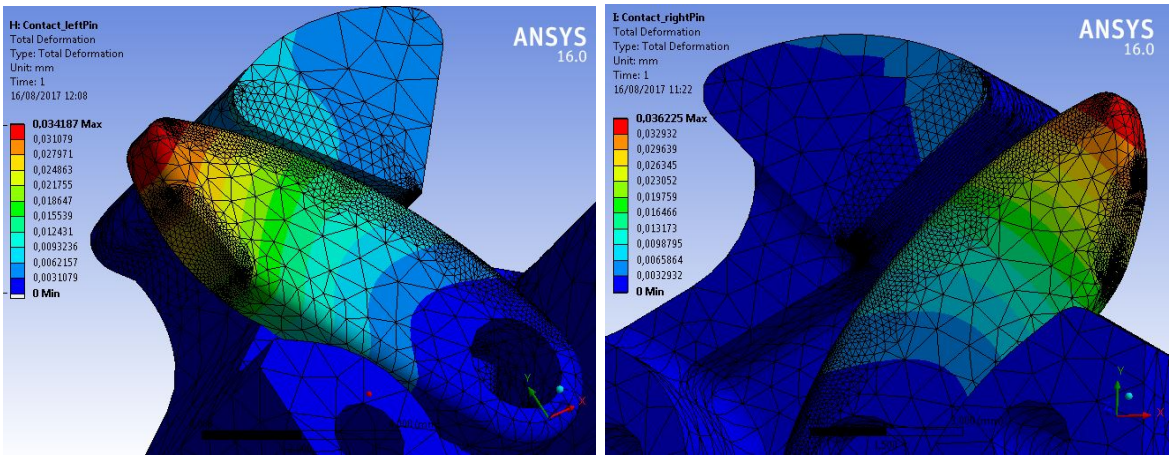

Figure 42: Adjusted Model 1, 2; Case 2: Total deformation of the first (left) and second (right) model.

The maximal (van-Mises) stresses within the first adjusted model are between 963 MPa and 688 MPa and within the second adjusted model between 904 MPa and 703 MPa as shown in Figure 43 - 47.

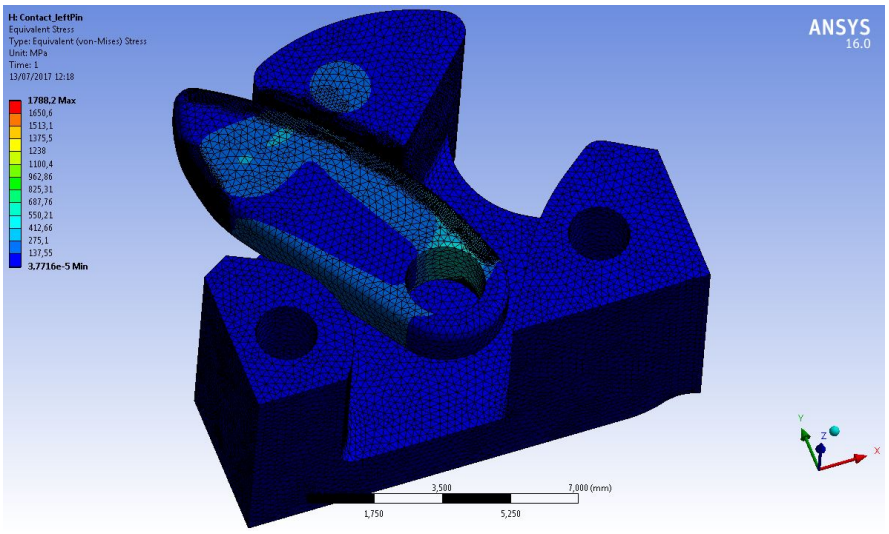

Figure 43: Adjusted Model 1, Case 2: (van-Mises) stresses. Entire model.

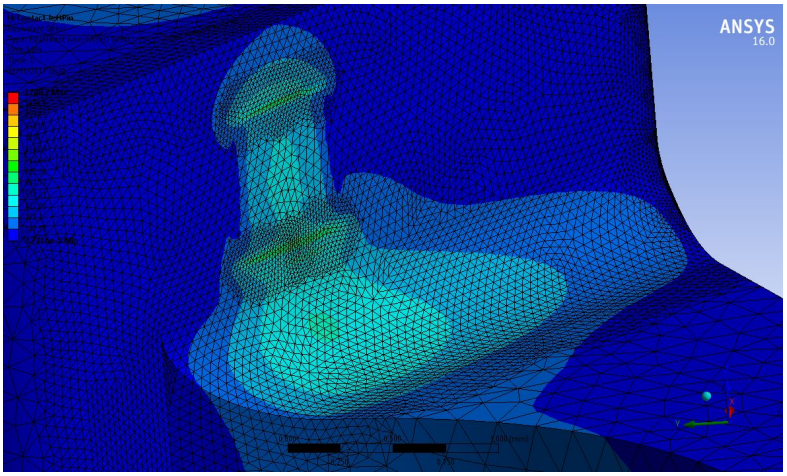

Figure 44: Adjusted Model 1, Case 2: (van-Mises) stresses. Cam pin, contact area with rounding between the cam pin and its basement.

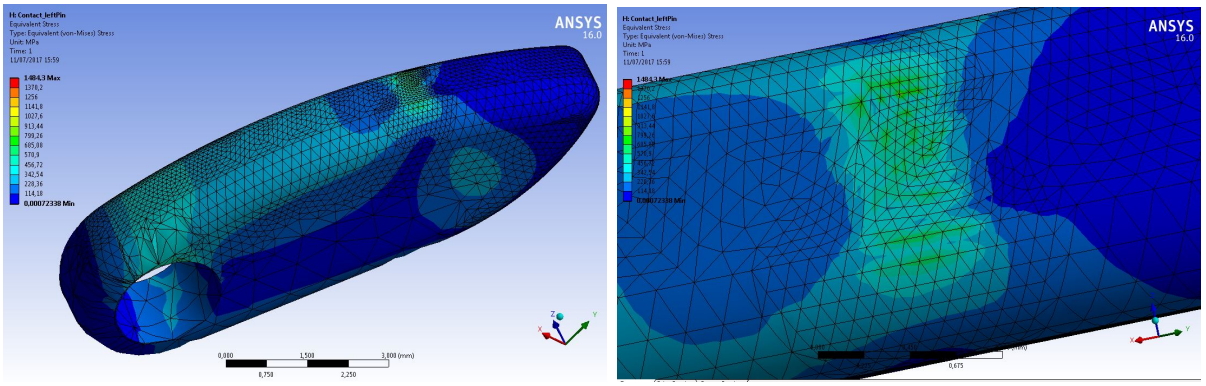

Figure 45: Adjusted Model 1, Case 2: (van-Mises) stresses. Left: Selector pin, contact surface visible. Right: Close up of the contact area of the selector pin.

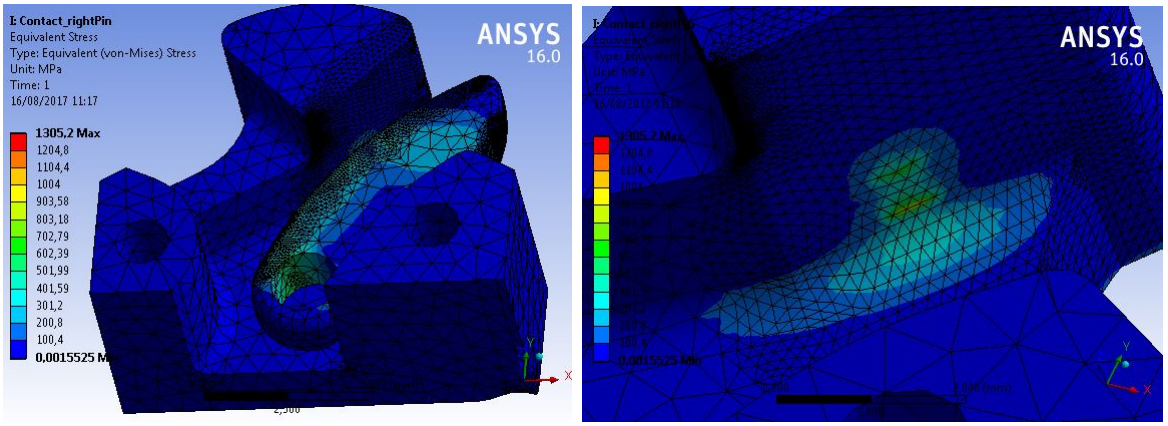

Figure 46: Adjusted Model 2, Case 2: (Van-Mises) stresses. Left: Entire model. Right: Cam pin, contact area and the rounding between the cam pin and its basement.

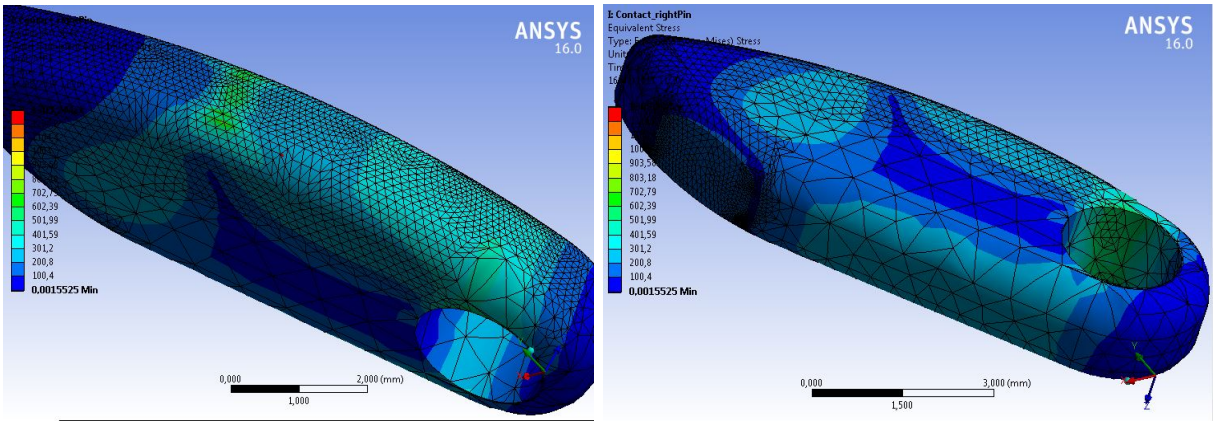

Figure 47: Adjusted Model 2, Case 2: (Van-Mises) stresses. Left: Selector pin, contact surface visible. Right: Selector pin, contact area not visible.

The maximal pressure at the contact area of the first model is between 2833 MPa and 2518 MPa and of the second model between 2371 MPa and 1844 MPa as shown in Figure 48.

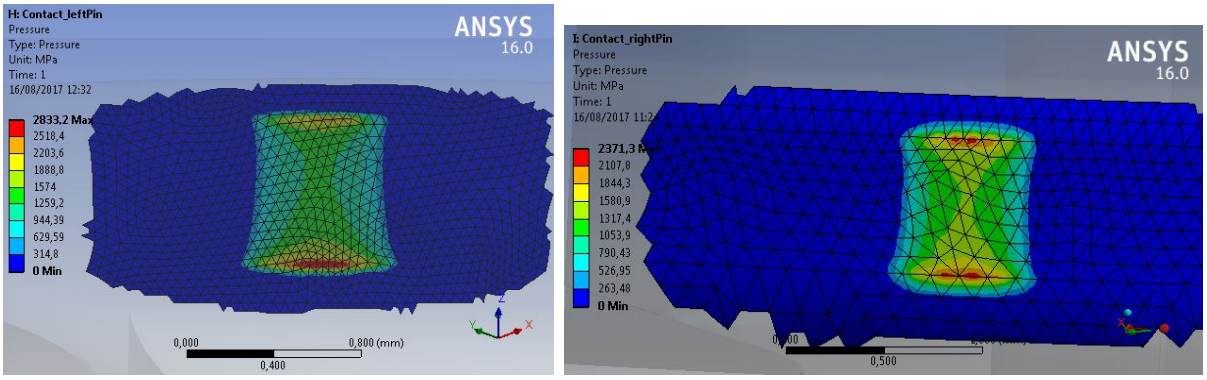

Figure 48: Adjusted Model 1, 2; Case 2: Obtained pressure at the contact areas of the first (left) and second model (right).

Discussion

As it can be seen from the results, the obtained deformations of all models in the first case are very small ranging from 0.0036 mm - 0.012 mm. Hence, it can be considered that the performance of the mechanism will not be influenced by these deformations. This can also be assumed to be true for the second case, even though the deformation increases between 0.034 mm and 0.13 mm. Despite, no performance limitations are expected because the major deformations take place at the tip of the pin, which is not part of the critical area. Critical areas regarding the deformations are the shafts of the selector pins, since the selector pins are moving in cavities with small tolerances with respect to the selector pins. Consequently, deformations on the shaft can lead to performance errors (mechanism could get stuck). However, no high deformations were present at the shaft.

Furthermore, the obtained stresses in the default design when the first case was used resulted in maximal stresses of up to 2058 MPa on the cam pin. This maximal stress

occurred only on a slim vertical node line at the contact edge of the cam pin. Yet, maximal stresses that occur either on single nodes and or in small areas can be neglected. Especially, when the areas of the maximal stresses are smaller than the actual mesh elements, since the high obtained stresses are results of the chosen mesh size. Thus, the near surrounding stresses are considered as the real maximal stresses. Therefore, the most present and now maximal stresses of the first default model of the first case were in the range of 950-1425 MPa (see Fig. 20). Furthermore, it is assumed that the enlargement of the edge's radius decreases the maximal stresses to satisfying results.

Besides, the rounding/curve between the cam pin and the basement of the cam obtained stresses of maximal 880 MPa, which is not acceptable since it is above the yield strength of the desired material (39NiCrMo3, $Rp_{0.2} = 785$ MPa [24]). Yet, the stresses obtained in that curve are assumed to be easily reduced by increasing its radius, lowering the stresses to an acceptable level.

However, since the design was additionally analyzed when it was loaded with 50 kg, more changes of the design were required since the stresses of the entire model increased by far. The maximal (van-Mises) stresses reached a value of 17465 MPa. Yet, the maximal stresses occurred only on two single nodes and result from the chosen mesh size. However, even when neglecting these maximal stresses, the surrounding stresses still reached values of 10748 MPa, which are not acceptable, since they exceed the mentioned yield strength. Consequently, changes of the dimensions and geometry had to be made to compensate for the high stresses.

Based on these changes, increasing the radi and the widths of the elements, the stresses were reduced by 27.8-87.9% for the first case of the first model, by 43.8-87.6% for the first case of the second model, by 57.5-91% for the second case of the first model and by 38.2-94.1% for the second case of the second model. Besides, the pressures of all evaluated conditions decreased as well. Thus, by 48.1% and 86.4%. for the first and second model of the first case.

Anyhow, the deformations were only reduced in three conditions (Case 1, Model 1; Case 2, Model 1 and 2) between 46.2% and 73.8%. In the first case of the second model, the adjustments increased the deformation by 27.8%, which was an unexpected result. However, the maximal deformation of the corresponding default model is at the contact area, instead the adjusted model obtained its maximal deformation at the pin of the tip. Yet, this does not explain the increase itself, but it indicates that the design adjustments switched the position of the maximal deformation. Although, all other FEM analyses showed the same behavior regarding the deformation, thus, it is possible that an error in the FEM set up occurred, explaining the different deformation behavior of the right selector pin.

Moreover, looking at all (van-Mises) stresses of the adjusted model of the first case, it can be stated that the resulting stresses indicate an successful design improvement. This is based on the stresses ranging from 57 MPa to 172 MPa being always below the yield strength. Nevertheless, the stresses of the second case of the adjusted model are only slightly below the yield strength with values between 402 MPa and 686 MPa when neglecting the maximal mesh size induced stresses. Otherwise, the stresses are ranging around the yield strength with a maximal achieved stresses between 799 MPa and 904

MPa.

Nevertheless, even when the yield strength is reached or slightly exceeded, the resulting plastic deformation is assumed to be not as critical as long the maximal stresses occur in small areas. The deformation will be based on compression instead of tension stresses and therefore the material will not be torn apart, but may change slightly its geometry in the affected areas. Hence, it can be considered that after the material has deformed, that the stresses in these areas will decrease.

Yet, as mentioned earlier, compression stresses are not considered as too critical, especially when they only occur in small areas. However, it would be optimal to either change the design further or to pick a material with a higher yield strength, if it is desired to achieve an even higher safety condition than the second case. Otherwise, since the second case represents a maximal, more critical case, it can still be considered as acceptable when lowering the maximal applied load. In addition, since the design criteria did not focus on a high loading of the orthosis, the design should be sufficient enough with the performed changes. Especially, because the modified design reaches acceptable values for the first case.

Furthermore, as stated previously, the pressure of the first default model obtains negative pressure values when the first case is applied. This behavior can be explained. During the FEM analysis, no 'Pinball Region' was set, which considers only the contacting nodes of the two elements in contact (selector pin and cam pin). Consequently, the nodes next to the actual contact of both elements were handled as being in contact, even though there was a small distance between these nodes. Due to this distance, the FEM analysis shows tension leading to negative values in the area next to the actual contact line.

Moreover, to relate the obtained FEM pressure to the real pressure conditions the equation 12 was used, resulting in a value of 954.8 MPa when loading the device 10^7 times. As it was stated in the results, this will lead to surface fatigue of the current chosen material when the load was applied for 10^7 times using the default models with the applied first case and the adjusted models under the application of the second case. Anyhow, the values, especially for the first default model under the first case and the adjusted models of the second case, may still be considered as acceptable for lower cycles taking into account that the P_{Hz} will be higher with a reduced number of cycles.

However, based on the FEM analyzes the following changes were made: The width of the selector pins were increased and its shape was adjusted, taking most of its previous curved geometry away. The input cam was thickened in the area of the cavity where the left selector pins move, and the radi in the corners were increased, which was also done in the cavity of the input cam for the right selector pin. Furthermore, the dimensions of the cam pin were in general increased, whereby the dividing tip of the cam pin is now the thinnest part and its width and length increases towards the output ring.

After all, it can be said that the adjustments improved the performance of the mechanism. Nevertheless, based on the changes, the input cam (outer steel part) resulted in a more complex design. Consequently, making the design more complicated to be manufactured, leading to increasing costs and production time of the items.

9 Component Issues

Based on the manufacturing process of specific elements, issues of some parts were obtained. The selector pins, the connectors as well as the forearm and upper arm element have been laser cut, thus, these parts have some additional unwanted material on few edges and often at their holes. Unfortunately, these additional material, as indicated in Figure 49, was not always completely removable. Hence, it has to be kept in mind that the following results influence the functioning of the mechanism. Furthermore, due to these unexpected conditions, some of the previously chosen tolerances are critical, especially regarding the width and depth of the selector pin cavity of the input cam. Therefore, some additional elements such as washers were used for the assembly of the mechanism to compensate for instance the additional material at the connector elements and the selector pins.

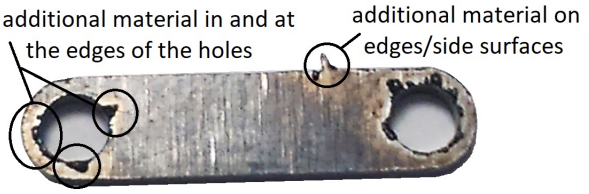

Figure 49: Unwanted, additional material demonstrated on a connector element, resulting from the manufacturing process.

10 MATLAB Codes

The following presented codes were used to compute the assumed torques of the conceptual designs, the optimal roller radius of the final designs and its radial roller forces and the forces within the crank slider mechanism. Furthermore, codes were created to analyze and compare the measured data of the unlocking torques and to generate the figures of the subjective evaluation. Equations related to the drum or disk brake were derived from Juvinall and Marshek [22].

Conceptual Designs

The following code was used to determine the first expected input-output torques/forces and their relations.

```
% Equations to determine the Input-Output force relations between the
% conceptual designs that have been created
 clear all; close all; clc;
% Select desired output force Fout [N]:
Fout = 100;
% basic parameter
g = 9.81;      % m/s^2
%% Push and Twist concept _1 (pen):
% angles [degree]
```

```
alpha = 50.10/180*pi;         % setting 1: 39.62; setting 2: 50.10
% length [m]
r  = 0.018; l = 0.01105; %0.01305;     % setting 1: r = 0.015; l = 0.01605;
%lm = 0.0072;
b1 = 0.00271; b2 = 0.0011;
% masses [kg]
m11 = 0; m21 = 0; m31 = 0;
% forces [N]
%Tin1 = 0.1;    %[Nm]
Fr11 = 0; Fr21 = 0;
% solving for output force:
% Fout1 = (Tin1*cos(asin(r/l*sin(alpha))))/...
%         (r*sin(alpha+asin(r/l*sin(alpha))));
T = (b1*Fout*(r*sin(alpha+asin(r/l*sin(alpha)))))/...
    (b2*cos(asin(r/l*sin(alpha))))
% solving for input Torque with defined output:
% syms t % t for Torque
% T = solve((Fout*b1)/b2 == (t*cos(asin(r/l*sin(alpha))))/...
%         (r*sin(alpha+asin(r/l*sin(alpha)))),t);
% T = double(subs(t,T));

%% Push and Twist, concept _2:
% % angles [degree]
alpha2 = 80/180*pi; %pushed down: 27.02; pulled up: 40.78 degrees
% length [m]
l1  = 0.015; l2  = 0.016; lm3 = 0.0072;
% masses [kg]
m_2 = 2; m12 = 0; m22 = 0; m32 = 0;
% forces [N]
%Fin2  = m_2*g;
Fr12  = 0; Fr22  = 0;
%Fbd2  = (Fin2-Fr12)/sin(alpha2);
        %(Fin2+(m12+m22)*g-Fr12)/sin(alpha2);
%solving for output force
%Fout = Fr22+(Fin2+-Fr12)*tan(alpha2);
        %Fr22+(Fin2+(m12-m22)*g-Fr12)/sin(alpha2)*cos(alpha2);
        % solving for input force with defined output force
syms fin2
Fin2 = solve(Fout == Fr22+(fin2-Fr12)*tan(alpha2));
Fin2 = double(subs(fin2,Fin2));

%% Concept_3 - pneumatic/hydraulic system
% dimensions bellow/cylinder of pipe, stage 1, stage 2
r_p  = 0.01/2;       % [m] not pipe, but other cylinder
r_s1 = 0.034/2;      % [m]
h_s1 = 0.008;        % [m]
r_s2 = 0.015/2;      % [m]
h_s2 = 0.008;        % [m]
% surfaces
Acy1 = r_p^2*pi;         % [m^2], cross-section CS
Acy2 = r_s1^2*pi;        % [m^2], cross-section CS
Al_s1 = 2*r_s1*pi*h_s1; % [m^2], lateralsurface LS
Ac_s2 = r_s2^2*pi;      % [m^2], cross-section CS
Al_s2 = 2*r_s2*pi*h_s2; % [m^2], lateralsurface LS
% solving for Pressure with defined output force
%Pc = Fout/Ac;   % [N/m^2] [Pa]
```

```
%Pl = Fout/Al;   % [N/m^2]

% solving for Input Force with defined output force
%Fin_s1l = Fout/Al_s1 * Acpipe;
Fcy1 = Fout/Acy2 * Acy1;
%Fin_s2l = Fout/Al_s2 * Acpipe;
Fin_s2c = Fout/Ac_s2 * Acy1;
% Stopping force Fst of drum
s   = 0.003;    % m      spring extension
Fsp = 0.5;      % N      Spring force  , 0.5
k   = Fsp/s;    % N/m    Federkonstante
Fb  = -k*s/2;   % N
%Fb= 2;
L=0.066;
R=0.033;
Fch=0;
Ffr=0;
%Fst = -Fb-Fout; % N
%Fa = Fcy1/Acy1*Acy2;
syms fcy1
Fcy1 = solve(0==(fcy1/Acy1*Acy2)*L+(Fout+Fb)*(L/2)+Fch-Ffr*R,fcy1);
Fcy1 = double(subs(fcy1,Fcy1))

%% Concept 8 - drum brake mechanically
p2o  = Fout;
a    = 0.025;
y    = 0.02;
beta = 45/180*pi;

Fin3 = (p2o*cos(beta)*y)^2/a

%% Concept 8, using a twister element (handle):
clc; clear all; close all;
Fout =100;
r = 0.020;
l = 0.010;

alpha = 13.61/180*pi;
syms tin1 % t for Torque
Tin1 = solve (Fout == (tin1*cos(asin(r/l*sin(alpha))))/...
         (r*sin(alpha+asin(r/l*sin(alpha)))), tin1);
Tin1 = double((subs(tin1,Tin1)))

%Tin1 = (Fout * (r*sin(alpha+asin(r/l*sin(alpha)))))/
%cos(asin(r/l*sin(alpha))) %correct, same result as 'solve' equation

%% Concept_4 - push down and shove
 alpha4 = 80/180*pi;
 Fin4 = Fout/tan(alpha4);
 Idea4 = 'Idea 4:\n alpha =%5.2f rad,\n Fin   = %4.3f Nm \n';

%% Concept_5 - gear system
% dimension of gears [m]
r1 = 0.008; % radius input gear
r2 = 0.013; % radius of planetary gear
%r3 = 0.034;
```

```
%Tout=Fout
%Ti = Fout*r1; To = Fout*r2; Tox= Ti * r2/r1; F  = To/r2
% -> Fout = Ti*1/r1; <-     %F =(Ti * r2/r1)/r2

% solving for input Torque with defined output:
Ti = Fout*r1   % Fout*r2*r1/r2
% Ti = (Tout*r1)%/r2;  % (Fout here Tout,[Nm]
% To = Ti*(r2/r1);  %
To = Fout*r2
```

Concept 6, 7 and 8 were evaluated more closely:

```
% Jessica Brand, % TU Delft/ Sant' Anna, 2017
clear all; close all; clc;
%% GENERAL PARAMETERS
m  = 5;          % kg, applied mass on forearm
l  = 0.33;       % m, forearm length/ lever arm
Tw = m*9.81*l;   % Nm, resulted Torque from the applied weight
%% Concept 6 - roller based clutch
b1   = 0.00071;      % lever arm
b2   = 0.0011;       % lever arm
r    = 0.016;        % 1.'arm' of twisting elemet
l    = 0.01105;      % 2.'arm' of twisting elemet

f    = 0.3;          % friction
N    = 12;           % # of rollers
R    = 0.0034;       % radius of roller

alpha = 10.08/180*pi;
%phi1  = 70.08/180*pi;
phi12 = 19.92/180*pi;
%phi2  = 53.4/180*pi;
phi22 = 36.6/180*pi;

Ft = Tw*2/(N*R);                      % tangential force
Fr = Ft*cos(alpha)/sin(alpha);        % radial force
Fu = 2*Fr*(f*cos(alpha)-sin(alpha))   % unlocking force

Fa   = -Fu*cos(phi12)/cos(phi22);
Fout = ((-Fa-Fu)*b1)/b2               % pulling force acting on slider

alpha1 = 43.1/180*pi;
   % alpha =< 43.1 -> no complex number,
   % the smaller alpha the better/smaller the releasing torque
   % 'original': 50.10 degrees

T    = (b1*Fout*(r*sin(alpha1+asin(r/l*sin(alpha1)))))/...
        (b2*cos(asin(r/l*sin(alpha1))))
        % torque to rotate the twisting element

% % % % % %  % % % % % % % %
%Tin1 = solve (Fout == (tin1*cos(asin(r/l*sin(alpha))))/...
%         (r*sin(alpha+asin(r/l*sin(alpha)))), tin1);
%Tin1 = double((subs(tin1,Tin1)))
```

```
%% CLUTCH DISK, concept 7
ri = 0.04;       % m, inner disk radius
ro = 0.035;      % m, outer disk radius
f  = 0.3;        % friction
N  = 2;          % 4 or 8; # of friction surfaces
%Tw = 100;
%F = 5; %N
% T = F*f*((ro+ri)/2)*N   % transmitted torque
Fc = Tw/(f*((ro+ri)/2)*N) % clamping force

% including screw part, for Screw M8
P     = 1.25*10^(-3);     % m, slope
d2    = 7.188*10^(-3);    % m
yk    = 0.16;             % friction on screw
dw    = 11.6*10^(-3);     % m
dm    = 8*10^(-3);        %?! % m
PG    = 5/180*pi;         %?!, Friction angle
Fv    = Fc;               % screw preloaded force = clamping force
phi   = atan((P/(d2*pi))/180*pi); % slope angle
Dkm   = (dw+dm)/2;                % mid 'head-(nuts-)plating diameter
Tlock = Fv*d2/2*(tan(phi+PG)+yk*Dkm/d2) % Locking Torque at screw

% DISK BRAKE
%Tw = 100;
f   = 0.3;          % friction on disks
rm  = 0.0375;        % radius from center to the middle of the pad
A1  = 0.05^2*pi;    % surface output cylinder (2nd cylinder)
Ain = 0.01^2*pi;    % surface input cylinder (1st cylinder)
a   = 0.02;         % lever arm
b   = 0.005;        % lever arm

%T   = 2*f*Fp*rm
Fp    = Tw/(2*f*rm) % Force on each braking pad
Finhy = Fp/A1*Ain   % Input force, hydraulic mechanism
%Finme = Fp*b/a      % Input force, mechanical mechanism

%% Concept 8, Drum Brake
% Parameters and equation by book DRUM BRAKE (book,

Fin = 100;             % Force activating the brakes

% non- selfenergizing %self-locking dimensions:
a   = 0.02975;%0.06152;
b   = 0.03369;%0.01626;
c   = b;
r   = 0.068/2;         % radius drum brake
f   = 0.3;             % friction coefficient

%b = f*a
N = Fin*c/(b-f*a);
T = f*Fin*c*r/(b+f*a)

FinTw = Tw*(b+f*a)/(f*c*r)

% r      = 0.068/2;       % radius m
```

```
% f      = 0.3;           % friction
% N      = 100;           % Norma force
% alpha1 = 11.51/180*pi;
% alpha2 = 141.51/180*pi;
% alpha3 = 65/180*pi;
%
% % Friction radius
% alpha = alpha3;
% rf    = (r*4*sin(alpha/2))/(alpha+sin(alpha));
%
% % Braking Torque Tb
% Tb    = f*N*rf
```

Optimal Roller Radius

In the following, the code is shown to determine the optimal roller radius. Equations are based on the paper by Controzzi et al. [17].

```
% Finding the optimal roller radius
clc; close all; clear all;

Fr      = 71.57%694.88;%689.61;                % [N], from excel
%N       = 12;                    % # of rollers -> nope Nmax
cf1     = -1.16;                 % from excel and paper
s       = 4;%*10^-3;             % desired spacing between rollers
R       = 33.2;%*10^-3;          % inner Ring radius
R2      = 24.43;%*10^-3;          % distance cam - center
v1      = 0.3;                  % steel
v2      = 0.3;                  % steel
E1      = 210000;%207000;%*10^10;         % steel
E2      = 210000;%207000;%*10^10;         % steel

sigmazz  = [];
Nmax     = [];
Frx      = [];
for r    = 0.25:0.125:20 %[0:0.1:8]      % 0.03
R1       = r;                            % roller radius
l        = 4*asin(r/(2*(R2-r)))*(R2-r);  % previously R2=R
delta    = (1/((1/2*R1)+(1/2*R2)))*((1-v1^2)/E1+(1-v2^2)/E2);

Nmaxx    = (2*pi*(R2-r))/(l+s);          % previously R2=R
Nmax     = [Nmax Nmaxx];

Frxx     = Fr/(Nmaxx/2);
Frx      = [Frx Frxx];
b        = sqrt((2*Frxx*delta)/(pi*l));

sigmazzx = b/delta*cf1;
sigmazz  = [sigmazz sigmazzx];  % safe data in vector

        % safe data in vector
end
```

```
r  = 0.25:0.125:20;%[0:0.1:8];

[minSig,Int]= min(-sigmazz);
rminSig     = r(:,Int)
rlow        = rminSig-0.6
rhigh       = rminSig+0.6

% plots
 figure
 plot(r, -sigmazz); hold on
     plot(rminSig, minSig, '*');
 hold off
     title('Relation between the stress and radius')
     xlabel('Radius, r [mm]')
     ylabel(' max. principle stress, \sigma [N/mm^2]')
     grid on
     grid minor

 figure
 plot(r, Nmax); hold on
     plot([rlow rlow], [0, 30], 'r');
     plot([3.48, 3.48],[0, 30], '--g');
     plot([0, 12],[12, 12], '--g');
     plot([rhigh, rhigh],[0, 30], 'r');
     title('Relation between the number of rollers and their radius')
     xlabel('Radius, r [mm]')
     ylabel('max. number of rollers, Nmax')
     grid on
     grid minor
% x = [r, Nmax];
%  figure
%  plot(r, Frx)
%  title('Frx - r')
%  xlabel('Radius r [mm]')
%  ylabel('max. number of rollers N')
%  grid on
```

Subjective Evaluation

In the following, the code for the subjective evaluation was used, especially for creating the plots.

```
% Jessica Brand  % TU Delft/ Sant' Anna, 2017
clear all; close all; clc;
% Subjective ealuation
% forearm values used
% [accaptable, accaptable (1-10mm), (not) accaptable (>10mm)]

a = [7;    9.23; 8.15; 8.09];
b = [7.61; 6.84];%;    0;    0];
c = [8.75; 7.96];%;    0;    0];

group = [repmat({'no changes'}, 4, 1);...
```

```
    repmat({'reduce by 1-10 mm'}, 2, 1); ...
    repmat({'reduce by > 10 mm'}, 2, 1)];

figure(1)
    boxplot([a;b;c], group)
    title('Accaptance related to the forearm diameter')
    ylabel('Forearm diameter d_f [cm]')
    xlabel('Accaptance with or without changes of the prototype diameter')
    grid on
    grid minor
    ylim([6,11])

% Bicep values
d = [8.09; 10.03; 9.14; 9.33];
e = [8.37; 8.09];
f = [9.39; 9.23];

group = [repmat({'no changes'}, 4, 1);...
    repmat({'reduce by 1-10 mm'}, 2, 1); ...
    repmat({'reduce by > 10 mm'}, 2, 1)];

figure(2)
    boxplot([d;e;f], group)
    title('Accaptance related to the biceps diameter')
    ylabel('Biceps diameter d_b [cm]')
    xlabel('Accaptance with or without changes of the prototype diameter')
    grid on
    grid minor
    ylim([6,11])
 %% Biceps and Forearm values together
close all;
group = [repmat({'no changes, f'}, 4, 1);...
    repmat({'1-10 mm, f'}, 2, 1); ...
    repmat({'> 10 mm, f'}, 2, 1);
    repmat({'no changes, b '}, 4, 1);...
    repmat({'1-10 mm, b'}, 2, 1); ...
    repmat({'> 10 mm, b'}, 2, 1)];

figure(3)
    boxplot([a;b;c;d;e;f], group)
    title('Accaptance Related to the Forearm (f) and Biceps (b) Diameter')
    ylabel('Forearm/Biceps diameter d_{f,b} [cm]')
    xlabel('Accaptance without or with reduction of the prototype diameter')
    grid on
    grid minor
    ylim([6,11])
```

Unlocking Torque of the New Design

The following code generates the theoretical unlocking torque of the new design, when the radial force is determined by the equations used in Controzzi et al. [17]

```
% Jessica Brand % TU Delft/ Sant' Anna, 2017
%% NEW  unlocking condition, set 2
clear all; close all; clc;
% angles [degree]
alpha1 = 51.7/180*pi; alpha2 = 4.11/180*pi; alpha3 = 19/180*pi;
alpha4 = 14.89/180*pi; alpha5 = 56.66/180*pi; alpha6 = 30.64/180*pi;
alpha7 = 19/180*pi;

% distances [mm]
l1 = 14;  l2 = 11;  l3 = 6.52;  l4 = 4.67;  l5 = 11.5;

%forces/moments [N]
%Fr = 715.67; %71.567; % for 1600 or 16000 max torque, excel table
%Fr =  4.67; % condition one: 150 g,  outputTorque = 104.48  Nmm
Fr = 14.02; % condition one: 450 g,  outputTorque = 313,43  Nmm
%Fr = 31.15; % condition one: 1000 g, outputTorque = 696.51  Nmm
%Fr = 62.31; % condition one: 2000 g, outputTorque = 1393.02 Nmm
%Fr = 93.46; % condition one: 3000 g, outputTorque = 2089.53 Nmm

Fb = (Fr*l3)/l4
R2 = (-Fr)*cos(alpha5)+Fb*cos(alpha6)
R1 = Fr*sin(alpha5)-Fb*sin(alpha6)

R3 = (-R2*l5+R1*l5)/l5
R4 = R1-R3*cos(alpha7)
R5 = R2+R3*sin(alpha7)

M = -R4*l1-R5*l1 % unlocking/input Torque,
Madjusted = M/2

%%%%%%%%%%%%%%%%%%%%%%%%%%%%%%%%%%%%%%%%%%%%%%%%%%%%%%%%%%%%
%% NEW  unlocked/pushed out condition, set 1 # NOT USED
clear all; close all; clc;
% angles [degree]
    % alpha1 = /180*pi;  % alpha2 = /180*pi; % alpha3 = 19/180*pi;
    % alpha4 = /180*pi;
alpha5 = 42.98/180*pi;   alpha6 = 5.58/180*pi;  alpha7 = 19/180*pi;
% distances [mm]
l1 = 14;   l2 = 11;   l3 = 7.08;   l4 = 2.83;   l5 = 7.42;
%forces/moments [N]
Fr = 100; %spring force
Fb = (Fr*l3)/l4
R2 = (-Fr)*cos(alpha5)+Fb*cos(alpha6)
R1 = Fr*sin(alpha5)-Fb*sin(alpha6)
R3 = (-R2*l5+R1*l5)/l5
R4 = R1-R3*cos(alpha7)
R5 = R2+R3*sin(alpha7)
M = -R4*l1-R5*l1
% NEW: unlocking forces/moments, (set 2)
% cut 1
```

```
N1 = -R1;
Q1 = -R2;
M1 = 0;
% cut 2
N2 = -R1-Fb*sin(alpha6);
Q2 = -R2+Fb*cos(alpha6);
M2 = -Fb*l4;
% cut 3
N3 = -R1-Fb*sin(alpha6)+Fr*sin(alpha5);
Q3 = -R2+Fb*cos(alpha6)-Fr*cos(alpha5);
M3 = -Fb*l4+Fr*l3;       % unlocking Torque

Matrix = [N1 N2 N3; Q1 Q2 Q3; M1 M2 M3]
```

Computing experimental Unlocking Torques

In the following, the code is shown used for computing the experimental unlocking torques of the new and old mechanism.

```
% Jessica Brand, % TU Delft/ Sant' Anna, 2017
clear all; close all; clc;
% COMPUTING UNLOCKING TORQUE OF THE NEW and OLD DESIGN
%%%%%%%%%%%%%%%%%%%%%%%%%%%%%%%%%%%%%%%%%%%%%%%%%%%%%%%%
% load worspace - NEW design (ND)
% load('w2_450g.mat')  % repetitions for weight: 450 g
% load('w3_1000g.mat') % repetitions for weight: 1000g
% load('w4_2000g.mat') % repetitions for weight: 2000g
% load('w5_3000g.mat') % repetitions for weight: 3000g

% load workspace - OLd design (OD)
% load('w22_450g.mat')  % repetitions for weight: 450 g
% load('w33_1000g.mat') % repetitions for weight: 1000g
% load('w44_2000g.mat') % repetitions for weight: 2000g
 load('w55_3000g.mat') % repetitions for weight: 3000g

% Mechanical Testing of the unlocking Torque
% l = 24;                     % [mm], lever arm to Fu, NEW Design
l = 64;                       % [mm], lever arm to Fu, OLD Design

% Repititions NEW and OLD Design
% In the following:
% for the new design: xi = row-1 (if not stated differently)
% for the old design: xi = m-1 (if nt stated differently)

% repetition 1
diffw1 = diff(wr1(:,2));     % ND, getting differences between ech values
[value,row] = (max(diffw1)); % ND, finding maximum difference between a and b
 %x1  = row-3;                % ND, get a previous value, before jump, (check in data)
  % ND: for weight5: -3       %  because, after the mechanism was unlocked
  %     for weight4: +1       %  the force decreased first before the force
                              %  jumped up, for NEW Design
 [m,n]=size(wr1); x1=m-2;    % OD
  %OD: W2 -6, W4: -4, W5: -2
```

```
 Fu1 = wr1(x1,2);            % ND, obtain unlocking Force
 Tu1 = Fu1*l;                % unlocking Torque of the repitition

% repetition 2
diffw = diff(wr2(:,2));
[value,row] = (max(diffw));
 % x2  = row-1;              % for New desigb
 [m,n]=size(wr2); x2=m-36;    % OD
  %OD: W2:-2, W3:-3, W4:-8, W5: -23
 Fu2 = wr2(x2,2);
 Tu2 = Fu2*l;

% repetition 3
diffw = diff(wr3(:,2));
[value,row] = (max(diffw));
 % x3  = row-16;             % ND: for weight4: -2; weight5: -16; ND
 [m,n]=size(wr3); x3=m-15;    % OD
  %OD: W2&3&4: -2, W5:-15
 Fu3 = wr3(x3,2);
 Tu3 = Fu3*l;

% repetition 4
diffw = diff(wr4(:,2));
[value,row] = (max(diffw));
% x4  = row-2;               % ND: for weight4: -2;
[m,n]=size(wr4); x4=m-16;       % OD
 %OD: W2&3 -3, W4: -2, W5:-16
 Fu4 = wr4(x4,2);
 Tu4 = Fu4*l;

 % repetition 5
diffw = diff(wr5(:,2));
[value,row] = (max(diffw));
 %x5  = row-1;                % ND
 % ND: weight 4&5:
 [m,n]=size(wr5); x5=m-2;     % OD
  %OD: W2&4: -4, W3&5: -2,
 Fu5 = wr5(x5,2);
 Tu5 = Fu5*l;

% mean and SD of repetition values of Fu (unlocking force)
Fur   = [Fu1, Fu2, Fu3, Fu4, Fu5];
Fu    = mean(Fur);
SD_Fu = std(Fur);
Tux   = Fu*l;

Tur   = [Tu1, Tu2, Tu3, Tu4, Tu5];
Tu    = mean(Tur);
SD_Tu = std(Tur);

% Plots
figure(1)
    plot(wr1(:,1),wr1(:,2)); hold on
    plot(wr1(x1,1),wr1(x1,2), '*');
    title('Unlocking Force Fu [N]');
    xlabel('Distance l [mm]');
```

```
    ylabel('Force [N]');
    grid on;
    grid minor;
figure(2)
    plot(wr2(:,1),wr2(:,2)); hold on
    plot(wr2(x2,1),wr2(x2,2), '*');
    title('Unlocking Force Fu [N]');
    xlabel('Distance l [mm]');
    ylabel('Force [N]');
    grid on;
    grid minor;
figure(3)
    plot(wr3(:,1),wr3(:,2)); hold on
    plot(wr3(x3,1),wr3(x3,2), '*');
    title('Unlocking Force Fu [N]');
    xlabel('Distance l [mm]');
    ylabel('Force [N]');
    grid on;
    grid minor;
figure(4)
    plot(wr4(:,1),wr4(:,2)); hold on
    plot(wr4(x4,1),wr4(x4,2), '*');
    title('Unlocking Force Fu [N]');
    xlabel('Distance l [mm]');
    ylabel('Force [N]');
    grid on;
    grid minor;
figure(5)
    plot(wr5(:,1),wr5(:,2)); hold on
    plot(wr5(x5,1),wr5(x5,2), '*');
    title('Unlocking Force Fu [N]');
    xlabel('Distance l [mm]');
    ylabel('Force [N]');
    grid on;
    grid minor;
```

Errors, Differences and Plots of the Unlocking Torques

The following code computes the errors between the theoretical and measured unlocking torques of the old and new design. Furthermore, the differences between obtained (van-Mises) stresses and deformation of the FEM outputs are generated.

```
% Jessica Brand % TU Delft/ Sant' Anna, 2017
clear all; close all; clc;
% ##########################################################
% Differences/Errors of experimental and theoretical unlocking torques
% New Design = ND, Old Design = OD
% ##########################################################
% Parametrs, values
Tro     = [313.43; 696.51; 1393.02; 2089.53]; % Resulting output torque
%Tum_new = [118.07; 190.57; 494.34; 610.44];   % ND, masured Tu
Tum_new = [124.1; 208.2; 471.9; 606];   % ND, masured Tu
Tum_old = [1777.5; 2236.9; 2853.4; 3488.9];   % OD, masured Tu

Tuo_new = [115.48; 256.62; 513.24; 769.85]; % ND, theo. Tu optimal,
Tus_new = [216.43; 480.88; 961.91; 1442.8]; % ND, theo. Tu with selector elements
Tus_adj = [108.2; 240.4; 481; 721.4];       % ND, adjusted theo. Tu with
                                            %     selector elements by a factor of 2
Tuo_old = [93.47; 207.71; 415.42; 623.13];  % OD, theo. Tu, optimal

% Error, ND: expe. - theo. Tu (with selector elements)
  E_mts = (Tus_new-Tum_new)./Tus_new*100;
% Error, ND: expe. - theo. Tu, optimal (without selector elements)
  E_mto_n = (Tuo_new-Tum_new)./Tuo_new*100;
% Error, OD: expe. - theo. Tu, optimal
  E_mto_o = (Tuo_old-Tum_old)./Tuo_old*100;
% Error, Tuo_old - Tuo_new: expe. - theo. Tu, optimal
  E_to_on = (Tuo_new-Tuo_old)./Tuo_new*100;
% Error, Tuo_old - Tum_new: expe. - theo. Tu, optimal
  E_mto_om = (Tuo_old-Tum_new)./Tuo_old*100;
% Error, Tuts - Tuo_new: expe. - theo. Tu, optimal
  E_to_os = (Tus_new-Tuo_new)./Tus_new*100;
% Eror Tus_adj - Tum_new
  E_mtadjs = (Tus_adj-Tum_new)./Tus_adj*100

% Difference theo. optimal:  Tuo_old -  Tuo_new
  Diff_Tu_on = Tuo_old-Tuo_new;
% Difference meas. old vs new:
  Diff_Tu_oldnew = Tum_old-Tum_new;
% Difference: measured output - input torque
  Diff_io_n = (Tro-Tum_new); % ND
  Diff_io_o = (Tro-Tum_old); % OD

% Behaviour
  Tuon_ro = Tuo_new./Tro; % output -theo.input, new, optimal
   % -> Linear behaviour
  Tusn_ro = Tus_new./Tro; % output -theo.input, new, selector elements
   % -> Linear behaviour
  Tuoo_ro = Tuo_old./Tro; % output -theo.input, old, optimal
   % -> Linear behaviour
```

```
  Tum_ro  = Tum_new./Tro;     % output -measured.input, new
  Tro_m   = Tro./Tum_new;
  Tro_mM  = mean(Tro_m);
  Tro_mSD = std(Tro_m);
  % -> almost Linear behaviour, some variations

 %Factor dfference Tum_old-Tum_new
  Tuon    = Tum_old./Tum_new;
  TuonM   = mean(Tuon);
  TuonSD  = std(Tuon);
% Factor dfference Tum_new-Tus_new
  Tums    = Tus_new./Tum_new;
  TumsM   = mean(Tums);
  TumsSD  = std(Tums);
 % Factor dfference Tum_new-Tuo_new
  Tumo    = Tuo_new./Tum_new;
  TumoM   = mean(Tumo);
  TumoSD  = std(Tumo);
 % Factor dfference Tum_old-Tut_old
  Tumto   = Tum_old./Tuo_old;
  TumtoM  = mean(Tumto);
  TumtoSD = std(Tumto);

%% Plots
close all;
 A = [313.4; 696.5; 1393; 2089.5]; %[450;1000,2000;3000]; [1;2;3;4];
 Tumn = [A,Tum_new];
 Tumo = [A,Tum_old];
 Tus_newx = [A,Tus_new];
 Tuo_oldx = [A,Tuo_old];
 Tuo_newx = [A,Tuo_new];
 Tus_adjx = [A,Tus_adj];

 a = 0;  b = 1600;  c = 3600;
 close all;

% ND: measured  vs theoretical torque (selector)
 figure(1)
    plot(Tumn(:,1),Tumn(:,2), '--*'); hold on
    plot(Tus_newx(:,1),Tus_newx(:,2), 'k--*');
    title('Measured vs. Theoretical Unlocking Torque (T_u), New Design');

    xlabel('Resulting Output Torque T_{ro} [Nmm]');
    ylabel('Unlocking Torque T_u [Nmm]');
    legend('measured T_u','theoretical T_u')
    grid on;
    grid minor;
    xlim([300,2200]); ylim([a,b]);
    set(gca,'YTick',[a: 200 :b]);

 % OD: measured  vs optimal theo. Tu
 figure(2)
    plot(Tumo(:,1),Tumo(:,2), '--*'); hold on
    plot(Tuo_oldx(:,1),Tuo_oldx(:,2), 'k--*');
    title('Measured vs. Theoretical Unlocking Torque (T_u), Current Design');
    xlabel('Resulting Output Torque T_{ro} [Nmm]');
```

```
    ylabel('Unlocking Torque T_u [Nmm]');
    legend('measured T_u','theoretical T_u')
    grid on;
    grid minor;
    xlim([300,2200]); ylim([a,c]);
    set(gca,'YTick',[a: 500 :c]);

 figure(3) % combines figure 1 and 2
    plot(Tumo(:,1),Tumo(:,2), 'r--*'); hold on
    plot(Tuo_oldx(:,1),Tuo_oldx(:,2), 'k--*');
    plot(Tumn(:,1),Tumn(:,2), 'r-*'); hold on
    plot(Tus_newx(:,1),Tus_newx(:,2), 'k-*');
    plot(Tuo_newx(:,1),Tuo_newx(:,2), 'g-o');
    plot(Tus_adjx(:,1),Tus_adjx(:,2), 'b-o');
    title('Experimental vs. Theoretical Unlocking Torques (T_u)');
    xlabel('Resulting Output Torque T_{ro} [Nmm]');
    ylabel('Unlocking Torque T_u [Nmm]');
    legend('T_{um-OD}',' T_{ut-OD}',' T_{um-ND}',...
        'T_{uts-ND}','T_{ut-ND}','T_{utsA-ND}')
    grid on;
    grid minor;
    xlim([300,2200]); ylim([a,c]);
    set(gca,'YTick',[a: 500 :c]);

%% ############################################################
% Differences/Errors FEM results default vs. adjusted model
% New Design = ND, Old Design = OD
% ############################################################
clear all; close all; clc;
% Values; order: [deform;stress_sp;stress_cp;stess_r;stress_h,pressure]
% sp = selector pin, cp = cam pin, r = radius/curve between cam pin and its
% basement, h = hole area of the selector pin

% Case 1
C1M1_d = [0.012;475;1425;316;158;1087];  % case1, model1, default design
C1M1_a = [0.0043;172;172;57;114;564];    % case1, model1, adjusted design

C1M2_d = [0.0036;704;1408;880;176;3234]; % case1, model2, default design
C1M2_a = [0.0046;174;174;148;99;440];    % case1, model2, adjusted design
% Case 2
C2M1_d = [0.13;5374;10748;2687;1344];    % case2, model1, default design
C2M1_a = [0.034;686;963;688;571];        % case2, model1, adjusted design

C2M2_d = [0.11;4870;6817;6817;974];      % case2, model2, default design
C2M2_a = [0.036;703;703;402;602];        % case2, model2, adjusted design

% Differences case 1
C1M1 = ((C1M1_d-C1M1_a)./C1M1_d)*100
C1M2 = ((C1M2_d-C1M2_a)./C1M2_d)*100
% Differences case 2
C2M1 = ((C2M1_d-C2M1_a)./C2M1_d)*100
C2M2 = ((C2M2_d-C2M2_a)./C2M2_d)*100
```

11 Technical Drawings

In the following, the technical drawings of the first manufactured stage of the new mechanism are shown in the following order:

1. Selector pin
2. Connector element
3. Twister element
4. Input cam, inner part (aluminum)
5. Input cam, outer part (steel)
6. Additional drawing for the input cam, outer part
7. Output ring
8. Output frame
9. Spacer (between bearings)
10. Cover plate of the input cam
11. Additional drawing of the input cover plate
12. Cover plate of the output frame
13. Forearm element
14. Roller
15. Upper arm element

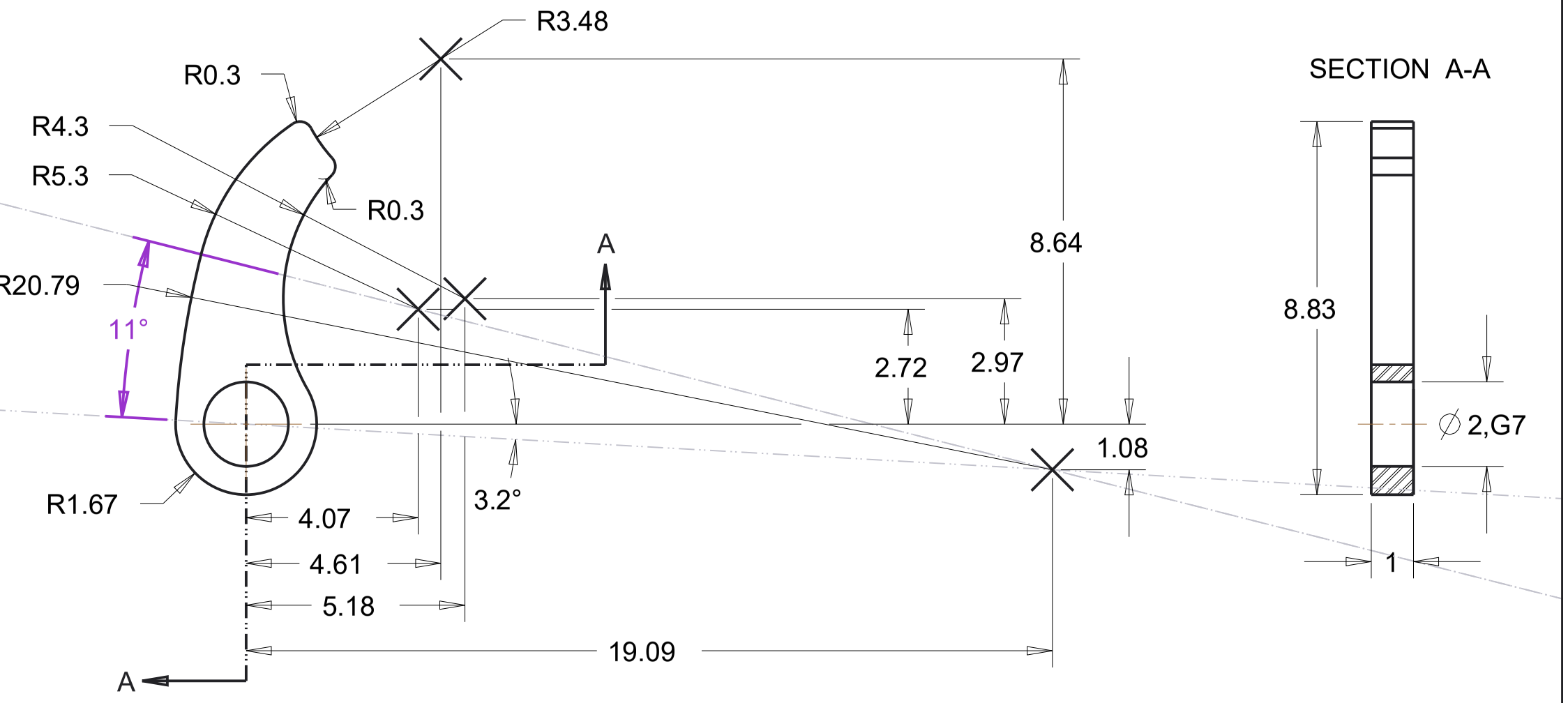

SECTION A-A

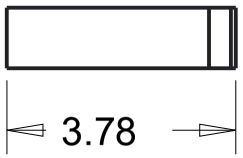

AH Lab - Artificial Hands Laboratory
The BioRobotics Institute - Scuola Superiore Sant'Anna

Part. N. 1	Denominazione: SELECTORPIN_NEWNEW_TRY4W			Materiale: stainless steel
Complessivo	Denominazione: Elbow Joint			Foglio: 1/1
Gruppo	Denominazione:			Scala: 8:1
Sottogruppo	Denominazione:			Data: Jun-13-17
Tolleranze generali UNI ISO 22768	Trattamenti speciali:	Disegnato	Lorenzo Bassi Luciani	Quantità: 12
		Controll.		Sostituisce il: il
		Approvato		Arch. N°:

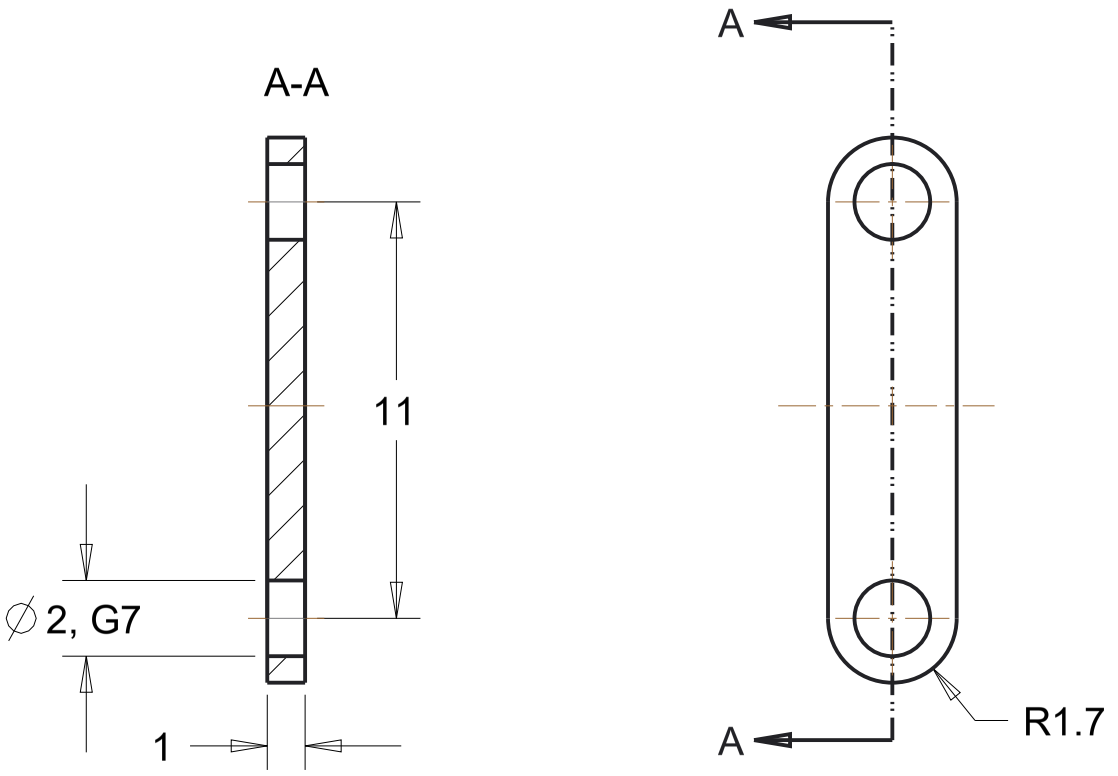

surface treatment: laser cut

AH Lab - Artificial Hands Laboratory The BioRobotics Institute - Scuola Superiore Sant'Anna				
Part. N. 2	Denominazione: CONNECTOR_S1_NEW			Materiale: stainless steel
Complessivo	Denominazione: Elbow joint			Foglio: 1/1
Gruppo	Denominazione:			Scala: 5:1
Sottogruppo	Denominazione:			Data: Jun-07-17
Tolleranze generali UNI ISO 22768	Trattamenti speciali:	Disegnato	Jessica Brand	Quantità: 6
		Controll.		Sostituisce il: il
		Approvato		Arch. N°:

SCALE 1.000

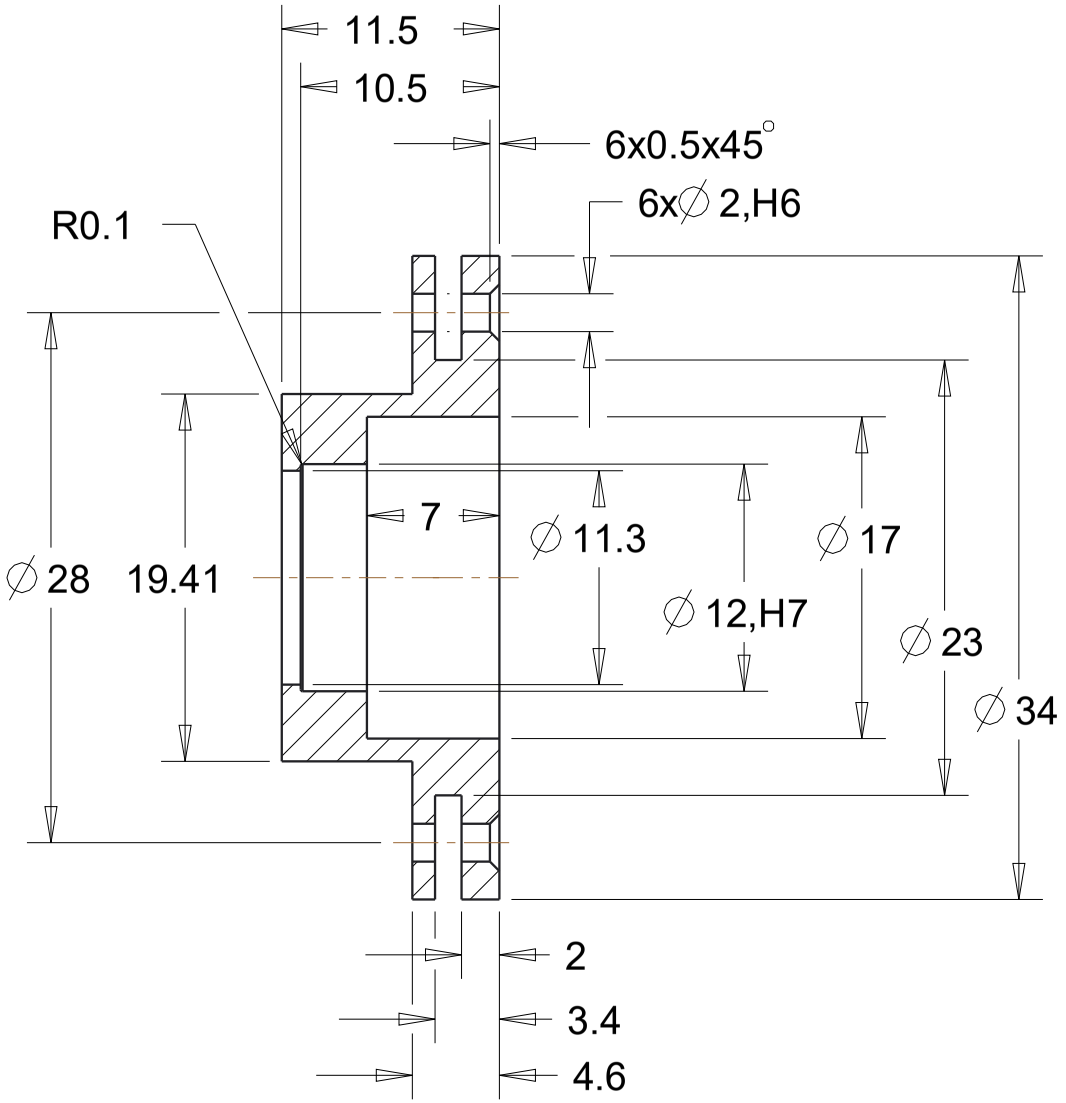

SECTION A-A

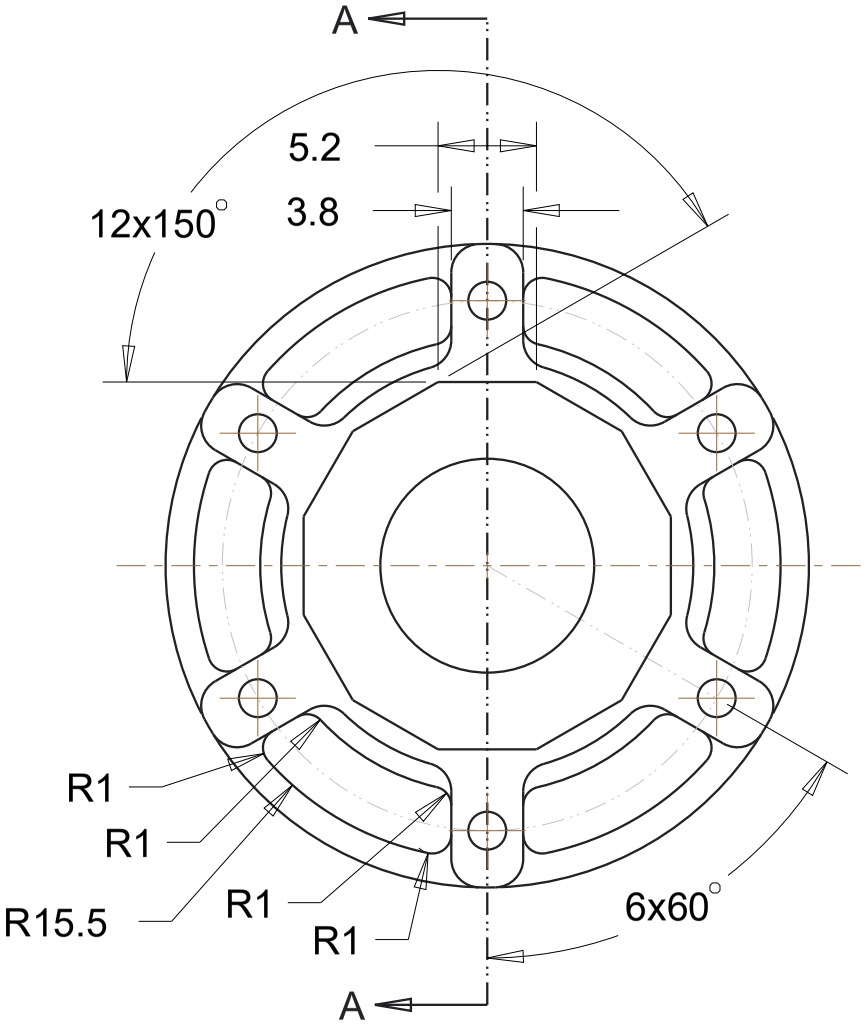

unlabeled R 1.5

SCALE 1.000

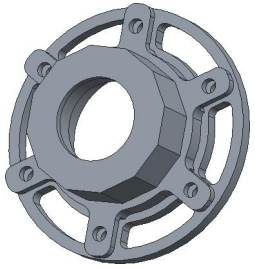

AH Lab - Artificial Hands Laboratory The BioRobotics Institute - Scuola Superiore Sant'Anna				
Part. N. 3	Denominazione: TWISTER_PLA_NEW			Materiale: Engal 7075
Complessivo	Denominazione: Elbow Joint			Foglio: 1/1
Gruppo	Denominazione:			Scala: 2.5:1
Sottogruppo	Denominazione:			Data: Jun-13-17
Tolleranze generali UNI ISO 22768 f	Trattamenti speciali:	Disegnato	Jessica Brand	Quantità: 1
		Controll.		Sostituisce il: il
		Approvato		Arch. N°:

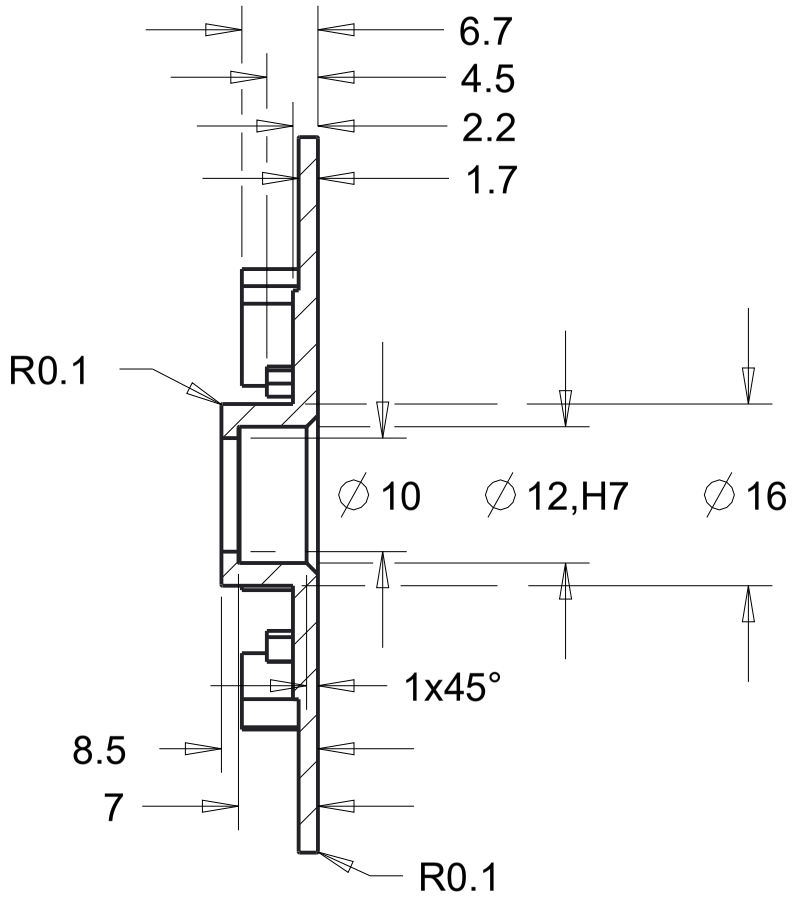

SECTION A-A

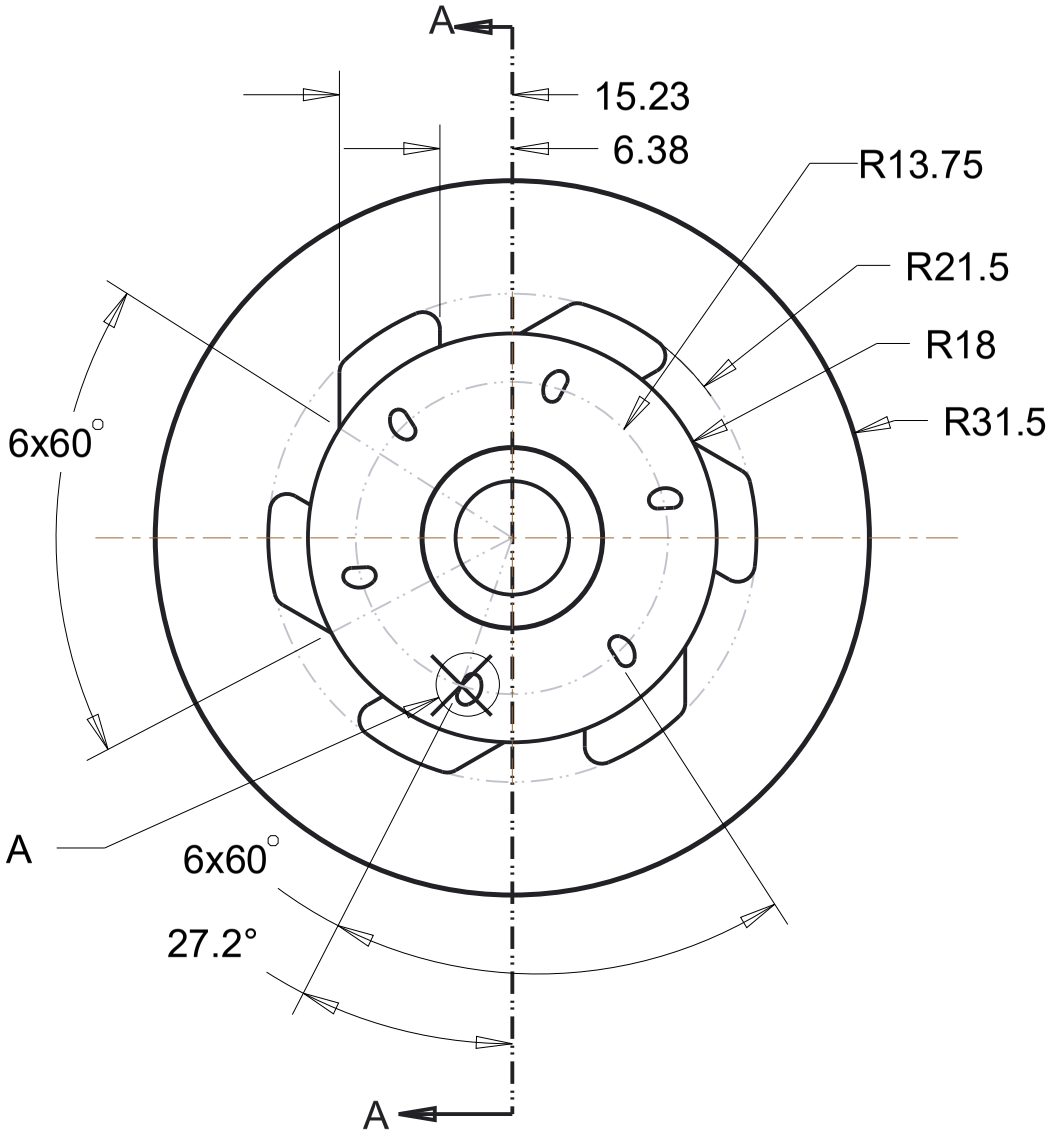

Detail A
SCALE 4.000

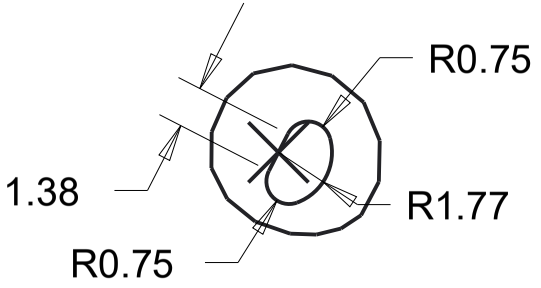

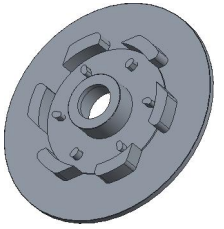

SCALE 0.500

AH Lab - Artificial Hands Laboratory The BioRobotics Institute - Scuola Superiore Sant'Anna				
Part. N. 4	Denominazione: CAM_PLA_NEWNEW_TRY2			Materiale: Engal 7075
Complessivo	Denominazione: Elbow Joint			Foglio: 1/1
Gruppo	Denominazione:			Scala: 1.5:1
Sottogruppo	Denominazione:			Data: Jun-08-17
Tolleranze generali UNI ISO 22768 f	Trattamenti speciali:	Disegnato	Jessica Brand	Quantità: 1
		Controll.		Sostituisce il: il
		Approvato		Arch. N°:

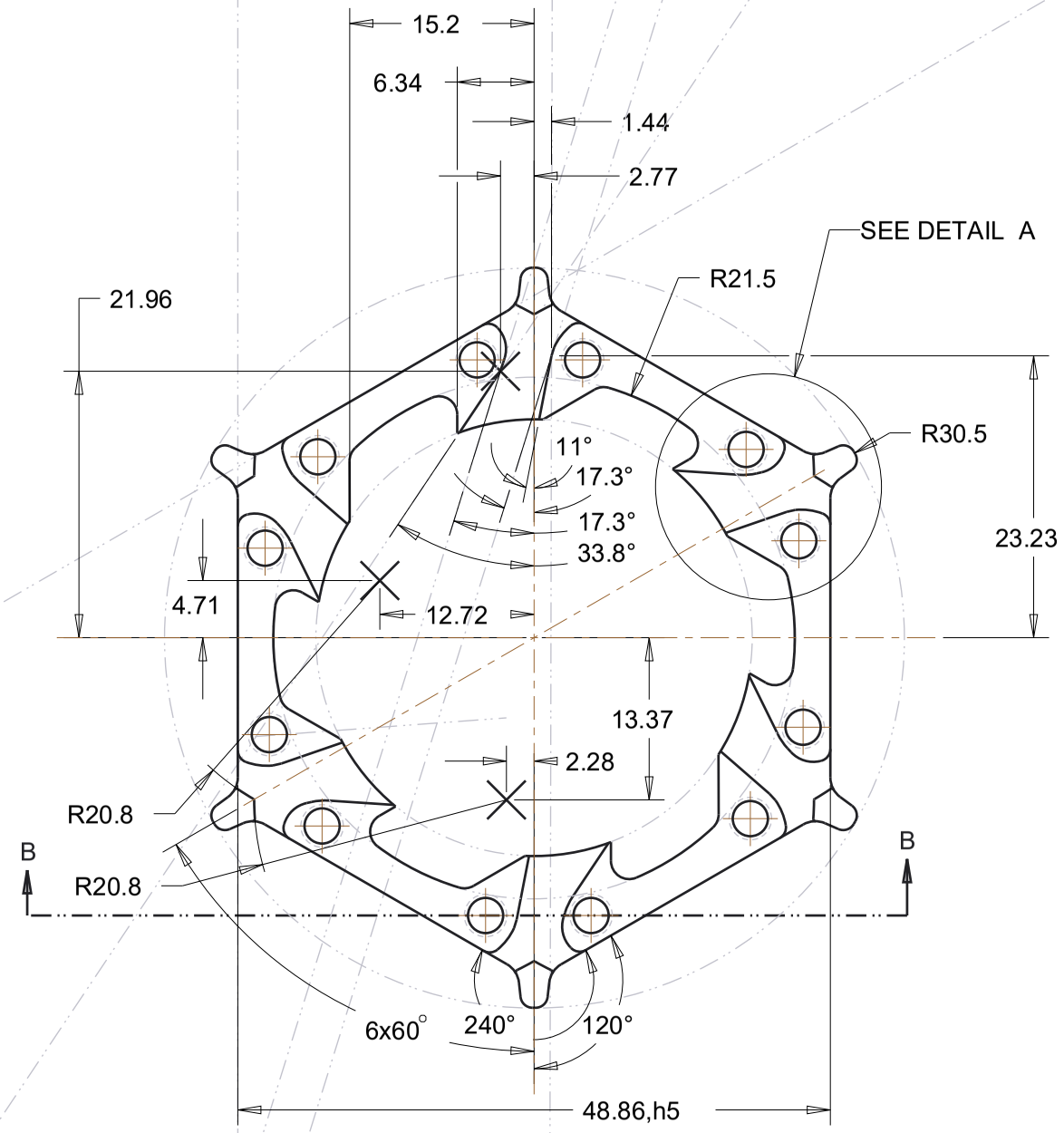

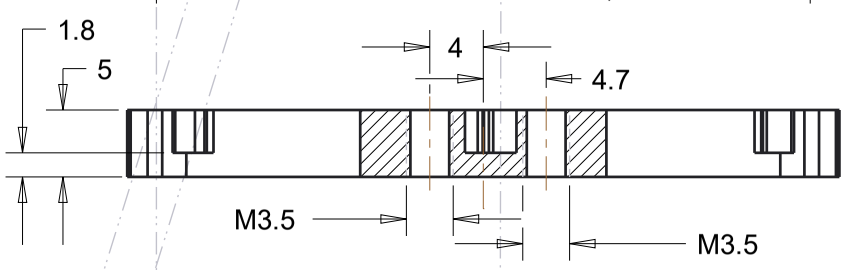

SECTION B-B

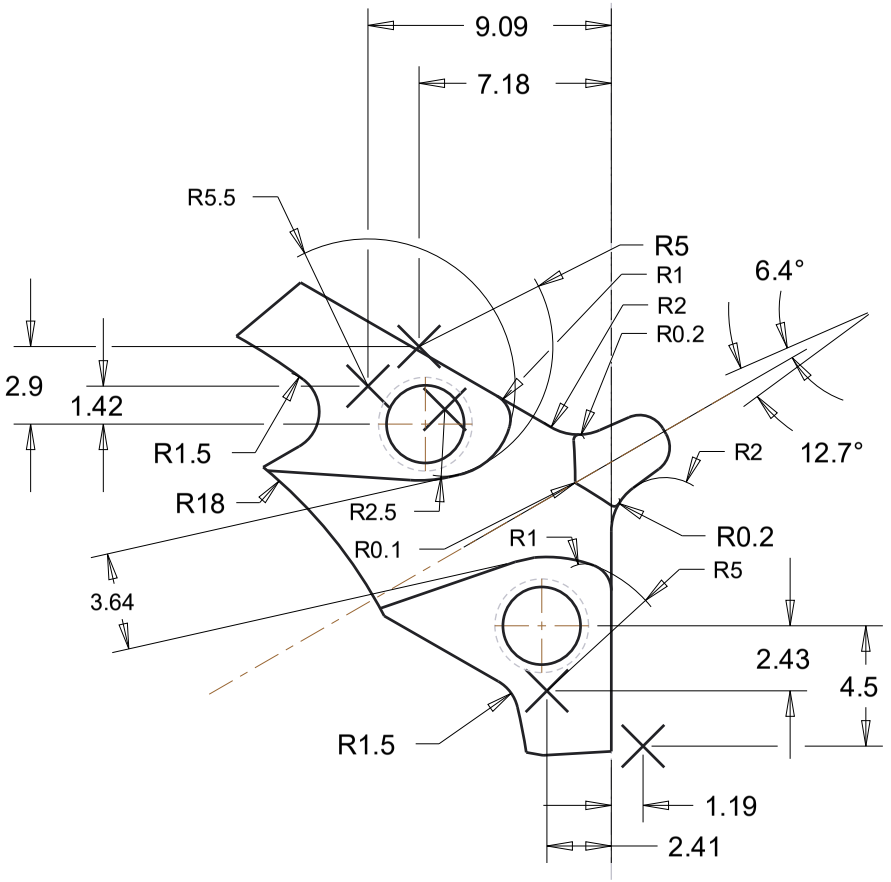

DETAIL A
SCALE 5.000

AH Lab - Artificial Hands Laboratory The BioRobotics Institute - Scuola Superiore Sant'Anna				
Part. N. 5	Denominazione: CAM_ME_NEWNEW_TRY2			Materiale: stainless steel
Complessivo	Denominazione: Elbow Joint			Foglio: 1/1
Gruppo	Denominazione:			Scala: 2.5:1
Sottogruppo	Denominazione:			Data: Jun-08-17
Tolleranze generali UNI ISO 22768 f	Trattamenti speciali:	Disegnato	Jessica Brand	Quantità: 1
		Controll.		Sostituisce il: il
		Approvato		Arch. N°:

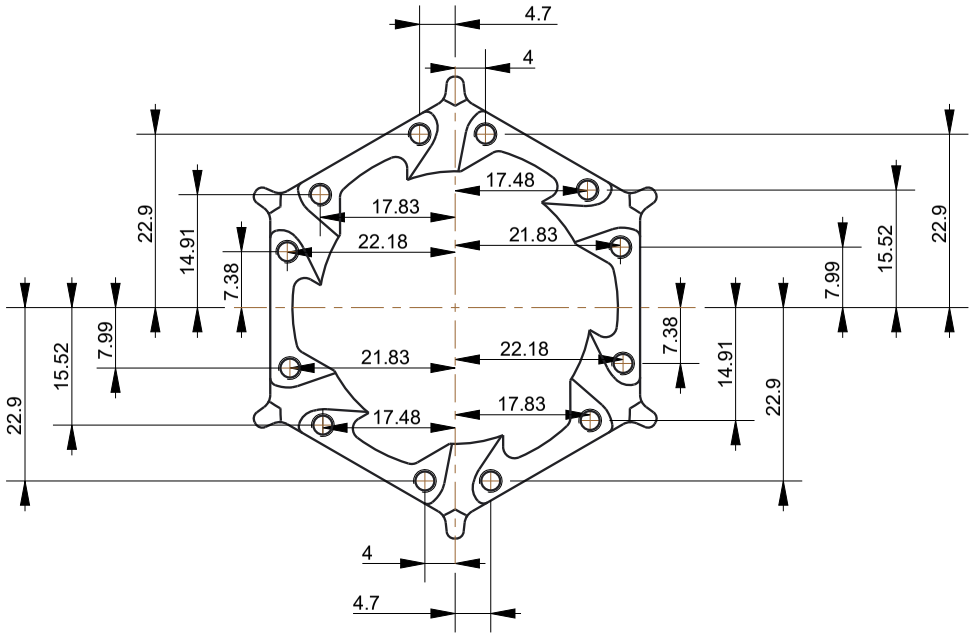

AH Lab - Artificial Hands Laboratory The BioRobotics Institute - Scuola Superiore Sant'Anna				
Part. N. 5	Denominazione: CAM_ME_NEWNEW_TRY2			Materiale: stainless steel
Complessivo	Denominazione: elbow joint			Foglio: 1/1
Gruppo	Denominazione:			Scala: 1:1
Sottogruppo	Denominazione:			Data: 17-Jun-23
Tolleranze generali UNI ISO 22768	Trattamenti speciali:	Disegnato	Jessica Brand	Quantità: 1
		Controll.		Sostituisce il: il
		Approvato		Arch. N°:

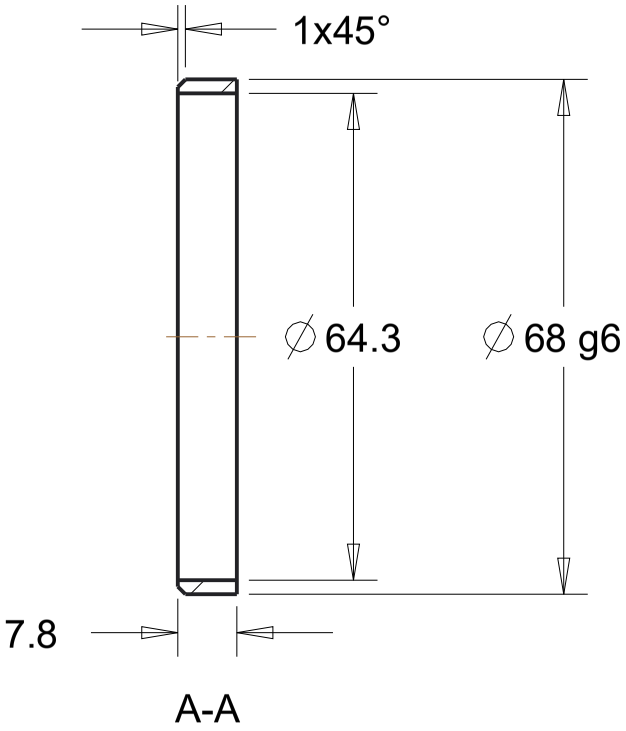

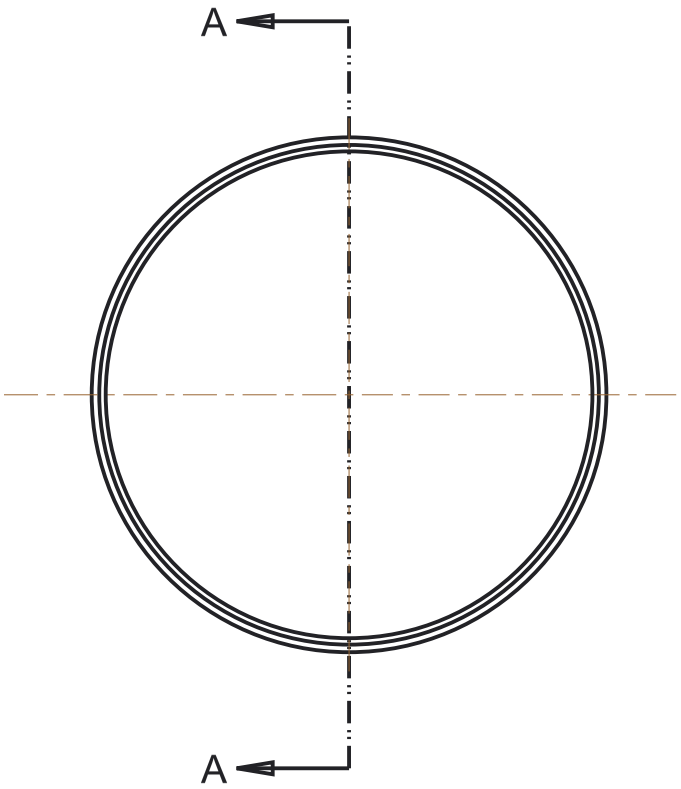

AH Lab - Artificial Hands Laboratory The BioRobotics Institute - Scuola Superiore Sant'Anna				
Part. N. 6	Denominazione: OUTPUTRING_NEW			Materiale: Stainless steel
Complessivo	Denominazione: Elbow Joint			Foglio: 1/1
Gruppo	Denominazione:			Scala: 1:1
Sottogruppo	Denominazione:			Data: Jun-08-17
Tolleranze generali UNI ISO 22768	Trattamenti speciali:	Disegnato	Jessica Brand	Quantità: 1
		Controll.		Sostituisce il: il
		Approvato		Arch. N°:

AH Lab - Artificial Hands Laboratory
The BioRobotics Institute - Scuola Superiore Sant'Anna

Part. N. 7	Denominazione: OUTPUTFRAME_PLA_NEW			Materiale: Engal 7075
Complessivo	Denominazione: Elbow Joint			Foglio: 1/1
Gruppo	Denominazione:			Scala: 1:1
Sottogruppo	Denominazione:			Data: Jun-08-17
Tolleranze generali UNI ISO 22768	Trattamenti speciali:	Disegnato	Jessica Brand	Quantità: 1
		Controll.		Sostituisce il: il
		Approvato		Arch. N°:

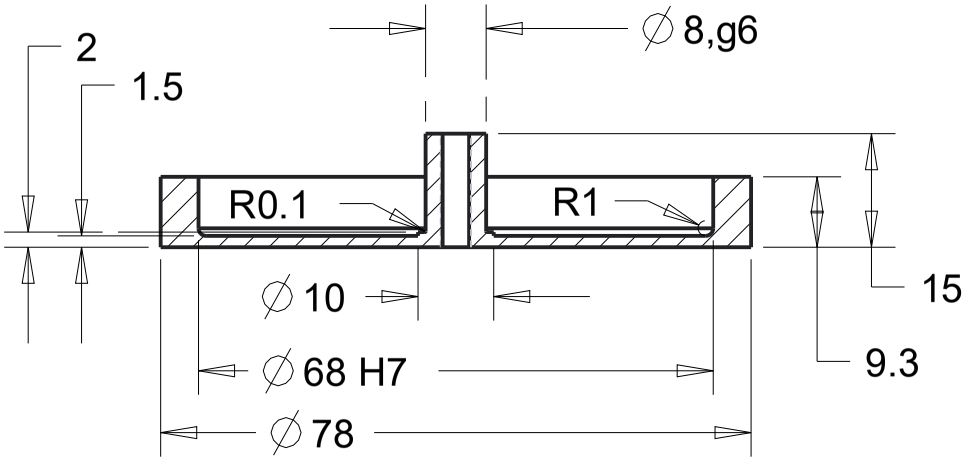

A-A

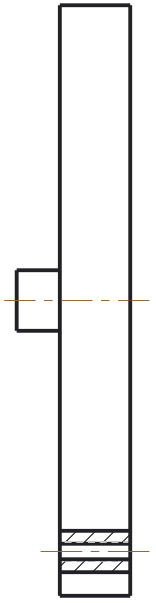

B-B

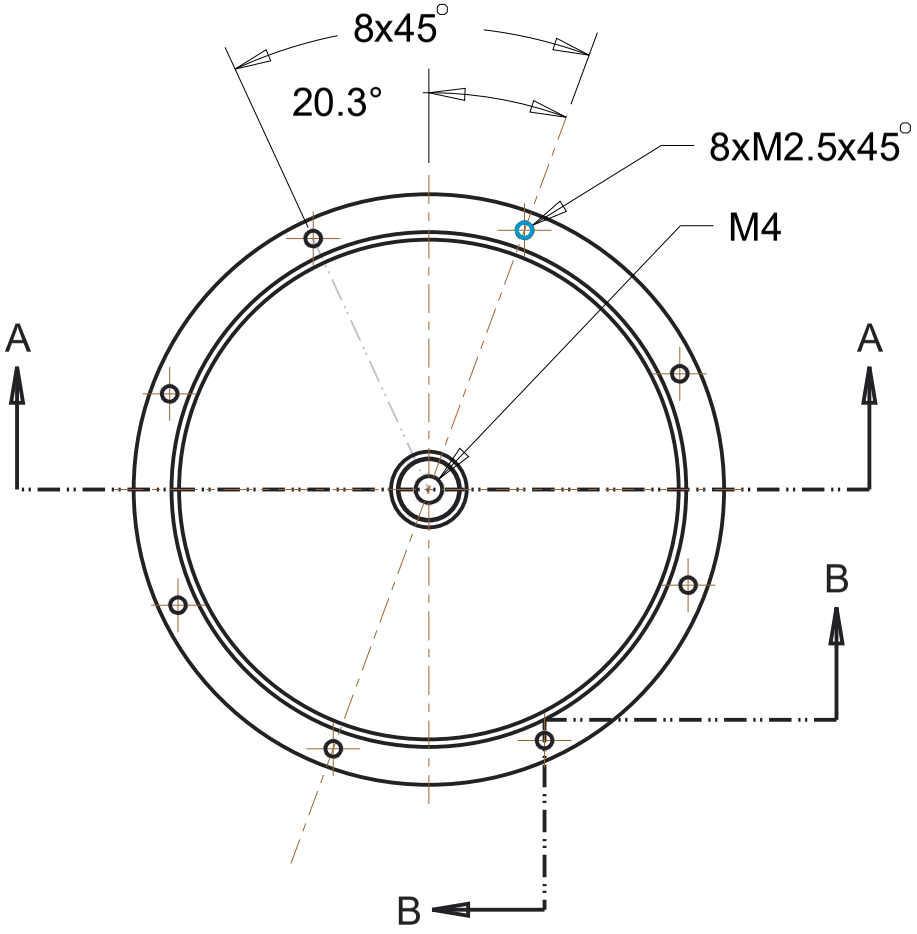

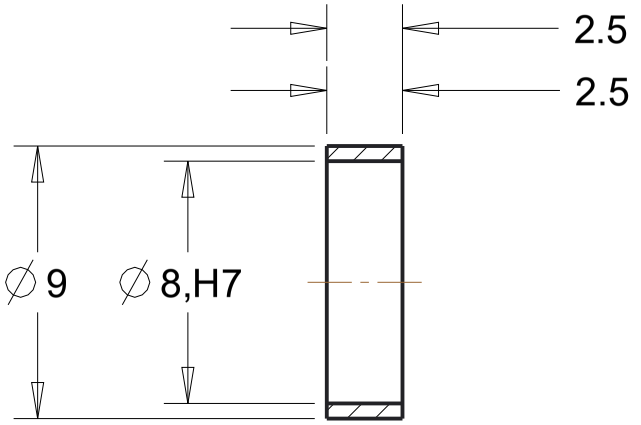

SECTION A-A

SCALE 1.000

AH Lab - Artificial Hands Laboratory The BioRobotics Institute - Scuola Superiore Sant'Anna				
Part. N. 9	Denominazione: SPACER			Materiale: Engal 7075
Complessivo	Denominazione: Elbow Joint			Foglio: 1/1
Gruppo	Denominazione:			Scala: 4:1
Sottogruppo	Denominazione:			Data: Jun-08-17
Tolleranze generali UNI ISO 22768	Trattamenti speciali:	Disegnato	Jessica Brand	Quantità: 1
		Controll.		Sostituisce il: il
		Approvato		Arch. N°:

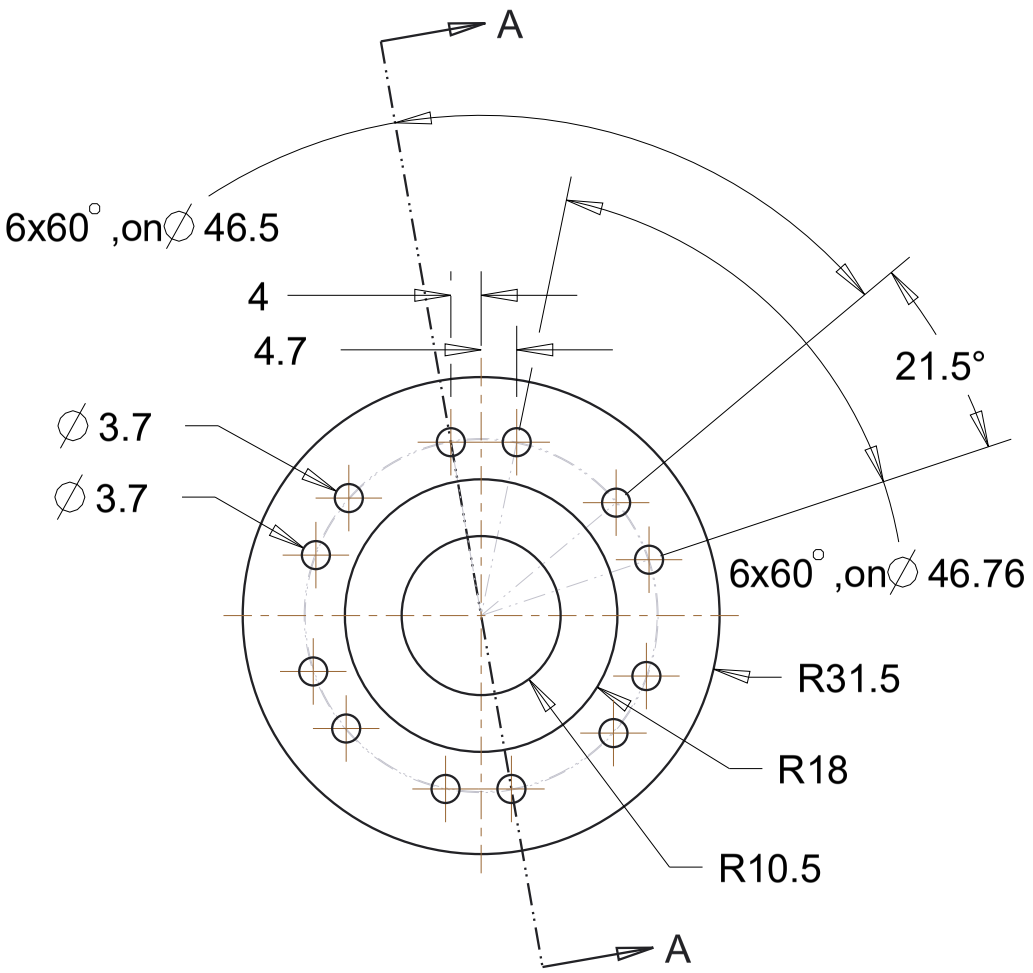

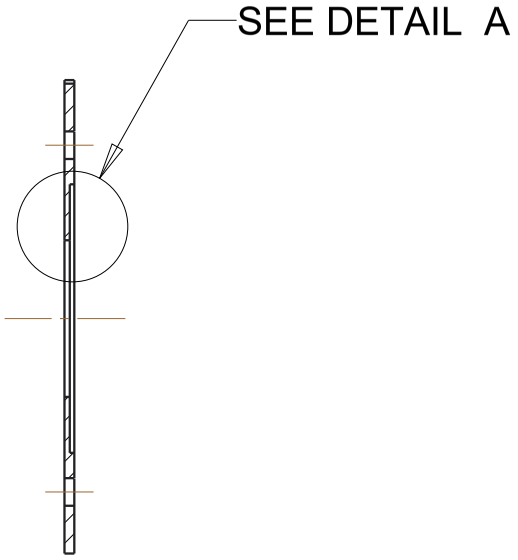

SECTION A-A

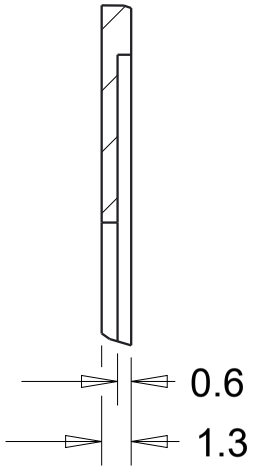

DETAIL A
SCALE 3.000

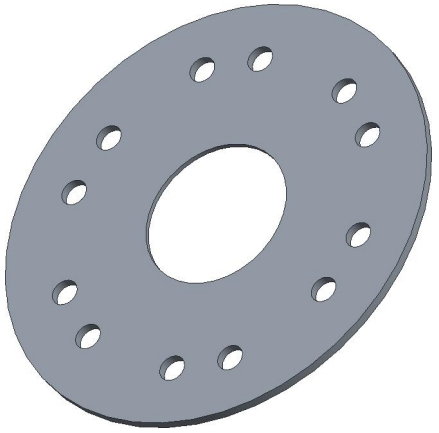

AH Lab - Artificial Hands Laboratory The BioRobotics Institute - Scuola Superiore Sant'Anna				
Part. N. 10	Denominazione: PLATE_S1_PLASTIC_NEWNEW			Materiale: Engal 7075
Complessivo	Denominazione: Elbow Joint			Foglio: 1/1
Gruppo	Denominazione:			Scala: 1:1
Sottogruppo	Denominazione:			Data: Jun-08-17
Tolleranze generali UNI ISO 22768	Trattamenti speciali:	Disegnato	Jessica Brand	Quantità: 1
		Controll.		Sostituisce il: il
		Approvato		Arch. N°:

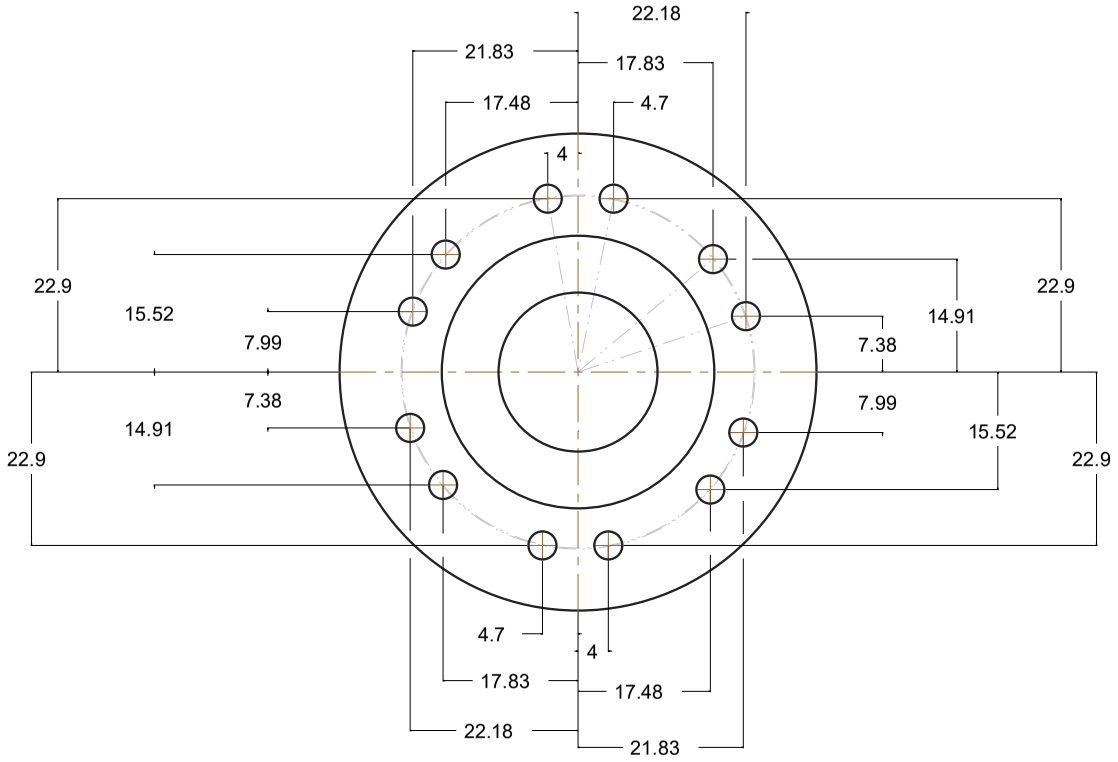

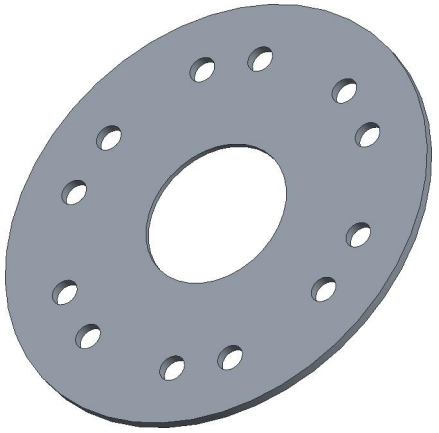

AH Lab - Artificial Hands Laboratory The BioRobotics Institute - Scuola Superiore Sant'Anna				
Part. N. 10	Denominazione: PLATE_S1_PLASTIC_NEWNEW			Materiale: Engal 7075
Complessivo	Denominazione: Elbow Joint			Foglio: 1/1
Gruppo	Denominazione:			Scala: 1:1
Sottogruppo	Denominazione:			Data: Jun-08-17
Tolleranze generali UNI ISO 22768	Trattamenti speciali:	Disegnato	Jessica Brand	Quantità: 1
		Controll.		Sostituisce il: il
		Approvato		Arch. N°:

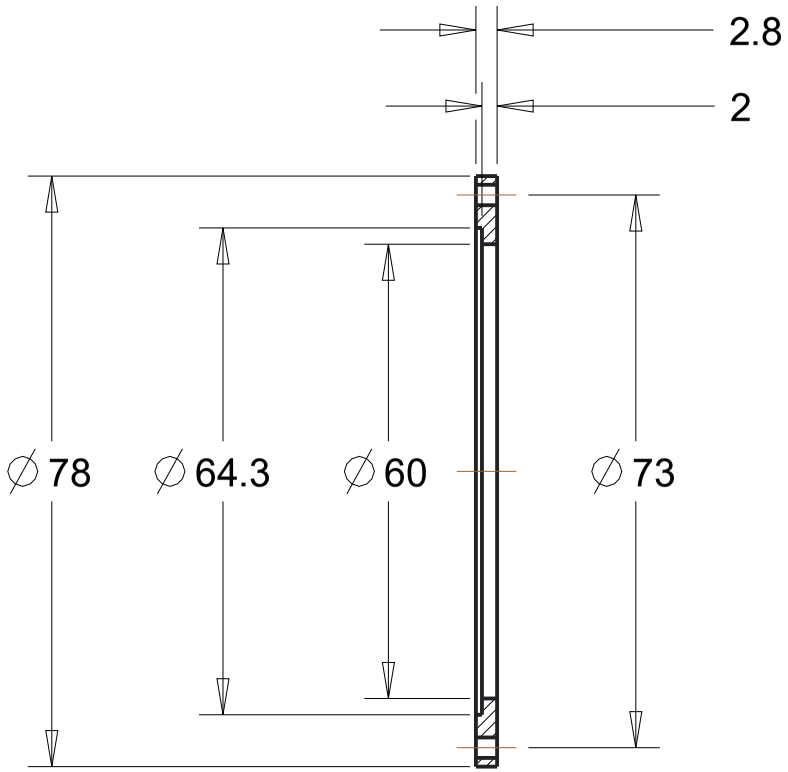

A-A

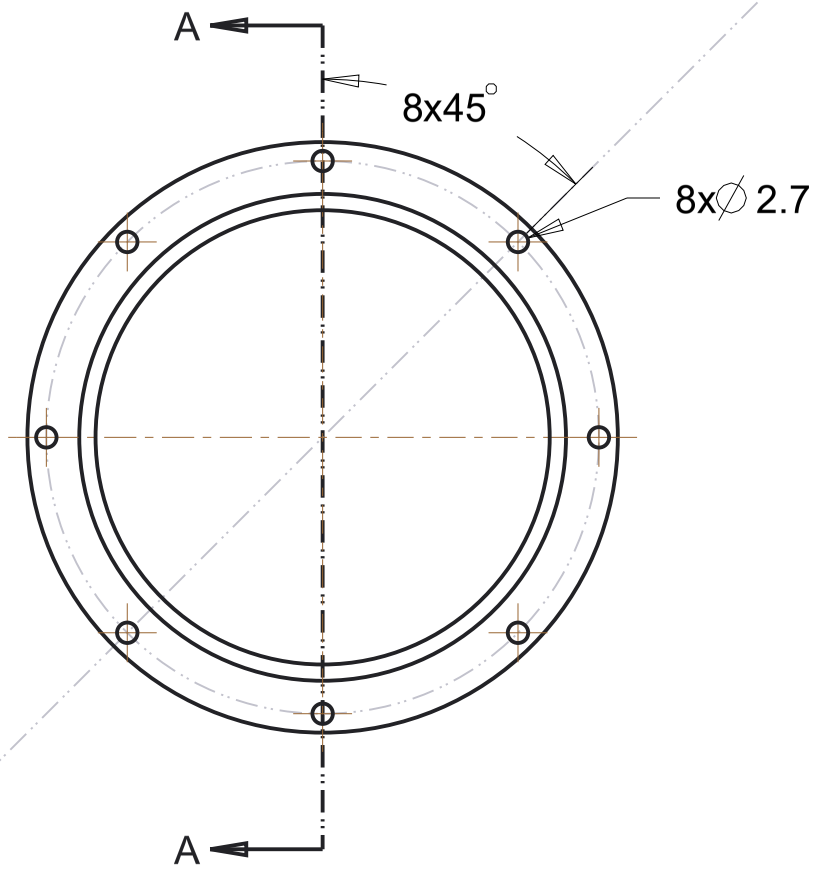

SCALE 0.500

AH Lab - Artificial Hands Laboratory The BioRobotics Institute - Scuola Superiore Sant'Anna				
Part. N. 11	Denominazione: PLATE_COVER_S1_NEWNEW			Materiale: Engal 7075
Complessivo	Denominazione: Elbow Joint			Foglio: 1/1
Gruppo	Denominazione:			Scala: 1:1
Sottogruppo	Denominazione:			Data: Jun-08-17
Tolleranze generali UNI ISO 22768	Trattamenti speciali:	Disegnato	Jessica Brand	Quantità: 1
		Controll.		Sostituisce il: il
		Approvato		Arch. N°:

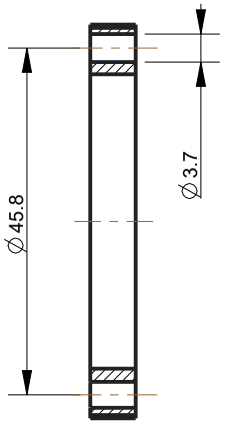

SECTION A-A

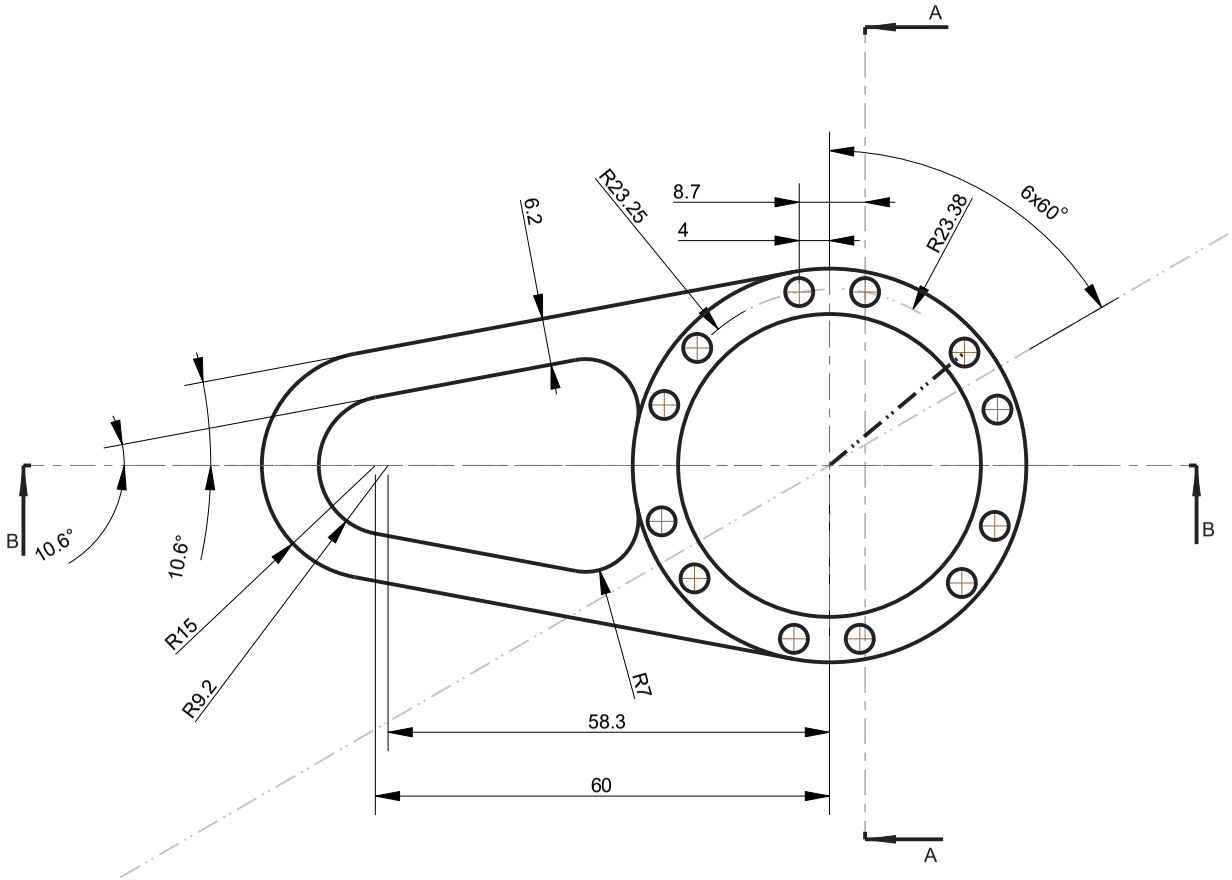

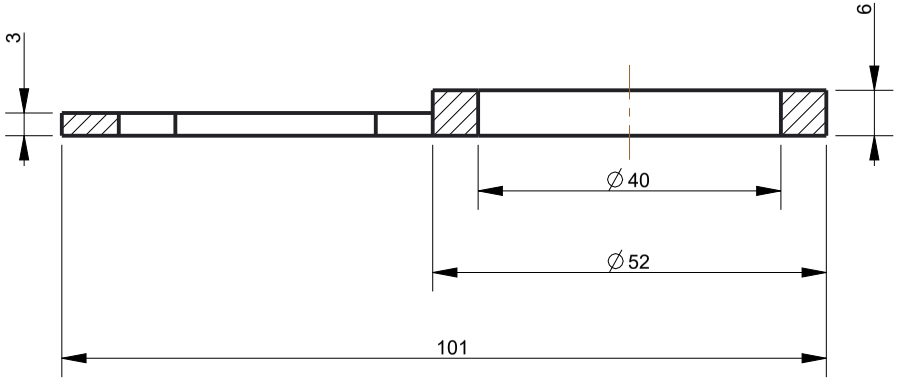

SECTION B-B

AH Lab - Artificial Hands Laboratory The BioRobotics Institute - Scuola Superiore Sant'Anna				
Part. N. 12	Denominazione: FOREARMELEMENT			Materiale: Engal 7075
Complessivo	Denominazione: Elbow Joint			Foglio: 1/1
Gruppo	Denominazione:			Scala: 1:1
Sottogruppo	Denominazione:			Data: Jun-14-17
Tolleranze generali UNI ISO 22768	Trattamenti speciali:	Disegnato	Jessica Brand	Quantità: 1
		Controll.		Sostituisce il: il
		Approvato		Arch. N°:

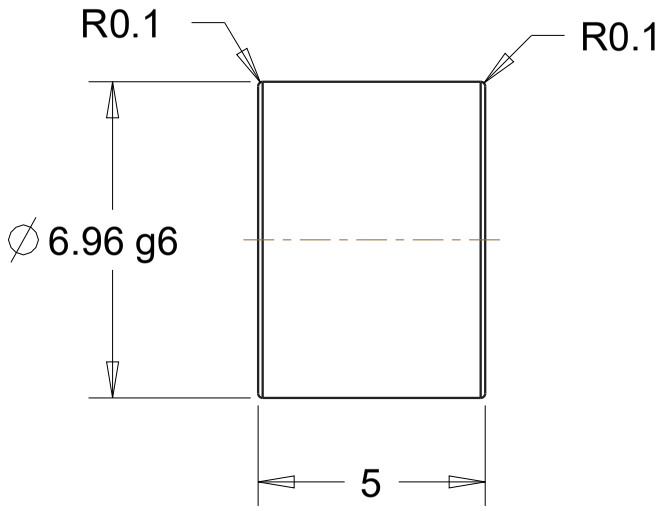

SCALE 1.000

AH Lab - Artificial Hands Laboratory The BioRobotics Institute - Scuola Superiore Sant'Anna				
Part. N. 13	Denominazione: ROLLER_656_NEW			Materiale: stainless steel
Complessivo	Denominazione:			Foglio: 1/1
Gruppo	Denominazione:			Scala: 6:1
Sottogruppo	Denominazione:			Data: Jun-08-17
Tolleranze generali UNI ISO 22768	Trattamenti speciali:	Disegnato	Jessica Brand	Quantità: 12
		Controll.		Sostituisce il: il
		Approvato		Arch. N°:

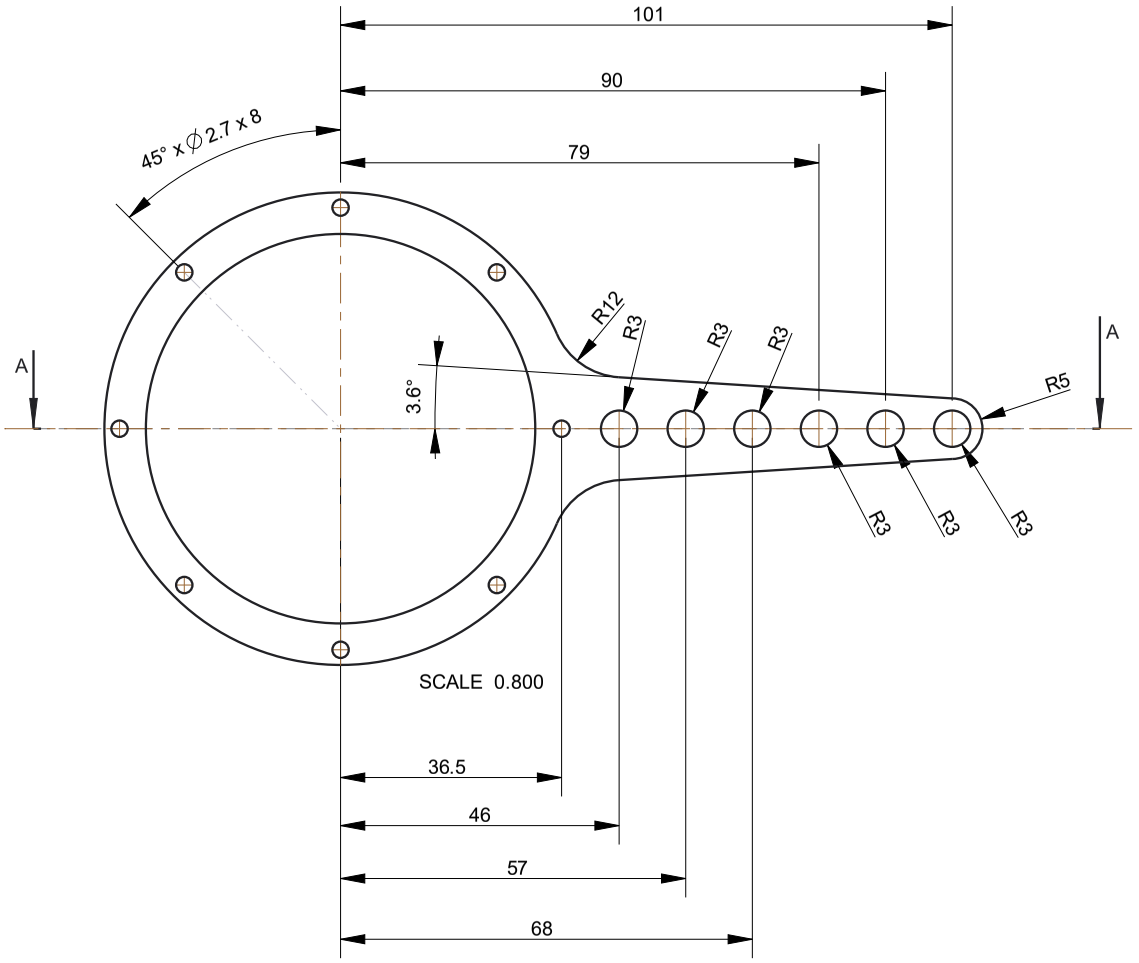

SCALE 0.500

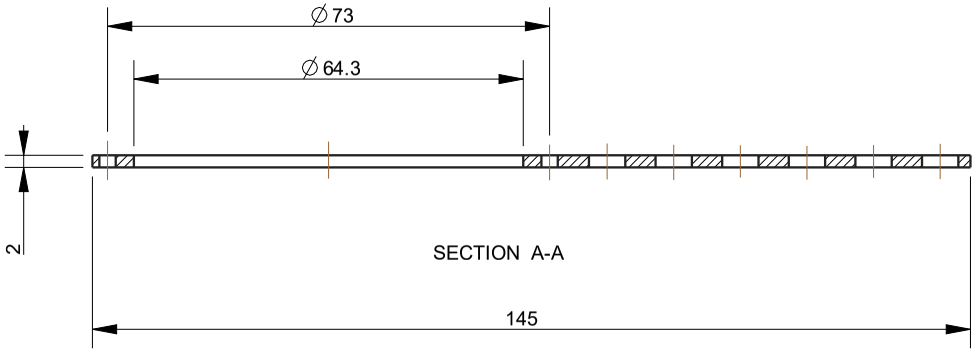

AH Lab - Artificial Hands Laboratory The BioRobotics Institute - Scuola Superiore Sant'Anna				
Part. N. 14	Denominazione: UPPERARM_ELEMENT_TEST			Materiale: Engal 7075
Complessivo	Denominazione: Elbow Joint			Foglio: 1/1
Gruppo	Denominazione:			Scala: 1:1.25
Sottogruppo	Denominazione:			Data: 17-Jun-19
Tolleranze generali UNI ISO 22768	Trattamenti speciali:	Disegnato	Jessica Brand	Quantità: 1
		Controll.		Sostituisce il: il
		Approvato		Arch. N°:

12 Abbreviation List

In the following, a list (see Table 6, 7) of all used abbreviations is given.

Table 6: Abbreviations, Part 1

Abbreviations	Original Names/Explanations	Units
α	Contact angle between roller and input cam	$^\circ$
A	Area	mm^2
a, b	Material parameters regarding its lubrication and condition	mm^2
CAD	Computer Aided Design	n/a
C_{f1}	Parameter of the principle stress	n/a
DOF	Degree of Freedom	n/a
d	Diameter	mm
D_{tot}	Total deformation	mm
Diff.	Differences between the default and adjusted design	%
E	Young's Module	MPa
E	Error between T_{uts} and T_{um}	%
FEM	Finite Element Method	n/a
F_u	Unlocking force	N
F_r	Radial force	N
F	(Tangential) force	N
g	Gravity constant	m/s^2
HB	Brinell Hardness	n/a
I	Moment of inertia	mm^4
L_m	Resulting output torque/applied load lever arm	mm
L_u	Unlocking force lever arm	mm
L	Length of element	mm
l	Distance between centerline and side surfaces of the input cam	mm
Mn_{ad}	Adjusted model, n = 1, 2	n/a
Mn_{de}	Default model, n = 1, 2	n/a
m	Load/mass	kg
ND	New Design	n/a
N	Total number of rollers	n/a
N_a	Number of rollers in use when a load is applied	n/a
N_{max}	Maximal number of rollers	n/a
OD	Old design	n/a
p	Pressure	MPa
$P_{Hz,10^7}$	Pressure that material withstands when it is loaded for 10^7 times	MPa
r	Roller radius	mm
R_{in}	Inner radius of the output ring	mm
ROM	Range of Motion	$^\circ$
$R_{p0.2}$	Yield strength at 0.2%	MPa
SSSA	Scuola Superiore Sant'Anna	n/a

Table 7: Abbreviations, Part 2

Abbreviations	Original Names/Explanations	Units
SD	Standard Deviation	n/a
S_y	Yield strength	MPa
σ_{cr}	Buckling strength	MPa
σ	Maximal principal stress	MPa
σ_{sp}	Maximal stresses of the selector pin	MPa
σ_{cp}	Maximal stresses of the cam pin	MPa
σ_r	Stresses in rounding/curve between cam pin and its basement	MPa
σ_h	Stresses at the area of the selector pin's hole	MPa
T_{max}	Maximal applied output torque	Nmm
T_u	Unlocking torque	Nmm
T_{ut}	Theoretical optimal unlocking torque	Nmm
T_{uts}	Theoretical unlocking torque including selecting mechanism	Nmm
T_{um}	Measured unlocking torque	Nmm
T_{ro}	Resulting/responding output torque	Nmm
v	Possion's ratio	n/a
VSA	Variable Stiffness Actuators	n/a
μ_s	Friction coefficient	n/a

Abbreviations that were used but only defined by equations, are not mentioned in the previous Table 6 and 7.